Volume 39 · Number 6 · 2010 · 327-341

Figure 3 TEM of (a) cyan, (b) magenta, (c) yellow and (d) black pigment dispersions; TEM for (e) cyan and (g) yellow inks; and SEM for (f) magenta and (h) black inks after one-year storage

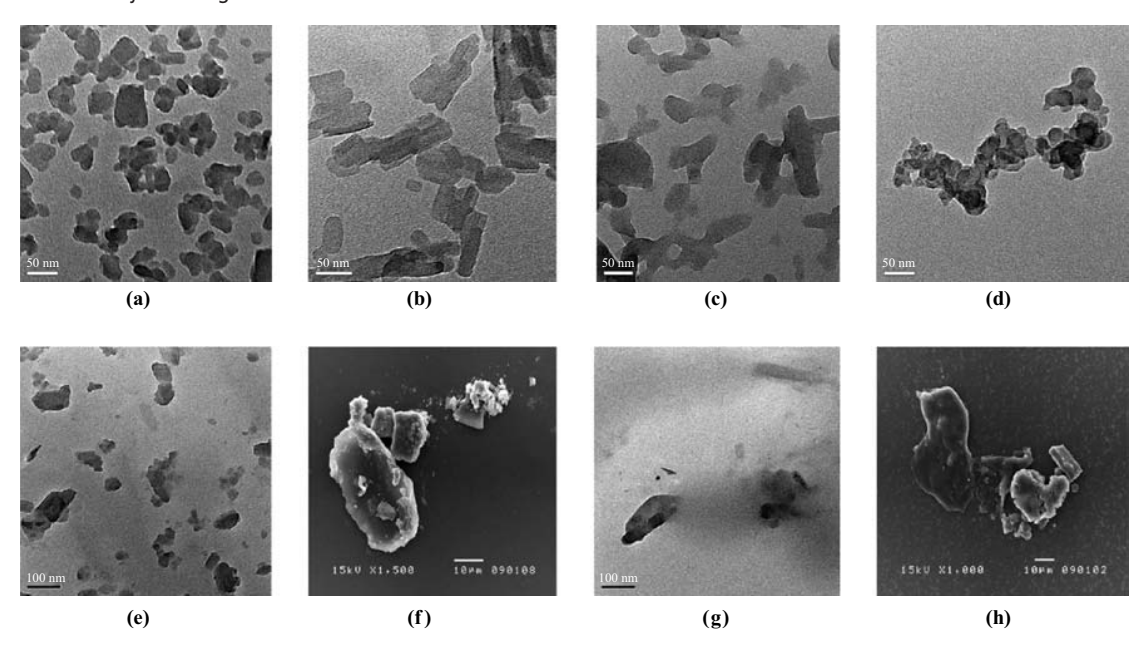
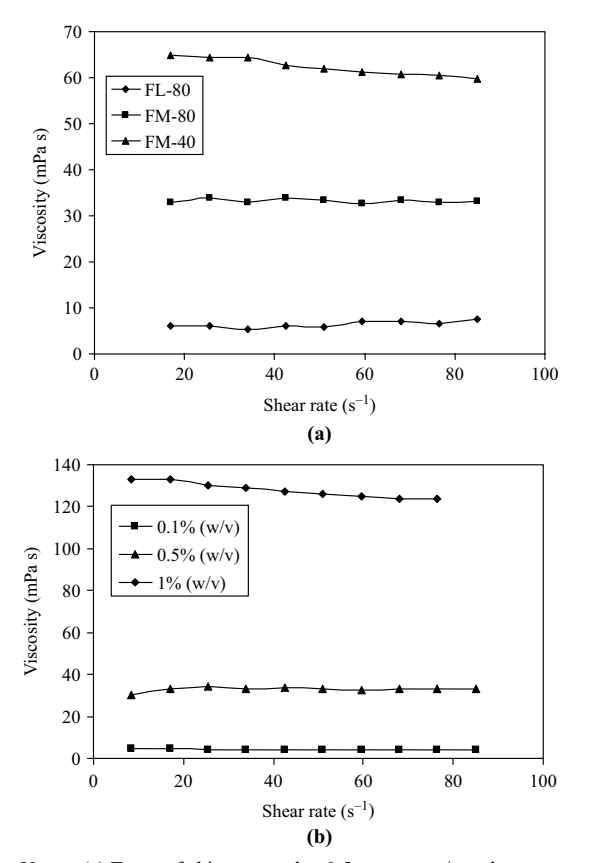


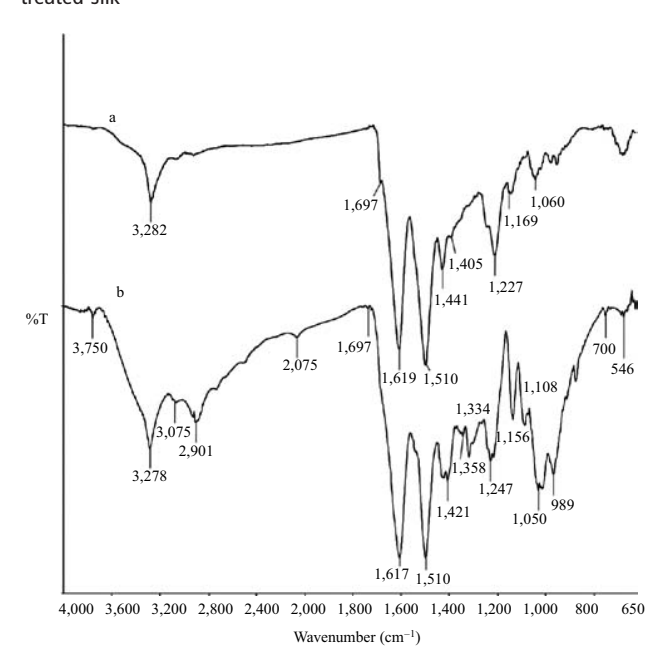
Figure 4 Viscosity of the chitosan solutions



Notes: (a) Types of chitosan used at 0.5 per cent w/v and (b) FM-80 at various loadings at 25°C; data are shown as the mean ± 1 (SD) and are derived from three replicates

concentration (FM-80) increases the viscosity of the padding solution (Figure 4(b)). Spectrum (a) of Figure 5 shows IR peaks of the non-treated silk fabric. In spectrum (b) of Figure 5 for chitosan-treated silk, a sharp strong NH₃⁺ stretching band in the 3,278-2,901 cm⁻¹ region resulting from superimposed O—H and NH₃⁺ stretching band are stronger than those in spectrum (a). The stronger peaks in spectrum (b) at 1,050-989 cm⁻¹ are assigned for the symmetric C—O—C stretching of chitosan. The asymmetric N—H stretching at 1,617-1,510 cm⁻¹ and more weakly near

Figure 5 FTIR-ATR spectra of (a) the non-treated silk and (b) chitosantreated silk



 $1,441-1,405\,\mathrm{cm^{-1}}$ are the asymmetrical and symmetrical $\mathrm{C(^-O)_2}$ stretching of the carboxylate ion group (Silverstein *et al.*, 1991). This indicates that chitosan has been incorporated on the fabric. Therefore, the addition of chitosan to the silk introduces synergistic effects to be generated on colour gamut.

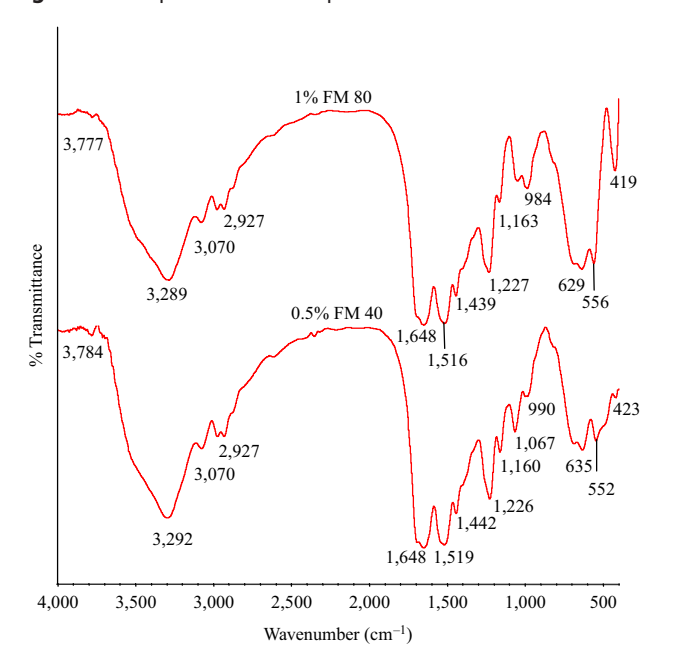
With the same degree of deacetylation (87-88 per cent), the three types of chitosan that were used in this work did not display any different chemical properties, for example with the IR spectra of silk fabric padded with the two types of chitosan, FM-80 and FM-40 (Figure 6). Moreover, the ink jet ink-printed silk fabrics that had previously been padded with chitosan solutions gave similar chemical surface properties, as shown by their IR spectra (Figure 7). Hydrogen peroxide bleaching of the fabric is to remove surface sericin and other waxy materials resulting in a clean and white surface for better wetting, adhesion and image permanency. Interactions between the ink and the substrate cannot be easily detected by simple spectroscopic methods because of the substrate dominance in comparison with the chitosan-treating solution. Thus, the dual objectives of developing improvements in the printing process with improvements in the colour-related properties were achieved initially. Further investigation of the extent of colour gamut expansion could provide an indication of the synergistic effects provided by the inks and the chitosan pre-treatment solution.

Effect of pre-treatment of the printed fabrics on operational properties

Colour gamut

For the three different types of chitosan, and across all the tested ranges of chitosan concentrations used, the colour gamuts (a*-b*, L*-a*, L*-b* and L*a*b*) of the pre-treated fabrics were overall greater, i.e. a larger gamut volume was attained than those printed colours applied to the non-treated

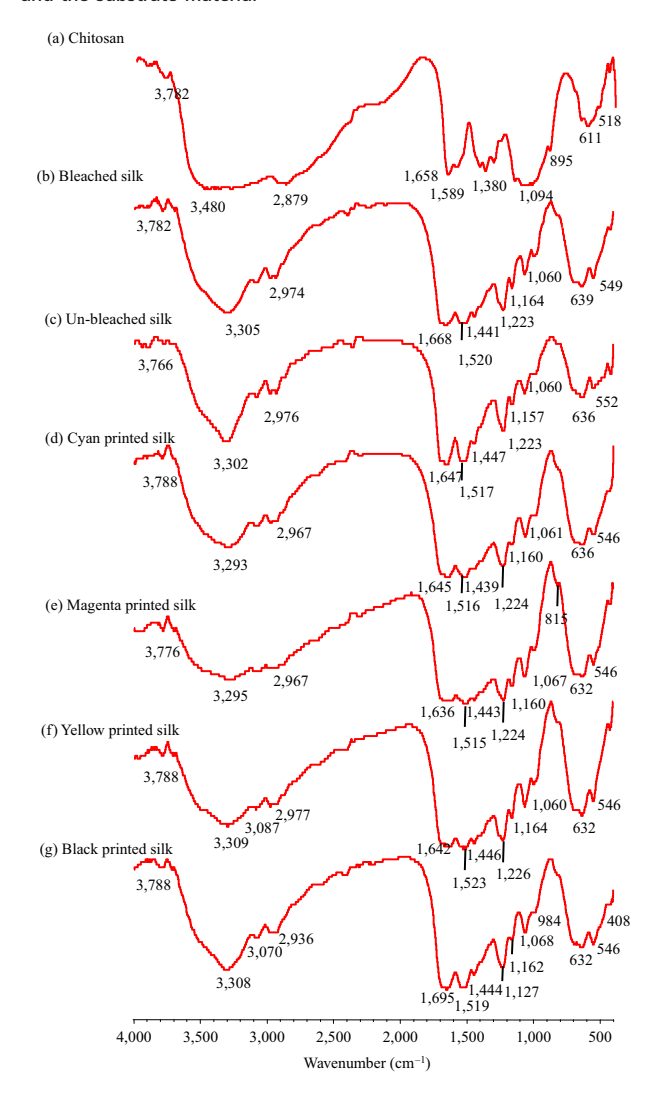
Figure 6 FTIR spectra of chitosan-padded bleached silk fabrics



Note: The upper line with 1 per cent w/v FM-80 solution and the lower line with 0.5 per cent w/v FM-40 solution

Volume 39 · Number 6 · 2010 · 327-341

Figure 7 FTIR spectra of the four-coloured ink jet ink printed fabrics and the substrate material

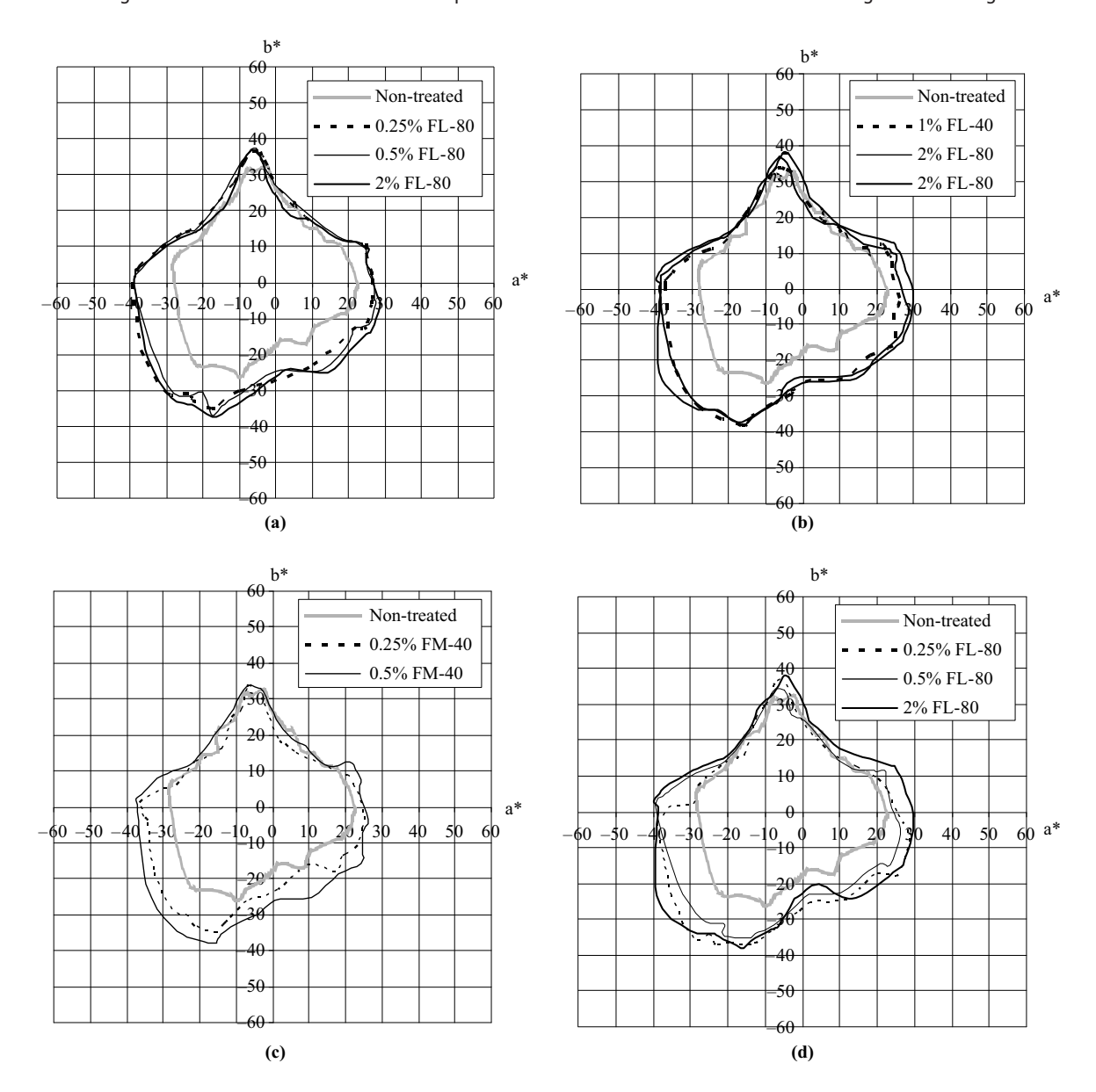


fabrics as shown in Figures 8-11. Likewise, lightness of the pre-treated fabrics was lower than those of non-treated ones (Figures 9-11), i.e. more colour saturation. Once the pigment was dispersed in water, the nanoparticles become interactive with the non-treated silk fibres, through hydrogen bonding and dipole-dipole interactions through the sulphonate or the carboxylic groups which are completely anionic under alkaline conditions. In addition, the alkalinity causes the silk fibres to swell, making them more accessible to the diffusion of the adsorbed nanoparticulate pigments from the surface towards the interior of the fibres.

Increasing the pre-treatment solution concentration for each of the three different molecular weight chitosans, resulted in a wider colour space where the chroma of the cyan colours, at many hue angles, became significantly saturated. A similar trend was also observed with the magenta colours but to a smaller extent. The colour strength of the fabrics printed following with the chitosan pre-treatments increased consistently, the chitosan concentration in the pre-treatment was increased. Amongst the three molecular weight

Volume 39 · Number 6 · 2010 · 327-341

Figure 8 a*-b* diagrams of the non-treated silk and the silk pre-treated with chitosan of different molecular weights and loadings



chitosans tested, the pre-treatment solution containing the medium molecular weight chitosan (FM-80), prepared at the highest concentration (2 per cent w/v), gave the largest colour gamut (the combined L*a*b* in Figure 11). This finding correlates well with its highest solution viscosity (Figure 4). Chitosan pre-treatment improves the colour gamut of the printing inks because the chitosan molecule contains amino groups (-NH₂) that are protonated (-NH₃⁺) under acidic conditions and can electrostatically interact with the sulphonate or carboxylate groups on the pigment surfaces, even at a low chitosan concentration (Jocic et al., 2005). Thus, the pre-treatment solutions provide the silk fabric with additional cationic functional groups that enhance the absorption of more ink on to the fabric surface. A colour gamut expansion on the treated fabric surfaces is related to the increases in the chroma (Figure 8). The function of the

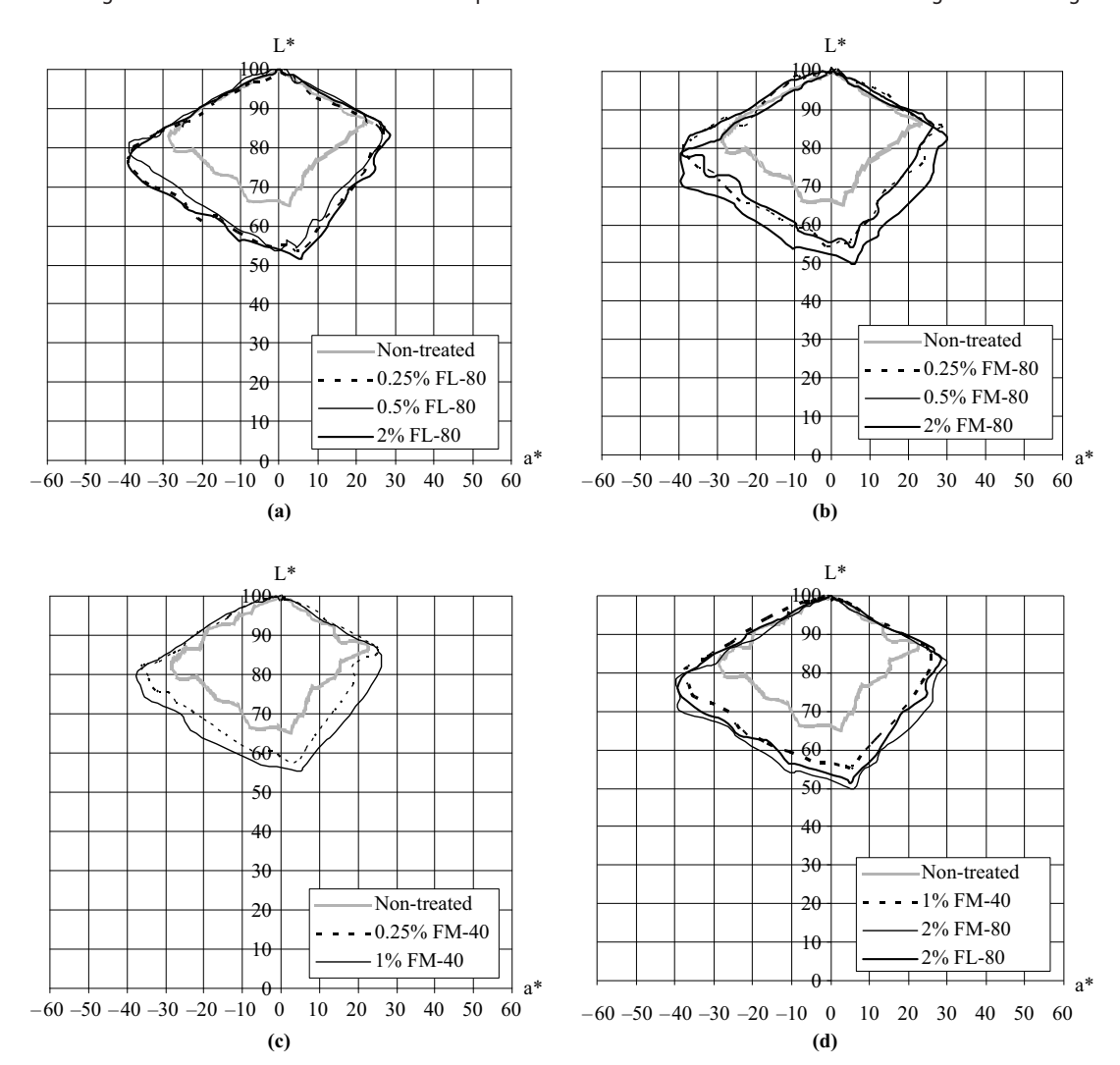
pre-treatment is to block ink penetration and to give retention of ink on the pre-treated surface. One of the chief concerns with treating silk fabric with chitosan is the increased stiffness of the treated fabrics (Leelajariyakul *et al.*, 2008; Phattanarudee *et al.*, 2009), and so it is desirable to use the smallest amount of chitosan in the pretreatment solution as possible to fulfil the need for a specific purpose.

Wash fastness

The inks contained the S-711 acrylic binder with its $T_{\rm g}$ of -31° C. This binder is designed to form a flexible film on the silk surface, giving the required properties to the fabric. The effect of the chitosan pre-treatment of silk on their wash fastness following printing was determined by following the K/S of the coloured fabrics, measured before and after the washings. The K/S values of the treated fabrics before and

Volume 39 · Number 6 · 2010 · 327-341

Figure 9 L*-a* diagrams of the non-treated silk and the silk pre-treated with chitosan of different molecular weights and loadings

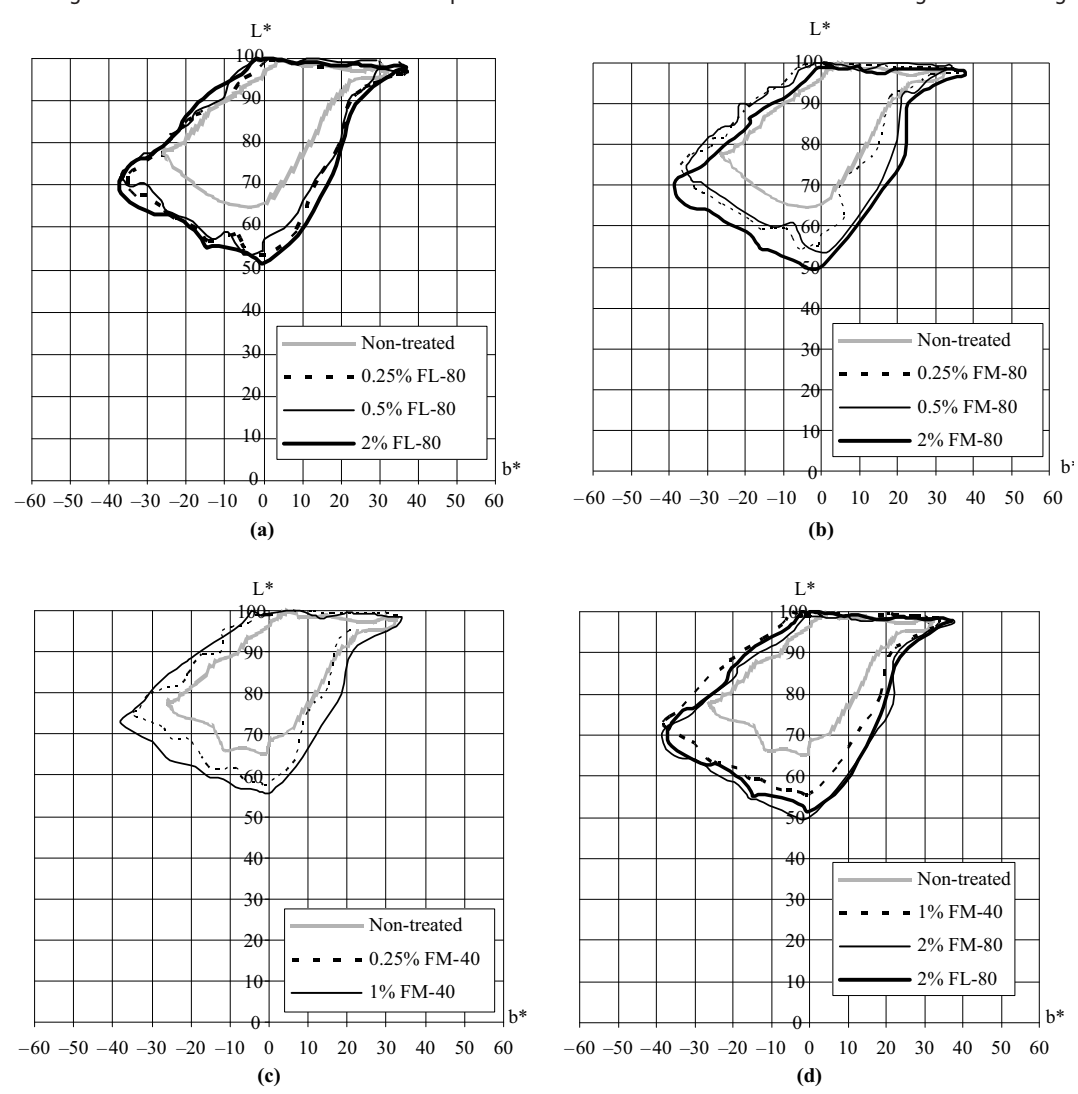


after washing were in unchanged range (0.4-0.5) for cyan and magenta inks, whereas the ranges of 1-1.3 and 1.7-2.5 were found in the yellow and black inks, respectively, depending on the treatment levels. The wash fastness of the printed fabrics was thus excellent for all of the pre-treatments (Table III), and the relative colour strength of the printed silk fabrics after washing is summarized in Table IV where a very small change in the K/S before and after washing, across all of the pre-treatments, was observed. Also, the pre-treatments moderately improved the wash fastness. The relative colour strength of the non-treated fabric was 0.82 for all colours, and the treated ones in the range of 0.9-1.2 for the cyan, magenta, yellow, and black inks, depending on the chitosan molecular weights and solution concentration. The chitosan pre-treatment of silk fabric thus enhanced the wash fastness properties. Comparing between the different chitosans used in the pre-treatments, the chitosan molecular weight and concentration had a slight effect on the wash fastness and colour gamut. At 2 per cent w/v of FL-80 and 1 per cent w/v of FM-80 and FM-40, all of the K/S values increased, especially for the black ink, when compared with the results on the coloured non-treated fabrics.

The amino group in chitosan has a pKa value of about 6.5. Thus, chitosan is positively charged and soluble in acidic to neutral solutions with a charge density that is dependent on the pH and on the percentage of deacetylation that the chitosan contains. The amino groups are protonated to (NH₃⁺ (a nucleophilic group) under slightly acidic pH conditions allowing ionic (electrostatic) interactions with electrophilic centres, such as carboxylate (-COO⁻) or sulphonate $(-SO_3^-)$ groups. The proposed electronic interaction is shown in Figure 12. A large pigment molecule with a correspondingly large surface area will provide a large number of potential reactive sites, such as the N-H, O-H or C=O groups. Thus, hydrogen-bonding interactions can occur to increase the strength of the binding over that of only the electrostatic interactions (Crini and Badot, 2008). All of these interactions, whether electrostatic, polar or H bonding, between the colorant and silk fabric, produce printed silks with an excellent wash fastness (Provost et al., 2009). Here, the cationic amino moiety increases the absorption potential of these negatively charged inks via an ionic bonding mechanism (Noguchi and Shirota, 2006; Li and Sun, 2007), since the amino groups in the pre-treating agent and the amino groups in

Volume 39 · Number 6 · 2010 · 327-341

Figure 10 L*-b* diagrams of the non-treated silk and the silk pre-treated with chitosan of different molecular weights and loadings



the silk are both protonated and can interact with the anionically surface-modified pigment particles, resulting in an increased interaction, increased ink binding and, consequently, an increase in the K/S values.

Carbon black pigments can contain hydrophilic carboxylic groups and hydroxyl groups from the production process (spectrum (d) in Figure 1). Such pigments can be additionally surface modified by the use of diazonium salts that contain the sulphonate functional group (Belmont, 1994). Thus, the carbon black pigments can be better dispersed under acidic conditions. It is known that carbon black is one of the most difficult-to-disperse pigments. Therefore, additional effective functional groups on the surface provide opportunity for the better development of superior black inks. The calculated K/S values, coupled with visual assessment, support the contention that these inks easily meet the appropriate performance criteria in that the visual ink density and the associated adhesion are both acceptable. The solid content of 50.7 per cent w/w of the Vanatex S-711 in the inks plays a very important role in the ability of the ink to interact with the padded chitosan on the silk fabric, i.e. holding more ink on

the surface. This would be expected to increase the colour gamut and the wash fastness.

Crock fastness

From the data given in Table V, it is clear that the non- and pre-treated printed silk fabrics provide the required minimal level of a good dry/wet crock fastness, at levels of 4-5. This is because the inks contained the binder (S-711 acrylic polymer) whose film is flexible (T_g of $-31^{\circ}C$) at room temperature and can withstand the rubbing processing. The chitosan pre-treatment slightly improved the fabric dry/wet crock fastness (at the 4/5 level). In dry conditions, chitosan loadings from pre-treatment with 0.25 and 0.5 per cent w/v solutions did not affect the dry rub resistance. However, a decline in the rub resistance (at the 4 level) was found under wet conditions, presumably due to a water-acid effect. For all of the chitosan pre-treatments, the dry crock fastness results were better than those of the wet crock fastness. The wet crock fastness was slightly decreased when the chitosan loading solution was more than 0.5 per cent w/v, but was essentially the same for the three different molar mass chitosans evaluated here (Leelajariyakul et al., 2008). The crock and the wash fastness

Volume 39 · Number 6 · 2010 · 327-341

Figure 11 L*a*b* of the untreated silk and the treated silk pre-treated with chitosan of different molecular weights and loadings

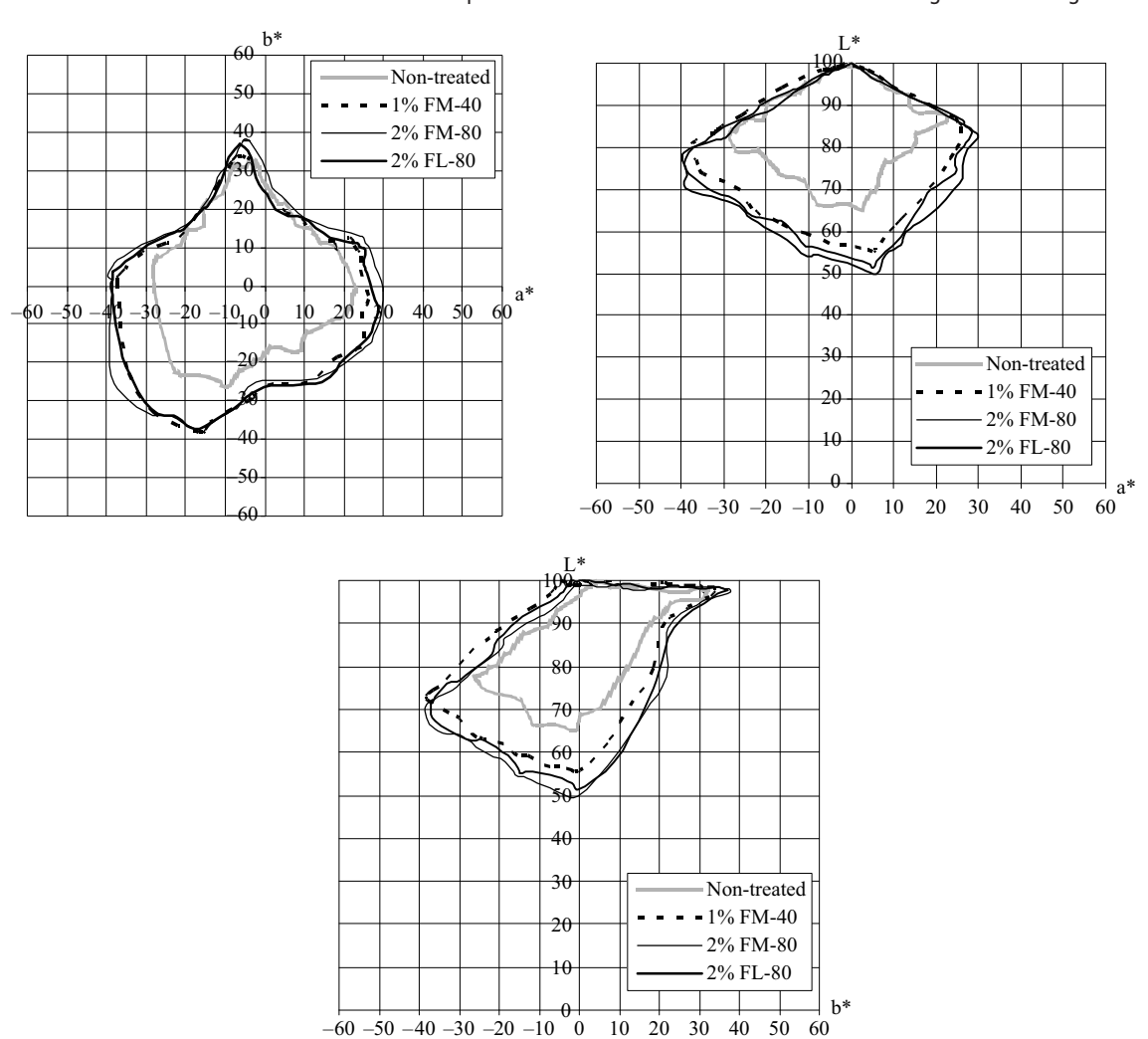


Table III K/S of the printed silk fabrics before and after washing

				K/S of	the printed sill	k with the inks			_
		Су	an	Mag	enta	Yel	low	Bla	ack
Condition of fabric treatment		Before washing	After washing	Before washing	After washing	Before washing	After washing	Before washing	After washing
Non-treated		0.42 ± 0.00	0.38 ± 0.01	0.45 ± 0.03	0.41 ± 0.02	1.18 ± 0.05	0.96 ± 0.07	1.41 ± 0.01	1.26 ± 0.04
Chitosan ^a (FL-80)	0.25	0.38 ± 0.04	0.40 ± 0.06	0.39 ± 0.02	0.40 ± 0.02	1.10 ± 0.04	1.08 ± 0.08	1.73 ± 0.03	1.75 ± 0.03
(%(w/v))	2	0.48 ± 0.04	0.47 ± 0.02	0.45 ± 0.03	0.45 ± 0.02	1.30 ± 0.01	1.28 ± 0.02	2.18 ± 0.04	2.24 ± 0.05
Chitosan ^b (FM-80)	0.25	0.4 ± 0.02	0.41 ± 0.02	0.37 ± 0.01	0.38 ± 0.01	0.99 ± 0.04	0.96 ± 0.03	2.54 ± 0.19	2.45 ± 0.06
(%(w/v))	1	0.45 ± 0.01	0.47 ± 0.03	0.47 ± 0.02	0.48 ± 0.01	1.29 ± 0.05	1.27 ± 0.06	2.20 ± 0.07	2.20 ± 0.02
	2	0.56 ± 0.06	0.55 ± 0.06	0.53 ± 0.01	0.51 ± 0.01	1.26 ± 0.09	1.23 ± 0.09	2.19 ± 0.14	2.15 ± 0.09
Chitosan ^c (FM-40)	0.25	0.42 ± 0.02	0.44 ± 0.02	0.41 ± 0.01	0.44 ± 0.02	1.14 ± 0.01	1.14 ± 0.04	1.92 ± 0.03	1.93 ± 0.04
(%(w/v))	1	0.45 ± 0.03	0.43 ± 0.02	0.45 ± 0.03	0.42 ± 0.03	1.34 ± 0.04	1.28 ± 0.05	2.54 ± 0.19	2.42 ± 0.24

Notes: $^aMW = 1.2 \times 10^5 \, g \, \text{mol}^{-1}$; $^bMW = 3.7 \times 10^5 \, g \, \text{mol}^{-1}$; $^cMW = 8.5 \times 10^5 \, g \, \text{mol}^{-1}$; all have an 87-88% degree of N-deacetylation; data are shown as the mean ± 1 (SD) and are derived from three replicates

Volume 39 · Number 6 · 2010 · 327-341

Table IV Relative colour strength of the printed silk fabrics after washing

	_	A			
Condition of treatment		Cyan	Magenta	Yellow	Black
Non-treated		0.82 ± 0.01	0.90 ± 0.00	0.81 ± 0.03	0.82 ± 0.02
Chitosan ^a (FL-80) (%(w/v))	0.25	1.04 ± 0.04	1.04 ± 0.01	0.98 ± 0.03	1.22 ± 0.00
	2	0.99 ± 0.03	1.00 ± 0.02	0.98 ± 0.02	1.23 ± 0.00
Chitosan ^b (FM-80) (%(w/v))	0.25	1.03 ± 0.03	1.03 ± 0.00	0.98 ± 0.01	0.98 ± 0.07
	1	1.03 ± 0.03	1.03 ± 0.01	1.04 ± 0.01	1.03 ± 0.02
	2	0.98 ± 0.00	0.96 ± 0.00	0.98 ± 0.01	0.98 ± 0.02
Chitosan ^c (FM-40) (%(w/v))	0.25	1.06 ± 0.01	1.06 ± 0.01	1.00 ± 0.02	1.01 ± 0.01
	1	0.95 ± 0.00	0.93 ± 0.00	0.96 ± 0.01	0.95 ± 0.03

Notes: ${}^aMW = 1.2 \times 10^5 \, \text{g mol}^{-1}$; ${}^bMW = 3.7 \times 10^5 \, \text{g mol}^{-1}$; ${}^cMW = 8.5 \times 10^5 \, \text{g mol}^{-1}$; all have an 87-88% degree of *N*-deacetylation; data are shown as the mean ± 1 (SD) and are derived from three replicates

Figure 12 Proposed scheme for the chitosan pre-treating agent and anionic pigment interactions

OHONH₂
$$OHO$$
 OHO O

are both governed by the strength of adhesion and by the interfacial bonding between the pigment particles/ink binder/pre-treated fabric surfaces.

Conclusion

Anionically surface-modified organic pigment dispersions were used to prepare four coloured polyacrylate binderbased ink jet inks within the pH range of 8-9. These inks exhibited Newtonian flow in which the viscosity at 25°C remained constant at 2.5 mPas under a 330 s⁻¹ shear-strain rate. The surface tension of the inks was approximately 44 mN m⁻¹ at 25°C, and the average particle sizes were approximately 100 nm. The zeta-potential of the inks was

strongly negative, in the range of -42 to $-51\,\mathrm{mV}$, and they were stable for over ten months (for the magenta and black inks) or one year (for the cyan and yellow inks), as confirmed by SEM and TEM micrographs. The inks were shown to be suitable for printing by the piezo ink jet method on both non-treated and chitosan pre-treated silk fabrics. The anionically surface-modified pigmented ink interacted with the protonated amino groups of chitosan giving improved ink deposition and fixation on the fabric surface. The colour gamuts of the treated fabrics were wider with the chroma of the cyan colour being the most improved followed by that of the magenta colour. The chitosan pre-treatment produced the better crock fastness and wash fastness of the printed fabrics than the non-treated ones.

Volume 39 · Number 6 · 2010 · 327–341

Table V Crock fastness of the non-treated and chitosan pre-treated silk fabrics

	Crock fastness								
	[Ory st	age		Wet stage				
Condition of treatment Non-treated	C 4	M 4	Y 4/5	К 4	C 4	M 4	Y 4	K 4	
Chitosan (FL-80) (%(w/v))	0.25	4/5	4/5	4	4/5	4/5	4/5	4	
	0.5	4/5	4/5	4	4/5	4/5	4/5	4	
	1	4	4	4	4/5	4	4	3/4	
	2	4	4	4	4/5	4	4	3/4	
Chitosan (FM-80) (%(w/v))	0.25	4/5	4	5	4/5	4/5	4/5	4	
	0.5	4/5	4/5	4	4/5	4/5	4/5	4	
	1	4/5	4/5	4	4/5	4/5	4	3/4	
	2	4/5	4/5	4	4/5	4	4	3/4	
Chitosan (FM-40) (%(w/v))	0.25	4/5	4/5	4	4/5	4/5	4/5	4	
	0.5	4/5	4/5	4	4/5	4/5	4/5	4	
	1	4/5	4/5	4	4/5	4/5	4/5	4	

Note: 1, 2, 3, 4 and 5 are the rating levels for poor, fair, fairly good, good and excellent, respectively

References

AATCC Crockmeter Method 8-2001 (2002), American Association of Textile Chemists and Colorists Technical Manual, AATCC, Research Triangle Park, NC, pp. 17-19. Bahmani, S.A., East, G.C. and Holme, I. (2000), "The application of chitosan in pigment printing", Journal of the Society of Dyers Colorists, Vol. 116 No. 3, pp. 94-9.

Bajaj, P. (2002), "Finishing of textile materials", Journal of Applied Polymer Science, Vol. 83 No. 3, pp. 631-59.

Belmont, J.A. (1994), "Process for preparing carbon materials with diazonium salts and resultant carbon products", US Patent 5,554,739, Application Date: 15 December.

Belmont, J.A., Johnson, J.E. and Adams, C.E. (1996a), "Aqueous inks and coatings containing modified carbon products", WO 96/18696A, 20 June.

Belmont, J.A., Johnson, J.E. and Adams, C.E. (1996b), "Ink jet ink formulations containing carbon black products", US Patent 5,571,311, 5 November 1996.

Berns, R.S. (2000), *Principles of Color Technology*, 3rd ed., Wiley, New York, NY.

Crini, G. and Badot, P.M. (2008), "Application of chitosan, a natural aminopolysaccharide, for dye removal from aqueous solution by adsorption process using batch studies: a review of recent literature", *Progress in Polymer Science*, Vol. 33 No. 4, pp. 399-447.

Fu, S. (2006) in Ujiie, H. (Ed.), Pigmented Ink Formulation, Digital Printing of Textile, Woodhead Publishing, Cambridge, pp. 220-30.

ISO 105-A03 (1993), "Textiles – tests for color fastness – part A03: grey scale for assessing staining", ISO 105-A03:1993.

ISO 105-C06 (1994), "Textiles – tests for color fastness – part C06: color fastness to domestic and commercial laundering", ISO 105-C06:1994.

Jason, H. (2004), "Surface modified pigments for ink jet ink application", available at: www.cabot.corp.com (accessed 8 November 2008).

Jocic, D., Vilchez, S., Topalovic, T., Nzvarro, A., Jovancic, P., Julia, M.R. and Erra, P. (2005), "Chitosan/acid dye

interactions in wool dyeing system", Carbohydrate Polymers, Vol. 60 No. 1, pp. 51-9.

Johnson, J.E. and Belmont, J.A. (1997), "Modified colored pigments and ink jet inks, inks, and coatings containing modified colored pigments", US Patent 5,922,118, application date: 9 June.

Johnson, J.E., Nanying, B. and Galloway, C.P. (2002), "Modified pigments having improved dispersing properties", US Patent 6,478,863, application date: 12 November.

Leelajariyakul, S., Noguchi, H. and Kiatkamjornwong, S. (2008), "Surface-modified and micro-encapsulated pigmented inks for ink jet printing on textile fabrics", *Progress in Organic Coatings*, Vol. 62 No. 2, pp. 145-61.

Li, D. and Sun, G. (2007), "Coloration of textiles with self-dispersible carbon black nanoparticles", *Dyes and Pigments*, Vol. 72 No. 2, pp. 144-9.

Noguchi, H. and Shirota, K. (2006), "Formulation of aqueous ink jet ink", in Ujiie, E. (Ed.), *Digital Printing of Textile*, Woodhead Publishing, Cambridge, pp. 233-51.

Oktem, T. (2003), "Surface treatment of cotton fabrics with chitosan", *Coloration Technology*, Vol. 199 No. 4, pp. 241-6.

Phattanarudee, S., Chakvattanatham, K. and Kiatkamjornwong, S. (2009), "Pretreatment of silk fabric surface with amino compounds for ink jet printing", *Progress in Organic Coating*, Vol. 64 No. 4, pp. 405-18.

Provost, J., Freche, M., Hees, U., Kluge, M. and Weiser, J. (2009), "Ink-textile interactions in ink jet printing – the role of pretreatments", available at: www.users.ecs.soton.ac.uk (accessed 1 January 2009).

Silverstein, R.M., Bassler, G.C. and Morrill, T.C. (1991), Spectrometric Identification of Organic Compounds, 5th ed., Wiley, Singapore, pp. 123-8.

Yuen, C.W.M., Ku, S.K.A., Kan, C.W. and Choi, P.S.R. (2007), "Enhancing textile ink-jet printing with chitosan", *Coloration Technology*, Vol. 123 No. 4, pp. 267-70.

About the authors



K. Chakvattanatham is currently a Technical Supervisor at Standard Can Company, Samutprakan, Thailand. She works in R&D and Customer Service Department and is involved in quality control assessment of packaging for food and paints. She obtained her BSc degree in Industrial Chemistry from King Mongkut's

Institute of Technology Ladkrabang, and her MSc degree in Printing Technology from the Department of Imaging and Printing Technology, Faculty of Science, Chulalongkorn University, in 2006. Her research expertise is in ink jet ink printing.



S. Phattanarudee is an Instructor at the Department of Imaging and Printing Technology of Chulalongkorn University, Bangkok, Thailand. She obtained her BSc degree in Materials Science from Chulalongkorn University, and her MSc and PhD degrees in Polymer Science and Engineering in 2003 from

Lehigh University, Bethlehem, Pennsylvania, USA. Her research areas are emulsion polymerization and coatings.





S. Kiatkamjornwong is currently a Full Professor of Polymer Science and Engineering at the Department of Imaging and Printing Technology, Faculty of Science, Chulalongkorn University, Bangkok, Thailand. She obtained her BSc and MSc degrees in Chemistry and Physical Chemistry, respectively, from the Faculty of

Science, Chulalongkorn University, and her PhD degree in Polymer Science and Engineering from Lehigh University, Bethlehem, Pennsylvania, USA, in 1983. Her research interests are in the areas of superabsorbent polymers, imbiber beads, modification of green polymers, digital printing and environment in polymers and printing. S. Kiatkamjornwong is the corresponding author and can be contacted at: ksuda@chula.ac.th



วารสารราชบัณฑิตยสถาน

วารสารราย ๓ เดือน

ที่ปรึกษา

ศาสตราจารย์ ดร.ปัญญา บริสุทธิ์นายกราชบัณฑิตยสถานดร.โสภา ชูพิกุลชัย ชปิลมันน์อุปนายกราชบัณฑิตยสถาน

ประธานคณะบรรณาธิการ

รองศาสตราจารย์อัศนีย์ ชูอรุณ ราชบัณฑิต

คณะบรรณาธิการ

รองศาสตราจารย์ ดร.ชยันต์ พิเชียรสุนทร ราชบัณฑิต ศาสตราจารย์ ดร.มงคล เดชนครินทร์ ราชบัณฑิต ศาสตราจารย์ ดร.ณัชชา พันธุ์เจริญ ภาคีสมาชิก ภาคีสมาชิก รองศาสตราจารย์ ดร.นิตยา กาญจนะวรรณ รองศาสตราจารย์ ดร.ผลิน ภู่จรูญ ภาคีสมาชิก ภาคีสมาชิก รองศาสตราจารย์มาลิทัต พรหมทัตตเวที รองศาสตราจารย์ ดร.วรวุฒิ หิรัญรักษ์ ภาคีสมาชิก ศาสตราจารย์ ดร.สมชาย วงศ์วิเศษ ภาคีสมาชิก

นางสาวกนกวลี ซูชัยยะ เลขาธิการราชบัณฑิตยสถาน

 นายประภาส แก้วสวรรค์
 ฝ่ายประสานงาน

 นางสาวศยามล แสงมณี
 ฝ่ายประสานงาน

 นางสาวสมทรง ศกุนตนาค
 ฝ่ายประสานงาน

กองบรรณาธิการ

นางสาวสุปัญญา ชมจินดาผู้อำนวยการกองวิทยาศาสตร์นางณัฐมาตย์ มูสิกะเจริญนักวรรณศิลป์ชำนาญการนายพรรษา ไทรงามนักวรรณศิลป์ชำนาญการนางสาวรัตติกาล ศรีอำไพนักวรรณศิลป์ชำนาญการนางสาวอารี พลดีนักวรรณศิลป์ชำนาญการนางสาวลักขณาวรรณ อนันธวัชนักวรรณศิลป์ปฏิบัติการ

ผู้จัดการ

นางนัยนา วราอัศวปติ เลขานุการกรม



The Journal of the Royal Institute of Thailand

Quarterly Journal

ADVISORY BOARD

Panya Borisutdhi President of the Royal Institute

Sobha Chupikulchai Spielmann Vice-President of the Royal Institute

EDITOR-IN-CHIEF

Asanee Chooarun FRI

EDITORIAL BOARD

FRI Chayan Picheansoonthon FRIMongkol Dejnakarintra **AFRI** Malithat Promathatavedi **AFRI** Natchar Pancharoen **AFRI** Nitaya Kanchanawan **AFRI** Palin Phoocharoon **AFRI** Somchai Wongwises **AFRI** Vorawoot Hirunruk

Kanokwalee Chuchaiya Secretary-General

Prapas KaewsawanCoordinatorSayamol SangmaneeCoordinatorSomsong SakuntanakCoordinator

DEPARTMENTAL STAFF

Supanya Chomchinda

Director of Science Division

Literateur, Professional Level

Nutthamard Musikacharoen

Literateur, Professional Level

Literateur, Practitioner Level

MANAGER

Naiyana Vara-asvapati Secretary



วารสารราชบัณฑิทยสถาน The Journal of the Royal Institute of Thailand

ปีที่ ๓๕ ฉบับที่ ๑ มกราคม-มีนาคม ๒๕๕๓		Volume 35 Number 1 January-March 2010
พรปีใหม่	ဝ	NEW YEAR'S GREETINGS
ประธานคณะบรรณาธิการแถลง	b	EDITOR-IN-CHIEF'S NOTE
สำนักธรรมศาสตร์และการเมือง		THE ACADEMY OF MORAL AND
		POLITICAL SCIENCES
มนุษยนิยมแนวปรัชญาจีน	m	The Chinese Humanism
สิทธิ์ บุตรอินทร์		Siddhi Butr-Indr
อัตถิภาวนิยม จิตวิทยาอัตถิภาวะ และการดำรงอยู่	ම ර	Existentialism, Existential Psychology and
ของมนุษย์ในปัจจุบัน		Current Human Existence
นพมาศ อุ้งพระ		Nopamas Oungphra
การก้าวเข้าสู่เศรษฐกิจคาร์บอนต่ำด้วยการซื้อขาย	۵o	Moving toward Low Carbon Economy through
คาร์บอนเครดิต		Carbon Credit Trading
วรวุฒิ หิรัญรักษ์	-	Vorawoot Hirunruk
สำนักวิทยาศาสตร์		THE ACADEMY OF SCIENCE
การใช้สารละลายเคมีปรับปรุงคุณภาพของดอกไม้	డం	Usage of Preservative Solutions Improves
หลังการเก็บเกี่ยว		Quality of Cut Flowers
		Saichol Ketsa
สายชล เกตุษา		Saichol Kelsa
สายชล เกตุษา		Saichol Ketsa

ปีที่ ๓๕ ฉบับที่ ๑ มกราคม-มีนาคม ๒๕๕๓

Volume 35 Number 1 January-March 2010

การพัฒนาแหล่งพลังงานทดแทนเพื่อผลิตไฟฟ้า ในประเทศ

ปรีดา วิบูลย์สวัสดิ์ วุฑฒิ พันธุมนาวิน

ระบบการจัดการพลังงานในอุตสาหกรรม

ศิริจันทร์ ทองประเสริฐ มานิจ ทองประเสริฐ

การวัด Bidirectional Reflectance Distribution Function และการจำลองแบบการสะท้อน ของผ้าไหม

สุดา เกียรติกำจรวงศ์ บุญยเกียรติ ฉายเทพประสิทธิ์ ชวาล คูร์พิพัฒน์

สำนักศิลปกรรม

ภาษารักของฌอร์ฌ ซ็อง

จินตนา ดำรงค์เลิศ

ตำนานเดี๋ยวขิมเพลงลาวแพน ทางของ หลวงประดิษฐไพเราะ (ศร ศิลปบรรเลง)

ชนก สาคริก

ลักษณะคำประพันธ์ของบทละครเรื่องโรเมโอ และจูเลียต พระราชนิพนธ์ในพระบาทสมเด็จ พระมงกุฎเกล้าเจ้าอยู่หัว

โชษิตา มณีใส

র্মাত Alternative Energy Sources for Electrical

Power Development of Thailand

Prida Wibulswas

Vutthi Bhanthumnavin

ನೆನ Energy Management System in Industry

Sirichan Thongprasert

Manit Thongprasert

೨೦೧ Measurement of Bidirectional Reflectance

Distribution Function and Reflectance

Modeling of Silk Fabrics

Suda Kiatkamjornwong Boonyakiat Chaitepprasith

Chawan Koopipat

THE ACADEMY OF ARTS

೧೧೮ George Sand's Language of Love

Chintana Damronglerd

ລາຍ The History of the Khim Solo of Lao Phaen:

Luang Praditpairoh (Sorn Silapabanleng)

Version

Chanok Sakrik

and The Versification of Romeo and Juliet written

by King Rama VI

Chosita Maneesai

รูปปั้นอาถรรพ์ใน La Vénus d' Ille ของปรอสแปร์ เมรีเม จุฑารัตน์ เบญจฤทธิ์ ปฏิทินฮิจเราะห์ในประเทศไทย ลอย ชุนพงษ์ทอง The Hijrah Calendar of Thailand Loy Chunpongtong นีลส์ โบร์ O๗๓ Niels Bohr	ปีที่ ๓๕ ฉบับที่ ๑ มกราคม-มีนาคม ๒๕๕๓		Volume 35 Number 1 January-March 2010
ของปรอสแปร์ เมรีเม	ปกิณกะ		MISCELLANEOUS
ปฏิทินฮิจเราะห์ในประเทศไทย ๑๖๕ The Hijrah Calendar of Thailand ลอย ชุนพงษ์ทอง Loy Chunpongtong นีลส์ โบร์	รูปปั้นอาถรรพ์ใน La Vénus d' Ille ของปรอสแปร์ เมรีเม จฑารัตน์ เบฌจถทธิ์	୦ଝଝ	of Prospère Mérimée
นีลส์ โบร์ ฉ๗๓ Niels Bohr	ปฏิทินฮิจเราะห์ในประเทศไทย	ඉවඳී	
		ഠസ്ന	



ปีที่ ๓๕ ฉบับที่ ๑ ม.ค.-มี.ค. ๒๕๕๓

การวัด Bidirectional Reflectance Distribution Function และการจำลอง แบบการสะท้อนแสงของผ้าไหม

สุดา เกียรติกำจรวงศ์**

ภาคีสมาชิก สำนักวิทยาศาสตร์ ราชบัณฑิตยสถาน

บุญยเกียรติ ฉายเทพประสิทธิ์^{**}

ชวาล คูร์พิพัฒน์**

บทคัดย่อ

ผ้าไหมเป็นสิ่งทอที่มีความมันวาวมากกว่าสิ่งทอประเภทอื่น เนื่องจากผ้าไหมมีลักษณะการสะท้อนแสง ที่มีความเฉพาะตัว ดังนั้น งานวิจัยนี้จึงศึกษาลักษณะการสะท้อนแสงของผ้าไหม โดยวัดค่าบีอาร์ดีเอฟ (BRDF, Bidirectional Reflectance Distribution Function) และนำเสนอแบบจำลองการสะท้อนแสงของพื้นผิวผ้าไหมที่ คำนึงถึงการสะท้อนของแสงฟุ้งและแสงกล้า โดยใช้วิธีการหาค่าความผิดพลาดกำลังสองน้อยสุด (least-square error) หาความสัมพันธ์ระหว่างค่าที่วัดกับแบบจำลอง เมื่อทดสอบแบบจำลองที่ได้พบว่า แบบจำลองที่นำเสนอนี้ มีความสัมพันธ์กับบีอาร์ดีเอฟที่วัดได้ของผ้าไหมมากกว่าแบบจำลองการสะท้อนแสงที่มีอยู่ทั่วไป ได้แก่ แบบจำลองการสะท้อนแสงของฟอง แบบจำลองการสะท้อนแสงของโอเรนและนายาร์ และแบบจำลองการ สะท้อนแสงของทอร์แรนซ์และสแปร์โรว์ ผู้วิจัยสามารถพยากรณ์ค่าการสะท้อนแสง วิเคราะห์ และอธิบาย ลักษณะการสะท้อนแสงของผ้าไหมได้จากแบบจำลองที่นำเสนอนี้

คำสำคัญ: บีอาร์ดีเอฟ, ผ้าไหม, แบบจำลองการสะท้อนแสง

คำนำ

ในยุคดิจิทัลที่การค้าขายใน
อินเทอร์เน็ตได้รับความนิยมอย่าง
กว้างขวาง ความสวยงามและเหมือน
จริงของสินค้าที่เป็นผ้าไหม หรือ
ผลิตภัณฑ์อื่นจากผ้าไหมเป็นสิ่งที่มีผล
ต่อการตัดสินใจซื้อของผู้บริโภค ความ
มันวาว (gloss) เป็นปัจจัยด้านคุณรูปที่
สำคัญอย่างหนึ่งที่เกิดจากสมบัติการ
สะท้อนแสงของผ้าไหม และมุมของ
แสงที่ตกกระทบและมุมมอง พื้นผิว
วัตถุใด ๆ สามารถเกิดการสะท้อนแสง
ใน ๑ ลักษณะ คือ การสะท้อนแสง
แบบฟุ้ง (diffuse reflection) การสะท้อน

แสงแบบกล้ำ (specular reflection) และ การสะท้อนแสงแบบผสมระหว่างแสง ฟุ้งกับแสงกล้ำ (mixed reflection) [Wyszecki and Stiles, 2000] ดังรูปที่ ๑ ปรกติพื้นผิววัตถุส่วนใหญ่มีการ สะท้อนแสงแบบผสม วัตถุที่มีความ มันวาวมากจะสะท้อนแสงกล้าออกมา มาก วัตถที่มีผิวด้านหรือผิวไม่เรียบจะ







นเบบฟุ้ง แสงแร

รูปที่ ๑ ลักษณะการสะท้อนแสง แบบฟุ้ง แบบกล้า และแบบผสม สะท้อนแสงฟุ้งออกมามาก ลักษณะ การสะท้อนแสงเหล่านี้ ทำให้มีผู้สร้าง แบบจำลองการสะท้อนแสงของพื้นผิว

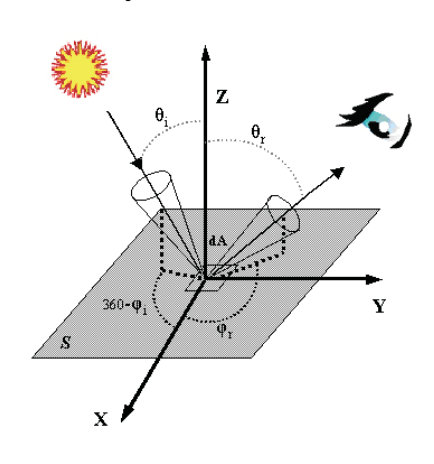
^{*} บทความนี้ปรับปรุงจากการบรรยายผลงานทางวิชาการในที่ประชุมสำนักวิทยาศาสตร์ เมื่อวันที่ ๑๗ กุมภาพันธ์ พ.ศ. ๒๕๕๓

^{**} ภาควิชาวิทยาศาสตร์ทางภาพถ่ายและเทคโนโลยีทางการพิมพ์ คณะวิทยาศาสตร์ จุฬาลงกรณ์มหาวิทยาลัย ถนนพญาไท แขวงวังใหม่ เขตปทุมวัน กรุงเทพฯ ๑๐๓๓๐



วัตถุงื้นมา เพื่อใช้พยากรณ์ค่าการ สะท้อนแสงของพื้นผิววัตถุและได้ นำไปใช้ในโปรแกรมสำหรับสร้างภาพ สามมิติในคอมพิวเตอร์ เช่น ภาพแบบ จำลองสินค้า ภาพการ์ ตูนแอนิเมชัน ภาพยนตร์ ความเหมือนจริงของรูปที่ สร้างขึ้นด้วยโปรแกรมเหล่านี้ขึ้นอยู่กับ ความสามารถในการจำลองค่าการ สะท้อนแสงของแบบจำลอง แบบจำลอง ชนิดหนึ่งอาจเหมาะกับวัตถุที่มีลักษณะ ผิวอย่างหนึ่ง แต่อาจไม่เหมาะกับวัตถุที่ มีพื้นผิวแตกต่างออกไป

Bidirectional Reflectance Distribution Function (BRDF) เป็นฟังก์ชันการ สะท้อนแสงในทิศทางต่าง ๆ ของพื้นผิว วัตถุ เมื่อเปลี่ยนมุมตกกระทบของแสง แบบจำลอง โดยทั่วไปกำหนดให้การ สะท้อนแสงรวมเป็นผลรวมระหว่าง การสะท้อนแสงแบบฟุ้งกับการสะท้อน แสงแบบกล้า ซึ่งมีตัวแปรเป็นมุมตก กระทบและมุมรับภาพ [Dana et al., 1999] ดังรูปที่ ๒



รูปที่ 🖢 BRDF ของพื้นผิววัตถุใด ๆ

สมการรูปแบบทั่วไปของ BRDF สามารถเขียนได้ดังสมการที่ ๑

$$L_{r} = k_{d}L_{d} + k_{s}L_{s} \tag{6}$$

โดยที่

- L. คือ การสะท้อนแสงของวัตถุ
- L_d คือ การสะท้อนแสงแบบฟุ้ง (diffuse reflection)
- $L_{_{\rm s}}$ คือ การสะท้อนแสงแบบกล้า (specular reflection)
- k_d คือ สัมประสิทธิ์ของการสะท้อน แสงแบบฟุ้ง (diffuse components reflection coefficient)

k_s คือ สัมประสิทธิ์ของการ สะท้อนแสงแบบแสงกล้า (specular components reflection coefficient)

$$k_d + k_s = 0$$

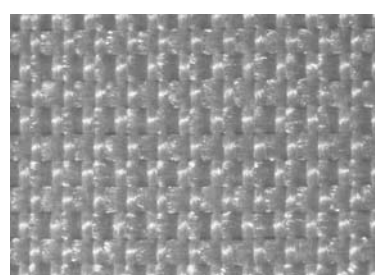
แบบจำลองการสะท้อนแสงของ
พื้นผิววัตถุมีอยู่ด้วยกันหลายแบบ ซึ่ง
สามารถพยากรณ์การสะท้อนแสง
แบบฟุ้งและแบบกล้าที่แตกต่างกัน
แบบจำลองพื้นฐานที่มองพื้นผิววัตถุมี
การสะท้อนแสงฟุ้งแบบอุดมคติคือ
แบบจำลองการสะท้อนแสงแบบ
แลมเบอร์เทียน (Lambertian reflection
model) [Dana et al., 1999] ส่วนแบบ
จำลองการสะท้อนแสงของโอเรนและ
นายาร์ (Oren and Nayar reflection
model) [Oren and Nayar, 1995] สามารถ
พยากรณ์การสะท้อนแสงแบบฟุ้งได้
แม่นยำมาก เพราะรวมลักษณะความ
ขรุขระของพื้นผิววัสคุไว้ในแบบจำลอง

ด้วย แบบจำลองที่พยากรณ์การสะท้อน แสงแบบกล้า ได้แก่ แบบจำลองของ ทอร์แรนซ์และสแปร์โรว์ [Torrance and Sparrow], แบบจำลองการสะท้อน แสงของคุก-ทอร์แรนซ์ (Cook-Torrance reflection model) [Dana et al., 1999] และแบบจำลองการสะท้อนแสงของ บลินน์ (Blinn reflection model) [Blinn, 1977] แบบจำลองแต่ละแบบได้คำนึง ถึงปริมาณแสงสะท้อนแบบกล้าที่รวม ปัจจัยด้านความขรุขระของพื้นผิว เอาไว้ด้วย และแบบจำลองที่เหมาะสม สำหรับพยากรณ์การสะท้อนแสงแบบ ผสม ก็คือ แบบจำลองการสะท้อนแสง ของฟอง (Phong reflection model) [Phong, 1975] ซึ่งเหมาะสมกับพื้นผิว เรียบ ๆ เช่น พลาสติก ในขณะที่ แบบจำลองการสะท้อนแสงของวาร์ด (Ward reflection model) [Ward, 1992] และแอชิกมิน-เชอร์ลีย์ (Ashikmin-Shirley reflection model) [Ashikmin and Shirley, 2000] ได้ปรับปรุงแบบจำลอง การสะท้อนแสงของฟอง (Phong)ให้ เหมาะสมมากขึ้นกับลักษณะพื้นผิวที่ หลากหลายและไม่สม่ำเสมอ แต่ แบบจำลองที่กล่าวมาข้างต้นยังไม่มี แบบใคที่สร้างขึ้นเพื่อใช้กับการ สะท้อนแสงของพื้นผิวผ้าใหม โดยเฉพาะ ดังนั้น งานวิจัยนี้จึงศึกษา ลักษณะการสะท้อนแสงของพื้นผิวผ้า ใหม โดยการวัดค่าบีอาร์ดีเอฟและนำ ค่าที่วัดได้มาสร้างเป็นแบบจำลองการ สะท้อนแสงที่สัมพันธ์กับค่าการ สะท้อนแสงของพื้นผิวผ้าใหม

ปีที่ ๓๕ ฉบับที่ ๑ ม.ค.-มี.ค. ๒๕๕๓

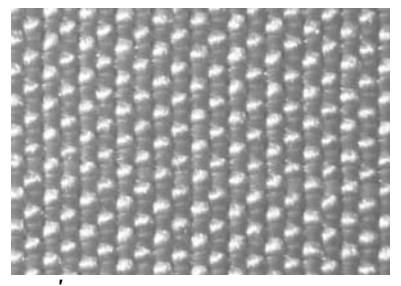
อุปกรณ์และวิธีการ

การทดลองนี้ได้ใช้ผ้าใหมสีขาวที่ ทอด้วยลายขัด ๑ ตัวอย่าง ผ้าใหม ตัวอย่างที่ ๑ ใช้เส้นไหม ๒ เส้นในการ ทอและเส้นใหมมาจากร้านใหมไทย คอลเล็กชัน ผ้าใหมตัวอย่างที่ ๒ และ ตัวอย่างที่ ๓ ใช้เส้นใหม ๒ และ ๔ เส้นในการทอและเส้นใหมมาจากร้าน จิม ทอป์มสัน ซึ่งมีลักษณะพื้นผิวตาม รูปที่ ๓ ถึง รูปที่ ๕ ตามลำดับ งานวิจัย นี้ได้แบ่งการทดลองออกเป็น 💩 ขั้นตอน ได้แก่ การทคลองตอนที่ ๑ เป็นการวัดค่าบีอาร์ดีเอฟของผ้าใหม ทั้ง ๓ ตัวอย่าง ด้วยเครื่องโกนิโอ สเปกโทรโฟโตมิเตอร์ (ยี่ห้อ มุราคามิ รุ่น จีเอสพี-๒๕ ประเทศญี่ปุ่น) ซึ่งได้ วัดค่าที่ศนย์การวิจัยฟรอนเทียร์เมดิคัล เกนจิเนียริง (Research Center for Frontier Medical Engineering) แห่งมหาวิทยาลัย ชิบะ ประเทศญี่ปุ่น โดยใช้มุมของ แหล่งกำเนิดแสง ที่ ๐, -๑๕, -๓๐, -๔๕, -bo และ -๗๕ องศา และใช้มมรับภาพ ମ୍ପି -ଟାଝ, -๖୦, -๔๕, -๓୦, -๑๕, ୦, ๑๕, ๑๐, ๔๕, ๖๐ และ ๗๕ องศา ตามลำดับ แล้วจึงนำค่าบีอาร์ดีเอฟที่ วัดได้มา เขียนกราฟเชิงขั้ว เพื่อทำให้สามารถ วิเคราะห์ลักษณะการสะท้อนแสงของ พื้นผิวผ้าใหม พร้อมทั้งสามารถหา ลักษณะเฉพาะตัวของการสะท้อนแสง ของผ้าใหมได้ ผู้วิจัยได้ทดลองตอนที่ ๒ ซึ่งเป็นการนำเสนอแบบจำลองการ สะท้อนแสงของพื้นผิวผ้าใหม โดยได้ ปรับปรุงจากแบบจำลองการสะท้อน แสงของฟอง และทดสอบแบบจำลอง ด้วยการหาความผิดพลาดที่น้อยที่สุด จากการเปรียบเทียบค่าที่คำนวณได้จาก แบบจำลองการสะท้อนแสงที่นำเสนอ กับค่าบีอาร์ดีเอฟที่วัดได้จากผ้าใหม และความผิดพลาดจากการเปรียบเทียบ ค่าที่คำนวณได้จากแบบจำลองการ สะท้อนแสงที่ใช้อยู่โดยทั่วไป ได้แก่ แบบจำลองการสะท้อนแสงของฟอง แบบจำลองการสะท้อนแสงของโอเรน และนายาร์ แบบจำลองการสะท้อน แสงของวาร์ด และแบบจำลองการ สะท้อนแสงของแอชิกมินและเชอร์ลีย์ เริ่มแรกผู้วิจัยได้หาค่าคงตัวใน แบบจำลองต่าง ๆ ที่สัมพันธ์กับ ลักษณะการสะท้อนแสงของผ้าใหม โดยใช้วิธีหาค่าความผิดพลาดกำลังสอง น้อยสุด (least-square error) จึงคำนวณ ค่าการสะท้อนแสงจากแบบจำลองที่มี ค่าคงตัวครบ แล้วจึงนำค่าที่คำนวณ ได้มาเปรียบเทียบหาความผิดพลาดกับ ค่าการสะท้อนแสงจากผ้าใหม โดยใช้ วิธีการหาค่ารากที่สองของกำลังสอง เนลี่ย (root-mean-square error) เพื่อหา แบบจำลองการสะท้อนแสงที่สัมพันธ์ กับค่าการสะท้อนแสงของผ้าใหมมาก

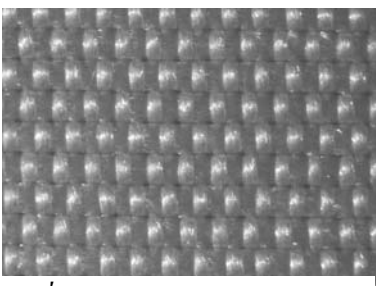


รูปที่ ๓ ลักษณะพื้นผิวของผ้าไหม ตัวอย่างที่ ๑

ที่สุด



รูปที่ ๔ ลักษณะพื้นผิวของผ้าไหม ตัวอย่างที่ ๒



รูปที่ ๕ ลักษณะพื้นผิวของผ้าไหม ตัวอย่างที่ ๑

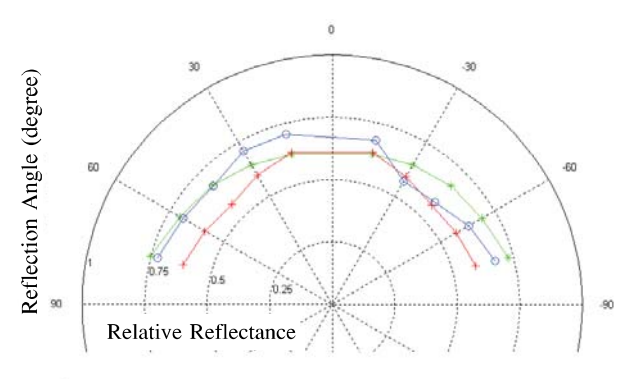
ผลการทดลองและวิจารณ์ ตอนที่ ๑ การวัดค่าบีอาร์ดีเอฟของ ผ้าใหม

ค่าบีอาร์ดีเอฟของผ้าใหมสีขาว ๓ ตัวอย่าง สามารถเขียนเส้นโค้งใน ระบบพิกัดเชิงขั้ว ได้ตามรูปที่ ๖-๑๑ โดยใช้มุมของแหล่งกำเนิดแสง ๐, -๑๕, -๓๐, -๔๕, -๖๐ และ -๗๕ องศา ตามลำดับ เส้นโค้งทั้ง ๖ เส้นนี้ เส้นสี แดง (+) คือ ค่าบีอาร์ดีเอฟของผ้าใหม ตัวอย่างที่ ๑ เส้นสีเขียว (*) คือ ค่า บีอาร์ดีเอฟของผ้าใหมตัวอย่างที่ ๒ และเส้นสีน้ำเงิน (๐) คือ ค่าบีอาร์ดีเอฟของผ้าใหมตัวอย่างที่ ๒ ของผ้าใหมตัวอย่างที่ ๑



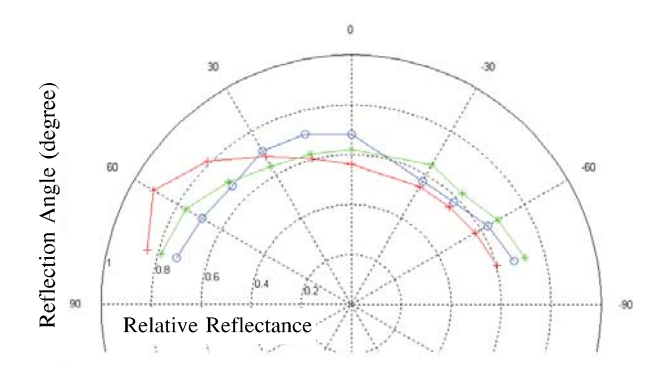
เส้นโค้งของค่าบีอาร์ดีเอฟของผ้า ใหมแสดงให้เห็นลักษณะการสะท้อน แสงของพื้นผิวผ้าใหม่ซึ่งแสงกระจาย ตัวออกรอบทิศทาง และเป็นสมบัติของ การสะท้อนแสงแบบฟุ้ง การกระจายตัว ของค่าการสะท้อนแสงยังมีแนวโน้มที่ เบ้ในทิศทางเดียวกันกับทิศทางของ แหล่งกำเนิดแสง แสดงให้เห็นว่า ค่าการ สะท้อนแสงกระจายตัวไปหนาแน่นใน ทิศทางตรงข้ามกับทิศทางของแหล่ง กำเนิดแสง ซึ่งเป็นทิศทางของแสง สะท้อนแบบกล้า ดังนั้น จึงสรุปได้ว่า แสงที่สะท้อนออกจากพื้นผิวของผ้า ใหม่มีการสะท้อนแสงแบบผสม

อย่างไรก็ตาม เมื่อพิจารณาเส้นโค้ง บีอาร์ดีเอฟของพื้นผิวผ้าไหมในส่วนที่ เป็นแสงฟุ้ง พบว่าเป็นการสะท้อนแบบ ฟุ้งที่ไม่เป็นอุดมคติ เพราะแสงสะท้อน มีความเข้มไม่เท่ากันในแต่ละทิศทาง และเมื่อพิจารณาในส่วนที่เป็นแสงกล้า จะพบว่า มุมของแสงสะท้อนที่มีความ เข้มสูงสุดไม่เป็นมุมตรงข้ามกับมุมของ แหล่งกำเนิดแสง แต่เกิดการเลื่อนตัวไป ในทิศทางอื่น ซึ่งแสดงให้เห็นว่า แสงที่

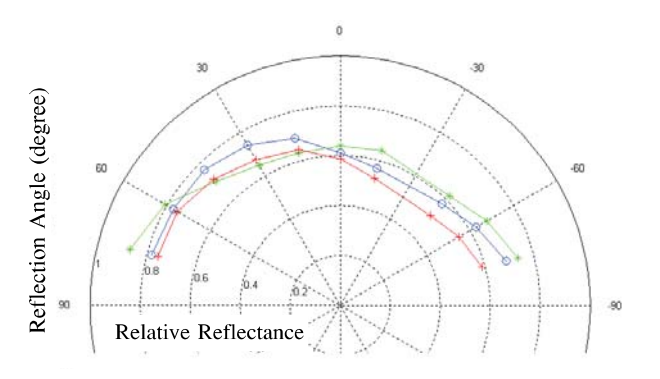


รูปที่ ๖ ค่าบีอาร์ดีเอฟของผ้าใหมตัวอย่างที่ ๑(+) ตัวอย่างที่ ๒(*) และตัวอย่างที่ ๓(o) เมื่อใช้มุมตก กระทบ o องศา

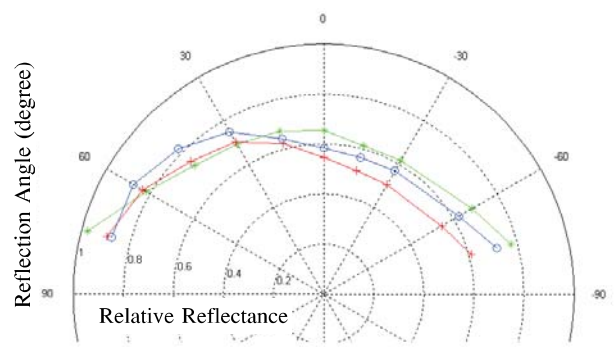
สะท้อนจากพื้นผิวผ้าใหมเกิด offspecular



รูปที่ ๗ ค่าบีอาร์ดีเอฟของผ้าใหมตัวอย่างที่ ๑(+) ตัวอย่างที่ ๒(*) และตัวอย่างที่ ๑(o) เมื่อใช้มุมตกกระทบ -๑๕ องศา



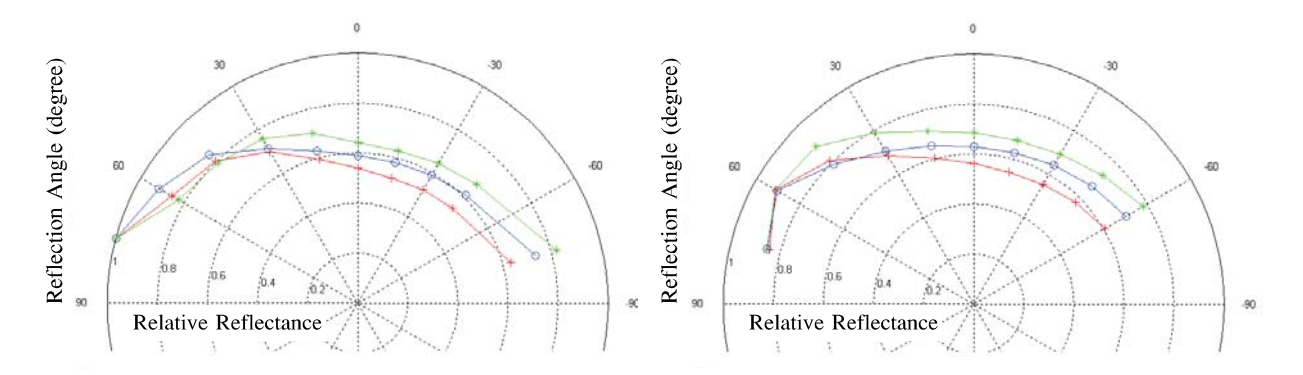
รูปที่ ๘ ค่าบีอาร์คีเอฟของผ้าใหมตัวอย่างที่ ๑(+) ตัวอย่างที่ ๒(*) และตัวอย่างที่ ๓(๐) เมื่อใช้มุมตกกระทบ -๓๐ องศา



รูปที่ ธ ค่าบีอาร์ดีเอฟของผ้าใหมตัวอย่างที่ ๑(+) ตัวอย่างที่ ๒(*) และตัวอย่างที่ ๓(o) เมื่อใช้มุมตก กระทบ -๔๕ องศา



ปีที่ ๓๕ ฉบับที่ ๑ ม.ค.-มี.ค. ๒๕๕๓



รูปที่ ๑๐ ค่าบีอาร์ดีเอฟของผ้าใหมตัวอย่างที่ ๑(+) ตัวอย่างที่ ๒(*) และตัวอย่างที่ ๓(o) เมื่อใช้มุมตก กระทบ -๖๐ องศา

รูปที่ ๑๑ ค่าบีอาร์คีเอฟของผ้าใหมตัวอย่างที่ ๑(+) ตัวอย่างที่ ๒(*) และตัวอย่างที่ ๑(o) เมื่อใช้มุมตก กระทบ -๘๕ องศา

ตอนที่ ๒ การเสนอแบบจำลอง การสะท้อนแสงและการทดสอบ แบบจำลอง

เนื่องจากสมบัติการสะท้อนแสงของผ้าใหมเป็นการสะท้อนแสงแบบผสม ผู้วิจัยจึงได้ปรับปรุงแบบจำลองการสะท้อนแสงของฟอง ในส่วนที่เป็นการสะท้อนแสงแบบฟุ้งและแบบกล้า โดยเพิ่มพารามิเตอร์ α และ β เพื่อปรับความกว้างของกรวยแสง และเพิ่มพารามิเตอร์ θ_{off} และ ϕ_{off} สำหรับปรับมุมสะท้อนแสงแบบ off-specular ดังแสดงในสมการที่ ๒

lpha คือ ค่าควบคุมความกว้างของกรวย แสงฟุ้ง (diffuse lobe)

 $oldsymbol{eta}$ คือ ค่าควบคุมความกว้างของกรวย แสงกล้ำ (specular lobe)

 $heta_r$ คือ มุมรับภาพในแนวมุมเงย (elevation)

 $heta_i$ คือ มุมของแหล่งกำเนิดแสงในแนว มุมเงย (elevation)

 $heta_{off}$ คือ มุม off-specular ในแนวมุมเงย (elevation)

 $oldsymbol{\phi}_r$ คือ มุมรับภาพในแนวมุมกวาด (azimuth)

 ϕ_i คือ มุมของแหล่งกำเนิดแสงในแนว

กล่าวมาข้างต้น มาเปรียบเทียบกับค่า บีอาร์ดีเอฟที่วัดจากผ้าใหม แล้ว คำนวณหาความผิดพลาดโดยใช้วิธีหา รากที่สองของกำลังสองเฉลี่ย (RMS) ซึ่งแสดงผลในตารางที่ ๑

เมื่อพิจารณาผลจากตารางที่ ๑ แล้ว จะเห็นว่า แบบจำลองการสะท้อนแสง ที่นำเสนอนี้ให้ความผิดพลาดน้อยกว่า แบบจำลองอื่น เช่น ผ้าไหมตัวอย่างที่ ๓ ใช้มุมของแหล่งกำเนิดแสง -๖๐ องศา มีค่า RMS ของแบบจำลองขึ่ง เสนออยู่ที่ ๐.๐๒๑๔ แบบจำลองของ ฟองมีค่าอยู่ที่ ๐.๐๒๑๘ แบบจำลองของ

$$L(\theta_i, \theta_r, \phi_i, \phi_r) = k_d \cos^{\alpha}(\theta_r, \phi_r) + k_s \cos^{\beta}[\theta_r + (\theta_i - \theta_{off}), \phi_r + (\phi_i - \phi_{off})]$$
 (b)

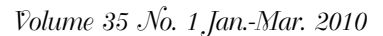
โดยที่

L คือ ค่าการสะท้อนแสงของผ้าใหม $k_{\scriptscriptstyle A}$ คือ สัมประสิทธิ์ความเข้มแสงของ แสงฟุ้ง

 k_s คือ สัมประสิทธิ์ความเข้มแสงของ แสงกล้ำ มุมกวาด (azimuth)

 $oldsymbol{\phi}_{o\!f\!f}$ คือ มุม off-specular ในแนวมุม กวาด (azimuth)

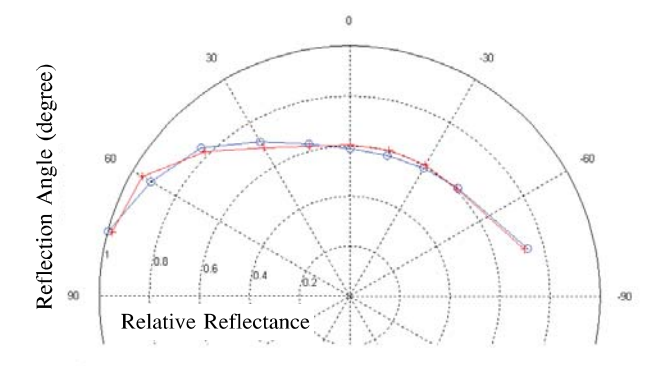
ผู้วิจัยได้ทคสอบแบบจำลอง โคยนำค่าบีอาร์คีเอฟที่คำนวณจาก แบบจำลองการสะท้อนแสงต่าง ๆ ที่ โอเรนและนายาร์อยู่ที่ ๐.๑๖๑๐ แบบจำลองของวาร์ด อยู่ที่ ๐.๑๐๓๖ และแบบจำลองของแอชิกมิน อยู่ที่ ๐.๑๐๓๖ ๐.๐๘๔๓ ซึ่งแสดงว่า ค่าบีอาร์ดีเอฟที่ ได้จากแบบจำลองการสะท้อนแสงที่ นำเสนอนี้สัมพันธ์กับค่าบีอาร์ดีเอฟ ของผ้าใหมมากกว่าแบบจำลองการ



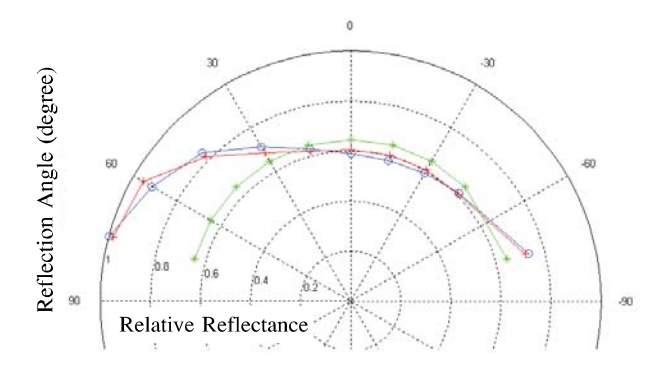


สะท้อนแสงอื่น และเมื่อนำมาเขียน เส้นโค้งเชิงขั้วจะเห็นว่า เส้นโค้งของ ค่าบือาร์ดีเอฟที่ได้จากแบบจำลองที่

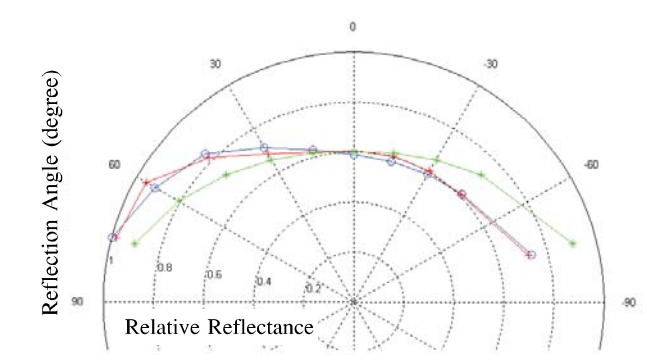
นำเสนอนี้ใกล้เคียงกับเส้นโค้งของ อื่น ดังแสดงใน รูปที่ ๑๒-๑๖ บือาร์ดีเอฟที่วัดจากผ้าใหม มากกว่าเส้น โค้งของค่าบีอาร์ดีเอฟจากแบบจำลอง



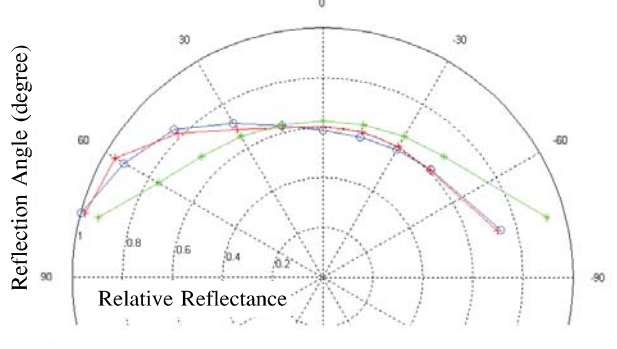
รูปที่ ๑๒ เส้น โค้งเปรียบเทียบระหว่างค่าการสะท้อน แสงที่วัดจากผ้าใหม(0) กับค่าการสะท้อนแสงที่ คำนวณจากแบบจำลองที่นำเสนอของผ้า ใหมตัวอย่าง ที่ ๓ ที่มุมตกกระทบ -๖๐ องศา



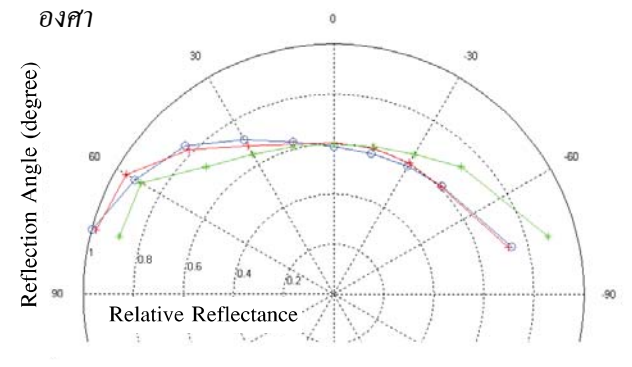
รูปที่ ๑๓ เส้น โค้งเปรียบเทียบระหว่างค่าการสะท้อนแสง ที่วัดจากผ้าใหม (0) กับค่าการสะท้อนแสงที่คำนวณจาก แบบจำลองที่นำเสนอ (+) และแบบจำลองฟอง (*) ของ ผ้าใหมตัวอย่างที่ ๓ ที่มุมตกกระทบ -๖๐ องศา



รูปที่ ๑๔ เส้น โค้งเปรียบเทียบระหว่างค่าการสะท้อนแสง ที่วัดจากผ้าใหม (0) กับค่าการสะท้อนแสงที่คำนวณจาก แบบจำลองที่นำเสนอ (+) และ แบบจำลองโอเรนและ นายาร์ (*) ของผ้าใหมตัวอย่างที่ ๓ ที่มุมตกกระทบ -๖๐



รูปที่ ๑๕ เส้น โค้งเปรียบเทียบระหว่างค่าการสะท้อนแสงที่ วัดจากผ้าใหม (o) กับค่าการสะท้อนแสงที่คำนวณจาก แบบจำลองที่นำเสนอ (+) และแบบจำลองวาร์ค (*) ของผ้า ใหมตัวอย่างที่ ๓ ที่มุมตกกระทบ -๖๐ องศา



รุปที่ ๑๖ เส้น โค้งเปรียบเทียบระหว่างค่าการสะท้อนแสงที่ วัดจากผ้าใหม (0) กับค่าการสะท้อนแสงที่คำนวณจากแบบ จำลองที่นำเสนอ (+) และ แบบจำลองแอชิกมินและเชอร์ลีย์ (*) ของผ้าใหมตัวอย่างที่ ๓ ที่มุมตกกระทบ -๖๐ องศา



ปีที่ ๓๕ ฉบับที่ ๑ ม.ค.-มี.ค. ๒๕๕๓

ตารางที่ ๑ ค่า RMS ของค่าการสะท้อนแสงจากแบบจำลองต่าง ๆ

	มุมตกกระทบ	ค่า RMS ของ							
ตัวอย่างที่	(องศา)	แบบจำลอง ที่นำเสนอ	แบบจำลอง ของฟอง	แบบจำลอง ของ โอเรนและ นายาร์	แบบจำลอง ของวาร์ด	แบบจำลอง ของ แอชิกมินและ เชอร์ลีย์			
	0	ഠ.ഠര്ക്ക	0.0මම්ක	୦.୦୭୭ଞ	୦.୦๒๒๕	ಂ.ಂಠುಠನ			
	-0&	ഠ.റെയെ	ට.බෛ ෆ	୦.୭๔๒๔	0.මෙಜීක	୦.୭୯୯			
	- ၈၀	ಂ.೦೯೬	ಂ.ಂಪಠಡ	೦.೦೯೦៦	ಂ.ಂದರಿದ	ം.ം പ്രിയ			
9	-૯હ	ಂ.ಂಠಿಕಾ	0.0000	୦.୧୩୧୯	o.മെന്	(n 600.0			
	-òo	ಂ.೦೯೯೦	୦.୭୭୭୭	ಂ.ಇಜಿಕಡ	ഠ.യെര്ത	ഠ.ംൈ			
	-හය	೦.೦೦& ๔	୦.୦୪ (ଜଣ)	ට.ගෙනරේ	ಂ.ಂಕಣಕ	ಂ.೦೦೦ ಜ			
	0	೦.೦ಡ೦೯	୦.୦୦ଖାଲ	೦.೦៤೦೯	୦.୦๒๙๓	ಂ.ಂಡಂಡೆ			
l o .	-0&	ට . ට ෆටෆ)	େଠାଇଟେ	ಂ.ಂದಣಿಕ	೦.೦ಡಡಿ	ಂ.ಂಜಿಡಂ			
	- ၈၀	0.0000	ಂ.ಂಡದಣಿ	ಂ.೧೯೬೮	o.050 &	૦.૦૪૬ૡ			
	-៤៥	ං.ටම්ගය්	ಂ.೦ಶಿಂಜೆ	ಂ.ಊಕಡ	0.05៤๓	୦.୦୩៦ଝ			
	- 50	୦.୦୩୯୯	୦.୦๕๗๗	ಂ.೩೭೦೬	0.05&5	രിയിറോ.ഠ			
	-හය	ට.ටමගේ	૦.૦&૭૦	ಂ.ඉද ೯೬	ಂ.ಂಶಿ&ನ	ಂ.ಂದ೯೦೬			
	0	ಂ.ಂಡದಣ	ં.૦૦ હૈંદ્ર	ಂ.ಂಡಕಕ	ಂ.ಂಡದಂ	૦.૦૯૬૯			
	-0&	०.०๔๔๔	০.০৫.১০	୦.୦୩၈၈	ಂ.ಂಡದಂ	ට.ට໕ටක			
ണ -	- ၈၀	୦.୦୭୦୧	୦.୦୩୦୩	o.oo& n)	ം.ംഎത്രജ	ಂ.ಾನ&			
	-૯&	ಂ.೦೯೬೪	୦.୦୪୭୭	୦.୭୩୦୩	೦.೧೦ ೬ ೬	ಂ.ಂಡಣಾ			
	-òo	ാ.ായരെ	ಂ.೦ಕೂದ	၀.၈၃၈၀	୦.୭୦୩៦	ಂ.ಂನಡಣ			
	-ଜାଝ	ಂ.ಂಜನ	ಂ.೦៥៥៦	೦.೯೯೯	ಂ.ಂಶಿಜೆದ	o . ૦૬૯૬			

สรุป

งานวิจัยนี้ได้วัดและวิเคราะห์ ลักษณะการสะท้อนแสงของพื้นผิวผ้า ไหม พบว่า ผ้าไหมมีการสะท้อนแสง แบบผสม และมีสมบัติพิเศษที่สะท้อน แสงกล้าแบบ off-specular ผู้วิจัยได้ สร้างแบบจำลองสำหรับทดสอบการ สะท้อนแสงของผ้าใหม่ขึ้น โดย ปรับปรุงจากแบบจำลองการสะท้อน แสงของฟองและได้เปรียบเทียบกับ แบบจำลองอื่น ๆ อย่างไรก็ตาม แบบจำลองที่นำเสนอนี้ได้มาจากการ วัดบีอาร์ดีเอฟเท่านั้น ดังนั้น การศึกษา เรื่องอิทธิพลของโครงสร้างผ้าใหม สมบัติเฉพาะของเส้นด้ายใหม จะช่วย ให้สร้างแบบจำลองการสะท้อนแสงได้ ถูกต้องและแม่นยำมากยิ่งขึ้น ซึ่งเป็น งานวิจัยในแนวลึกต่อไป



กิตติกรรมประกาศ

คณะผู้นิพนธ์ขอขอบพระคุณฝ่าย วิชาการ สำนักงานกองทนสนับสนน การวิจัย (สกว.) และสำนักงานคณะ กรรมการการอดมศึกษา (สกอ.) ที่ให้ การสนับสนุนการวิจัยเรื่องนี้ ผ่าน โครงการวิจัยเมธิวิจัยอาวุโส สกว. รหัสโครงการ RTA๕๐๘๐๐๐๔ นอกจากนี้ คณะวิจัยขอบคุณศูนย์การ วิจัยฟรอนเทียร์เมดิคัลเอนจิเนียริง (Research Center for Frontier Medical แห่งมหาวิทยาลัยชิบะ Engineering) ประเทศญี่ปุ่น ที่เอื้อเฟื้อให้ใช้อุปกรณ์ วิจัย ขอบพระคุณภาควิชาวิทยาศาสตร์ ทางภาพถ่ายและเทคโนโลยีทางการ พิมพ์ คณะวิทยาศาสตร์ จฬาลงกรณ์ มหาวิทยาลัย ที่เอื้อเฟื้อค่าใช้ก่ายและค่า เดินทางระหว่างประเทศ ซึ่งทำให้ สามารถทำงานวิจัยบางส่วนที่ประเทศ ญี่ปุ่น

เอกสารอ้างอิง

Ashikmin, M., and Shirley, P. 2000.

Anisotropic Phong BRDF Model. Journal of Graphic Tools, 5(2):25-32.

Blinn, J.F. 1977. Models of Light Reflection for Computer Synthesized Pictures.

International Conference on Computer Graphics and Interactive Techniques, Proceedings of the 4th annual conference on Computer Graphics and Interactive Techniques, pp. 192-198.

Dana, K.J., Ginneken, B.V., Nayar, S.K. and Koenderink, J.J. 1999. Reflectance and

Texture of Real-World Surfaces. ACM Transactions on Graphics, 18(1):1-34.

Oren, M., and Nayar, S.K. 1995.

Generalization of Lambert's Reflectance

Model. Computer Vision, 14(3):227-251.

Phong, B.T. 1975. Illumination for Computer Generated Pictures. Communications of the ACM, 18(6):311-317.

Torrance, K.E. and Sparrow, E.M. 1967.

Theory for off-specular Reflection from Roughened Surface. Optical Society of America, 57(9):1105-1114.

Ward, G.J. 1992. Measuring and Modeling Anisotropic Reflection. Computer Graphics, 26(2):265-272.

Wyszecki, G., and Stiles, W.S. 2000. Color Science. 2nd ed., Wilky Classic, pp. 51-52.

ปีที่ ๓๕ ฉบับที่ ๑ ม.ค.-มี.ค. ๒๕๕๓

Abstract

Measurement of Bidirectional Reflectance Distribution Function and Reflectance Modeling of Silk Fabrics

Suda Kiatkamjornwong

Associate Fellow of the Academy of Science, The Royal Institute, Thailand

Department of Imaging and Printing Technology, Faculty of Science, Chulalongkorn

University, Bangkok 10330, Thailand

Boonyakiat Chaitepprasith,

Chawan Koopipat

Department of Imaging and Printing Technology, Faculty of Science, Chulalongkorn University, Bangkok 10330, Thailand

Silk fabric is a fabric in which its gloss is perceived differently in comparison with other fabrics due to its specific reflectance. This research measured a Bidirectional Reflectance Distribution Function (BRDF) of three types of silk fabric having different weaving styles in conjunction with reflectance characteristics. Besides the measured BRDFs of the silk fabrics, its reflection model was then proposed. The proposed reflection model incorporates a specular reflection lobe and diffuse reflection lobe. The proposed model and the measured BRDFs of the three silk fabrics were fitted by the least-square error method. The measured BRDFs of the silk fabric were also fitted with Phong reflection model, Oren-Nayar reflection model and Torrance-Sparrow reflection. It was found that the proposed model fitted better with the measured BRDF than did the general models of Phong-reflection, Oren-Nayar reflection, and Torrance-reflection. The proposed model can thus be used to approximate, analyze and elucidate the characteristics of light reflection of the three silk fabrics.

Key words: BRDF, silk fabrics, reflection model

บทความที่ Under revision หรือ Under review

Journal of Applied Polymer Science

SYNTHESES, CHARACTERIZATION AND ANTIBACTERIAL ACTIVITY OF CHITOSAN GRAFTED HYDROGELS AND ASSOCIATED MICA-CONTAINING NANOCOMPOSITE HYDROGELS

Journal:	Journal of Applied Polymer Science
Manuscript ID:	Draft
Wiley - Manuscript type:	Research Article
Keywords:	swelling, hydrogels, nanocomposites, organoclay, biocompatibility

SCHOLARONE™ Manuscripts

SYNTHESES, CHARACTERIZATION AND ANTIBACTERIAL ACTIVITY OF CHITOSAN GRAFTED HYDROGELS AND ASSOCIATED MICACONTAINING NANOCOMPOSITE HYDROGELS

Supaporn Noppakundilograt¹, Kittichai Sonjaipanich², Nuttha Thongchul³ and Suda Kiatkamjornwong^{1*}

¹Department of Printing and Imaging Technology, Faculty of Science, Chulalongkorn University, Bangkok, 10330, Thailand. ¹E-mail: *supaporn.n@chula.ac.th*; *1corresponding author; ^{1*}e-mail: *ksuda@chula.ac.th*; Tel.: +66-2218-5587.

²Program of Petrochemistry and Polymer Science, Faculty of Science, Chulalongkorn University, Bangkok, 10330, Thailand. ²E-mail: kittichai_sonjai@hotmail.com.

³Institute of Biotechnology and Genetic Engineering, Chulalongkorn University, Bangkok, 10330, Thailand. ³E-mail: Nuttha.T@chula.ac.th.

SYNTHESES, CHARACTERIZATION AND ANTIBACTERIAL ACTIVITY OF CHITOSAN GRAFTED HYDROGELS AND ASSOCIATED MICACONTAINING NANOCOMPOSITE HYDROGELS

Abstract

Chitosan (CS) grafted poly[(acrylic acid)-co-(2-hydroxyethyl methacrylate)] (CS-g-poly(AA-co-HEMA)) at different molar ratios of AA and HEMA, and the associated nanocomposite hydrogels of CS-g-poly(AA-co-HEMA)/mica were synthesized by radical copolymerization. The grafting positions at the amino or hydroxyl groups in the CS were identified by Fourier transform infrared spectroscopy. CS-g-poly(AA-co-HEMA) hydrogels were intercalated in the mica and the amount of hydrogel insertion did not affect the spacing of the silicate layers in mica. The higher mica loadings produced a rougher surface of the nanocomposite hydrogel. The water absorbency of the CS-g-poly(AA-co-HEMA)/mica nanocomposite hydrogels decreased with increasing levels of mica loading to a lower level than those of the CSg-poly(AA-co-HEMA) hydrogels. Both CS-g-poly(AA) and CS-g-poly(AA-co-HEMA)/mica nanocomposite hydrogels exhibited a higher antiproliferative activity against Staphylococcus aureus than did the neat CS hydrogel with CS-g-poly(AA) revealing a very pronounced minimum inhibition concentration (MIC) of 1.56 mg ml ¹. The extent of mica loading in the CS-g- poly(AA-co-HEMA) nanocomposite hydrogels did not affect the MIC (12.5 mg ml⁻¹).

Keywords: Chitosan; Acrylic acid; 2-hydroxyethyl methacrylate; Mica;

Nanocomposite hydrogel; Antibacterial property

1. Introduction

Hydrogels are slightly crosslinked hydrophilic polymers that can swell and absorb at least 15 times of their dry weight. The relative density of hydrophilic groups and the degree of crosslinking of the hydrogel are the two main factors that affect the water absorbency of a hydrogel. Chitosan (CS) has found wide applications in the biomedical field, as well as other fields, because of its interesting biological properties, such as biocompatibility, biodegradability, hemostatic activity and bacteriostatic effects. Recently, CS-based hydrogels have been extensively researched and used in a wide field of applications because of their biocompatibility, biodegradability, nontoxicity and antibacterial activity,² as well as that CS is a plentiful, renewable and relatively cheap material. The hydrogels derived from CS grafted with hydrophilic vinyl monomers, such as acrylic acid (AA) or itaconic acid (IA), showed an increased water absorbency compared to CS alone.³⁻⁵ The 2-hydroxyethyl methacrylate (HEMA) monomer has long been used in biomedical applications because it improves the graft copolymer biocompatibility.⁶ HEMA monomer is harmful in the dental application if it does not completely polymerize, because it induces DNA damage, apoptosis and cell-cycle delay by the production of reactive oxygen species. However, it was found that the presence of antioxidant and/or CS can decrease the genotoxicity of HEMA monomer. 7,8 CS-g-poly(AA-co-HEMA) was reported to exhibit good cytocompatibility and hemocompatibility and thus possesses a high potential as an application for wound dressing.³ Suitable wound dressings normally possess an antibacterial activity for protecting the wound from infection, and have a water absorbency of around 25 - 32 times their dry weight so as to be able to remove secretion or pus from the wound. Bacterial infection is one of the main factors for the development of chronic wounds. Infected wounds may cause trauma and higher

treatment costs. Pathogens frequently associated with wound infections include *Staphylococcus aureus* (*S. aureus*), *Enterococcus* sp., *Escherichia coli*, *Pseudomonas aeruginosa*, *Enterobacter* sp., *Proteus mirabilis*, *Klebsiella pneumonia*, *Streptococcus* sp., and *Candida albicans*. *S. aureus* is the most commonly found human pathogens which cause wound infections, boils, pustules and other human skin infections. ¹⁰ Infection by *S. aureus* is accounted for about 20% frequency of occurrence in burns, wounds, and surgical sites. Due to the above mentioned, any developed wound dressing materials should therefore possess an inhibitory effect on the most frequently found *S. aureus* in wounds.

Generally, the gel strength of a bio-absorbent is naturally rather weak and this unfortunately limits its useful applications. To improve the gel strength, thermal and inherently antibacterial properties of CS and/or grafted CS, clay minerals, such as montmorillonite, 11 rectorite 12,13 and sepiolite, 14 have been used as a filler incorporated into the CS to produce CS/nanocomposite hydrogels. Wang et al. 15 found that the antibacterial activity against *S. aureus* of CS/rectorite nanocomposite film was better than that of the neat CS film. This result agreed with the research reporting that clay minerals alone did not destroy bacteria, but they could adsorb and kill bacteria when the antimicrobial materials were intercalated into silicate layers. 16

Mica is a clay mineral known as a 2: 1 phyllosilicate and its general formula is $AM_{2-3}T_4O_{10}X_2$, where A is usually Na, K or Ca. The M can be Fe, Al and Mg; T is Si and/or Al and X is (OH), O, Cl and F.¹⁷ It is composed of two-dimensional layers of an edge-shared octahedral sheet that is fused to form two tetrahedrals by the shared oxygen ions of one octahedral sheet and two tetrahedral sheets.¹⁸ Mica showed the antimicrobial activity, but it has a tendency of cytotoxicity with a larger platelet size than that of montmorillonite.¹⁹ Nanosilicate platelet of montmorillonite has a low

cytotoxicity with antibacterial activity. ^{19,20} However, only a few research reports on CS/mica nanocomposite hydrogels are available, leaving its potential suitability for many applications, including as a wound dressing material, unknown. Therefore, the synthesis and characterization of grafted CS/mica nanocomposite hydrogels was the main aim of this research. The effects of the reaction parameters on the morphology, water absorption and antibacterial activities of the resultant hydrogels were investigated.

2. Experimental

2.1 Materials

CS with a viscosity average molecular weight of 57,000 g mol⁻¹ and an 85% deacetylation degree was purchased from Seafresh Industry Public Co., Ltd. (Bangkok, Thailand). Industrial grade AA and HEMA monomers were kindly supplied by Thai Mitsui Specialty Chemicals Co., Ltd. (Bangkok, Thailand). N, N'-Methylenebisacrylamide (*N*-MBA) crosslinker Ν. N. N'. and tetramethylethylenediamine (TEMED) co-initiator were purchased from Fluka (Buchs, Switzerland). Ammonium persulphate (APS), purchased from Ajax (Australia), was used as the initiator. Swelling mica was purchased from Wako Pure Chemical Industries, Ltd. (Osaka, Japan). Deionized water, used as the reaction medium, was obtained from an Elga Deionizer (Model LA611, Marlow international, Bucks, U.K.). Sodium ampicillin (drug grade) was purchased from T.P. Drug Laboratories (Bangkok, Thailand). Staphylococus aureus (S. aureus) isolate from textile wastewater was provided by the National Center for Genetic Engineering and Biotechnology (NSTDA, Pathum thani, Thailand). Mueller-Hinton Broth (MHB) and Mueller-Hinton Agar (MHA), used for the growth of S. aureus were from Difco, New Jersey, USA.

2.2 Syntheses

2.2.1 Synthesis of grafted CS hydrogels

CS (1 g) was added into 30 ml of 2% w v⁻¹ acetic acid solution in a 500-ml four-necked round-bottom flask with a mechanical stirrer (Ika RW 28, IKA® Werke GmbH & Co. KG, Staufen Germany), assembled with a half-moon shaped Teflon blade paddle and a condenser. The mixture was stirred for 30 min at room temperature and then heated at $60 \pm 2^{\circ}$ C under nitrogen gas which was fed constantly through the gas inlet at 10 ml min⁻¹ for 30 min. APS (0.01-0.15 g) was then added and stirred for 10 min, followed by the sequential addition of either AA or HEMA or both and N-MBA (0.01 - 0.15 g) to the desired final concentration and stirred for 5 min. Finally, TEMED was added (0.01 - 0.4 g) to the mixture and stirred at 250 rpm for another 60 min. The reaction was then cooled down to room temperature and adjusted to pH 8 by 1 M sodium hydroxide solution. The product was dewatered with acetone, cut into pieces of approximately 1 x 1 cm square and dried in an oven at 50°C for 24 h. The dried product was extracted with an excess amount of methanol in a Soxhlet apparatus for 24 h to remove the unreacted components and obtain the CS grafted polymer (e.g. CS-g-poly(AA-co-HEMA)). The extracted product was dried in the oven at 50°C for 24 h, milled and sieved through a 100 mesh sieve to obtain the hydrogel particles in the range of 50 - 100 mesh (200 - 400 micrometers).

2.2.2 Synthesis of CS-g-poly(AA-co-HEMA)/mica nanocomposite hydrogels

The desired amount of mica was dispersed in the mixture of AA and HEMA monomers for 60 min by stirring at 250 rpm with a magnetic stirrer. CS (1 g) was dissolved in 30 ml of 2% v v⁻¹ solution of acetic acid, and then added into a 500-ml four-necked round-bottomed reaction flask equipped with the mechanical stirrer and a

condenser. The reactor was then immersed in a temperature controlled water bath, stirred at 250 rpm under a constant nitrogen gas fed through the gas inlet tube for 30 min before APS (0.1 g) was added and stirred for 10 min. The well-dispersed mica suspension was added into the solution of CS and APS, stirred at 250 rpm and heated to $60 \pm 2^{\circ}$ C under the nitrogen gas circulation for 30 min before *N*-MBA (0.1 g) was then added and stirred for 5 min. Finally, TEMED (0.4 g) was added and stirred for another 60 min. The polymerization product was cooled down and the product was obtained by the same procedure as described above for the grafted CS hydrogels.

2.3 Grafting ratio and efficiency of the grafted CS hydrogels by acid hydrolysis

The grafted CS hydrogel (0.5 g) was dissolved in 50 ml of 1 M HCl in a 125-ml Erlenmeyer flask which was assembled with a condenser and refluxed at 120°C for 2 h. After the acid hydrolysis, the remaining solid (grafted copolymer) was filtered, dried and weighed. The filtrate was neutralized to pH 7 by 1 M sodium hydroxide solution and then precipitated by ethanol. The precipitate was filtered and dried at room temperature for 24 h to obtain its dry weight. Finally, the filtrate from the precipitation step was evaporated to remove the residual solvent. The white solid was dried at room temperature and weighed. The remaining solid and precipitate after acid hydrolysis were investigated for functional groups by Fourier Transform Infrared Spectroscopy (FT-IR; model Tensor 27, Billerica, USA) using KBr pellets. The grafting ratio, grafting efficiency and homopolymer content were calculated from Equations (1) - (3):²¹⁻²³

% grafting efficiency =
$$\frac{\text{Weight of remaining solid after acid hydrolysis} \times 100}{\text{Weight of homopolymer} + \text{Weight of grafted copolymer}}$$
 (1)

% grafting ratio =
$$\frac{\text{Weight of remaining solid after acid hydrolysis} \times 100}{\text{Weight of precipitate from ethanol}}$$
 (2)

% homopolymer = Weight of grafted CS hydrogel before Soxhlet

extraction - weight of grafted CS hydrogel after Soxhlet

extraction (3)

2.4 Identification of functional groups of grafted CS hydrogels and CS-g-poly(AA-co-HEMA)/mica nanocomposite hydrogels

The functional groups of mica, the grafted CS hydrogels and grafted CS-g-poly(AA-co-HEMA)/mica nanocomposite hydrogels were characterized by FT-IR.

2.5 Characterization of the grafted CS hydrogels and CS-g-poly(AA-co-HEMA)/mica nanocomposite hydrogels

The surface morphologies of the mica, and the grafted CS and grafted CS/mica nanocomposite hydrogels were photographed on a scanning electron microscope (SEM, model JSM-5410LV, Tokyo, Japan) without prior cross sectioning. Each sample was fixed on an aluminum stub and coated with gold. X-ray diffraction (XRD) patterns of the samples were recorded using Bruker AXS (model D8 Discover, Bruker AXS Munich, Germany) with Cu radiation, voltage of 40 kV, a current of 40 mA and scanned from 1 - 35° with a scanning rate of 0.02° min⁻¹. The transmission electron micrographs (TEM) were taken on JOEL (JEM-2100, Jeol Ltd., Tokyo, Japan).

2.6 The effect of the reagent contents on water absorbency of grafted CS hydrogels and CS-g-poly(AA-co-HEMA)/mica nanocomposite hydrogels

The water absorbencies of the grafted CS hydrogel and the grafted CS-g-poly(AA-co-HEMA)/mica nanocomposite hydrogels were carried out with distilled water at room temperature in a closed system to minimize water evaporation. Distilled water (200 ml) was added to 0.1 g of the dry grafted hydrogels or the nanocomposite hydrogels. The hydrogel was swollen to equilibrium for 24 h and the swollen gel was then filtered through a 100-mesh aluminum screen sieve for 2 h. The water absorbency was determined for at least three replications for each synthesized product by Equation (4):

Water absorbency
$$(Q) = \frac{(W_s - W_d)}{W_d}$$
 (4)

where W_s is the weight of swollen hydrogels or nanocomposite hydrogels (g) and W_d is the weight of the dry hydrogels or nanocomposite hydrogels (g).

2.7 Antibacterial activity

2.7.1 Turbidity method

The CS, CS-g-poly(AA), CS-g-poly(HEMA) and CS-g-poly(AA-co-HEMA) hydrogels, and the CS-g-poly(AA-co-HEMA)/mica nanocomposite hydrogels, each weighing 250 mg, and distilled water were sterilized by UV radiation for 1 h prior to the test.

The diluted stock culture of *S. aureus* was adjusted to 0.5 units by sterile deionized water. The *S. aureus* suspension (2.5 ml) was inoculated into 47.5 ml of sterile Mueller-Hinton Broth (MHB) in a 250 ml sterile Erlenmeyer flask. For each hydrogel type, the sterile sample (250 mg) was then added to the *S. aureus* suspension in MHB media and incubated at 37°C while being shaken at 250 rpm. At every two hours a 50 ml aliquot was harvested and the swollen gel removed by filtration through

filter paper no. 1 (Schleicher & Schuell, Whatman, Kent, U.K.) prior to measuring the OD_{610 nm} of the filtrate as a measure of the growth of *S. aureus* using a spectrophotometer (Spectronic 21, Bausch & Lomb Inc., Rochester, New York, U.S.A). The OD results of the growth with or without the hydrogel were plotted versus time to obtain the bacterial growth profiles. The culture time at which the antibacterial activity of the grafted CS hydrogel was found to be maximal by the optical density measurement was used to evaluate the total replication competent (viable) bacterial number using the total plate count method (see section 2.7.2. below) so as to calculate the mean colony-forming units per milliliter (CFU ml⁻¹), and from this the relative degree of inhibition of bacterial proliferation can be obtained.

2.7.2 Total plate count method

The six and eight hour old *S. aureus* cultures in MHB were diluted with sterile deionized water to 10⁸ - 10⁹ CFU ml⁻¹ and then 100 µl aliquots of each diluted *S. aureus* suspension were spread on each MHB plate. The plates were incubated for 24 h at 37°C where upon the number of viable bacteria was counted. Mean CFU ml⁻¹ and the relative inhibition were calculated by Equations (5) and (6), respectively. The negative control was the sterilized *S. aureus* cultured in MHB.

$$CFU/ml = \left(\frac{mean \ numbers \ of \ counted \ colonies}{amount \ of \ dilute \ S. aureus \ for \ spread \ plate \ (ml)}\right) \times dilution \ factor$$
(5)

Relative inhibition =
$$100 - \left(\frac{CFU / ml \ of \ the \ sample}{CFU / ml \ of \ negative \ control}\right) \times 100$$
 (6)

2.7.3 Minimum inhibition concentration (MIC)

The antibacterial activity was determined in terms of the minimum inhibition concentration (MIC). The diluted stock culture of *S. aureus* was adjusted to 0.5 A_{610} units by sterile deionized water and 100 μ l was inoculated into 4.9 ml of sterile MHB in a 10 ml test tube. The hydrogels, each evaluated at the five concentrations of 0, 3.12, 6.25, 12.5 and 25 mg ml⁻¹, were added to the 0.01 A_{610} unit suspensions of *S. aureus* (see above) in sterile MHB. The cultures were then incubated at 37°C with shaking at 120 rpm for 24 h. The mean CFU ml⁻¹ of each sample tested were measured by the total plate count method as above and the experiment was performed in triplicate. The MIC was thus determined from the derived CFU ml⁻¹ and statistical significance (ANOVA) was accepted at the 99% significant level or $\alpha = 0.01$.

3. Results and discussion

3.1 Characterization of the grafted hydrogels

3.1.1 Grafted CS hydrogels

The spectrum of the CS hydrogel (Figure 1(a)) shows the characteristic amino group peaks at 3428 cm⁻¹ for N-H stretching, 1640 cm⁻¹ for the C=O stretching of amide I,²⁴ 1594 cm⁻¹ for the N-H bending of amide II, 1381 cm⁻¹ for the -NHCO stretching of amide II²⁵ and 1253 cm⁻¹ for C-N stretching.²⁶ The characteristic peaks of the saccharide structure in CS exhibit at 1152 cm⁻¹ for the bridge O stretching,^{23,27} and 1085 cm⁻¹ and 1031 cm⁻¹ for the C₃-OH and C₆-OH stretching, respectively.²⁵ In addition, the absorption peak at 1420 cm⁻¹ is the O-H and C-H vibration which indicates the presence of a hydroxyl group.²⁴ The peak of C-H stretching appears at 2921 and 2864 cm⁻¹.²⁷

The CS-*g*-poly(AA) hydrogel spectrum (Figure 1(b)) shows a new absorption peak at 1724 cm⁻¹ assigned to C=O stretching of the carboxyl group from the grafted poly(AA) part,²⁷ which was shifted from the peak at 1713 cm⁻¹ of the carboxyl group of poly(AA). In addition, the new absorption peaks at 1563 cm⁻¹ and 1402 cm⁻¹ are ascribed to asymmetric and symmetric stretching of the carboxylate anion of poly(AA) in the CS-*g*-poly(AA) hydrogel.³ The absorption peak at 1594 cm⁻¹, assigned to N-H bending of CS, disappeared in the CS-*g*-poly(AA) hydrogel. Thus, the NH₂ group is grafted in the CS backbone.²⁸ Moreover, the characteristic peaks of the saccharide structure of CS in the CS-*g*-poly(AA) hydrogel was shifted to 1065 cm⁻¹ and 1019 cm⁻¹ (C₃-OH and C₆-OH stretching) and the peak of O-H bending at 1420 cm⁻¹ disappeared (Figure 1(b)). From these results, the poly(AA) chains were confirmed to be grafted at both the NH₂ and OH sites on the CS backbone.

The CS-*g*-poly(HEMA) spectrum (Figure 1(c)) shows an absorption peak at 1730 cm⁻¹, assigned to C=O asymmetric stretching, which indicates the presence of the ester carbonyl group of poly(HEMA),³ and a new absorption peak at 746 cm⁻¹ that is attributed to the CH₂ rocking of the poly(HEMA) moiety.²⁹ The absorption peak of N-H stretching of CS also disappeared. Thus, the NH₂ group of CS had been reacted in the graft polymerization.²⁸ The characteristic peaks of the saccharide structure of CS in the CS-*g*-poly(HEMA) hydrogel were shifted to 1069 cm⁻¹ and 1021 cm⁻¹ (C₃-OH and C₆-OH stretching) and the CS O-H bending peak at 1420 cm⁻¹ disappeared. Thus, the poly(HEMA) was grafted at both NH₂ and OH sites on the CS backbone as well.

The CS-g-poly(AA-co-HEMA) hydrogel spectrum (Figure 1(d)) shows the absorption peak at 1722 cm⁻¹ that is assigned to the C=O asymmetric stretching and so indicates the presence of the ester carbonyl group of the poly(HEMA) moiety,³ and

a new absorption peak at 753 cm⁻¹ that is attributed to the CH₂ rocking of the poly(HEMA) moiety.²⁹ In addition, it also shows peaks at 1585 cm⁻¹ (C=O asymmetric stretching) and 1402 cm⁻¹ (C=O symmetric stretching) of the carboxylate anion in the poly(AA) moiety.³ Moreover, the characteristic peaks of the saccharide structure of CS in the CS-*g*-poly(AA-*co*-HEMA) hydrogel (Figure 1(d)) shifted to 1074 and 1021 cm⁻¹ (C₃-OH and C₆-OH stretching) and the peak of O-H bending at 1420 cm⁻¹ (Figure 1(a)) disappeared (Figure 1(d)). Thus, poly(AA-*co*-HEMA) was also grafted at both the NH₂ and OH sites on the CS backbone.

3.1.2 CS-g-poly(AA-co-HEMA)/mica nanocomposite hydrogels

The FT-IR spectrum of mica is shown in Figure 1(e). It shows a peak of O-H stretching at 3600 - 3400 cm⁻¹ that indicates the presence of the hydroxyl group. The absorption peaks at 2924 and 2852 cm⁻¹ are attributed to the C-H stretching of the organic part and indicate that the mica used is synthetic mica. It also shows the absorption peaks of H-O-H bending of water at 1637 and 1620 cm⁻¹, ³⁰ and Si-O and Al-O stretching peaks at 1016 and 473 cm⁻¹. ³¹

The FT-IR spectra of CS-*g*-poly(AA-*co*-HEMA)/mica nanocomposite hydrogels, containing mica at 7, 10 or 15% w w⁻¹ of the monomer, are shown in Figure 1(f-h), respectively. In comparison with the spectra of mica (Figure 1(e)), the characteristic peaks of CS are shifted to 1636 and 1389 cm⁻¹, whilst the characteristic peaks of poly(AA-*co*-HEMA) are also shifted to 1724, 1572, 1404 and 754 cm⁻¹. In addition, new absorption peaks appear at 473, 469 and 467 cm⁻¹ (Figure 1(f-h), respectively), all of which are attributed to the Al-O stretching of mica. The intensity of the absorption peak at 1016 cm⁻¹ (Si-O stretching) increased with increasing mica loadings in the CS-*g*-poly(AA-*co*-HEMA)/mica nanocomposite hydrogels, which

indicates the existence of mica in the CS-g-poly(AA-co-HEMA) nanocomposite hydrogel. Based on these FT-IR data, the AA or HEMA group is grafted at the OH group of the C-6 position and/or the amino group of CS. The FT-IR peaks in the spectra further confirmed that CS-g-poly(AA-co-HEMA)/mica nanocomposite hydrogels with various loadings of mica were successfully synthesized.

3.2 The grafting performance of grafted CS hydrogels

Analysis of the acid hydrolysis suggests the grafting ratio of the CS-gpoly(AA) hydrogel (87%) is lower than that of the CS-g-poly(AA-co-HEMA) (269%) and CS-g-poly(HEMA) hydrogels (343%). However, the grafting ratios of CS-gpoly(AA-co-HEMA) and CS-g-poly(HEMA) hydrogels were calculated from the weight differences because a poly(HEMA) C=O peak at 1710 and 1722 cm⁻¹ is still observed. Thus, at least some poly(HEMA) is still incorporated in the precipitate after acid hydrolysis, it means that the acid hydrolysis of the CS-g-poly(HEMA) was not completed. In comparison with the amount of CS, a greater amount of HEMA was used and so HEMA can generate an interpenetrate polymer network (IPN) hydrogel³² on the CS backbone. This result reflects the high grafting ratio as expected. The grafting efficiency of CS-g-poly(AA), CS-g-poly(AA-co-HEMA) and CS-gpoly(HEMA) hydrogels is 93, 94 and 96%, respectively. The amount of homopolymer normally generated during graft polymerization and the homopolymer chains could form the IPN chains. Therefore, the amount of homopolymer cannot be derived directly just from the Soxhlet extraction and acid hydrolysis. Therefore, the amounts of free poly(AA), poly(AA-co-HEMA) and poly(HEMA) found are only 3, 5 and 3%, respectively, which are considered to be quite small, and would probably have been incorporated as the IPN in the polymeric hydrogels.

3.3 Surface morphology

The surface morphologies of the CS, mica, CS-g-poly(AA-co-HEMA) hydrogel and CS-g-poly(AA-co-HEMA)/mica nanocomposite hydrogels with 5 to 15% (w w⁻¹ of the monomer) mica loadings are shown as the representative SEM micrographs in Figure 2. The relatively smooth surface of the CS hydrogel and the flat sheets of mica at approximately 1 - 3 micrometers along with their aggregated state is clearly visible (Figure 2(a,b)). The surface of the CS-g-poly(AA) hydrogel (see Figure 2(c)) exhibits the larger porous structure in many areas than those of CS-g-poly(HEMA) (see Figure 2(d)) and CS-g-poly(AA-co-HEMA) hydrogel (see Figure 2(e,f)). The surface morphology of the CS-g-poly(HEMA) hydrogel shows a gel network surrounded by a wide spread of uniformly distributed micro-pores and this is especially regular on the surface of the CS-g-poly(AA-co-HEMA) hydrogel (Figure 2(d)). The CS-g-poly(AA-co-HEMA) hydrogel surface exhibits further a nano-porous structure (Figure 2(e,f)).

morphologies of the CS-g-poly(AA-co-HEMA)/mica internal nanocomposites containing 5 - 15% w w⁻¹ mica of the monomer (Figure 2(g-j)) are slightly different from those of the mica-free CS-g-poly(AA-co-HEMA). It is seen that the higher the mica loading, the more the surface roughness increased and that the mica flakes are imbibed in the inner areas of the gel. When the mica loadings were high, they were agglomerated, aggregated, resided, deposited and covered the whole surface. Based on these results, CS-g-poly(AA-co-HEMA)/mica polymer nanocomposite hydrogels are confirmed to have been successfully synthesized. One must state that no residual HEMA was retained in the resulting hydrogels because no indication of the double bonds peaks was found in the IR spectra because many extractions of the unused materials were made in solvent.

3.4 XRD and TEM analyses

The XRD pattern of the CS hydrogel (Figure 3(a)) shows the 2-theta of CS at 10.53° and 19.93°, which corresponds to the hydrated crystals of low crystallinity of the form I and crystallinity of the form II, respectively. 33,34 The XRD pattern of CS-gpoly(AA), CS-g-poly(HEMA) and CS-g-poly(AA-co-HEMA) exhibit the broader and weaker peaks at 20.19, 18.49 and 20.31°, respectively, whereas the 2-theta at 10.53° of all these three CS grafted hydrogels disappeared. These indicated that the crystallinity of the grafted CS was dramatically decreased. Changes in the intensity of the peaks at approximately 20° relate to different packing of the chains and/or different hydrogen bonding networks in the grafted CS. 35 Thus, the introduction of AA and/or HEMA chains onto the surface of the CS causes the breakdown of its crystallinity. These results confirmed that the grafting of polymer onto the CS chain occurred. 33,34,36 The XRD patterns of mica revealed 2-theta values of 7.13 and 9.22° that correspond to a basal spacing of 13.58 and 9.58 Å, respectively. The XRD patterns of the CS-g-poly(AA-co-HEMA)/mica nanocomposite hydrogel reveal that the 2-theta value of mica in the nanocomposite hydrogels were shifted towards a lower angle (6.27°) and that the interlayer spacing of mica increased by 1.7 Å compared with that of the swelling mica. This confirms that intercalation had taken place and that the CS-g-poly(AA-co-HEMA)/mica nanocomposite hydrogels are intercalated composites with more spacing in the silicate layers.³⁷ In addition, it also shows that increasing the mica loadings from 5 to 15% (w w⁻¹ based on the weight of monomer) does not affect the intercalated structure of the CS-g-poly(AA-co-HEMA)/mica nanocomposite hydrogels but rather they exhibit the same basal spacing. These results agree well with the previous report of Wang and coworkers.¹²

Representative TEM micrographs of the CS-*g*-poly(AA-*co*-HEMA)/mica nanocomposite hydrogels with mica loadings of 5, 7, 10 and 15% w w⁻¹ of the monomer are shown in Figure 4. The dark lines in Figure 4 belong to the mica structure and the bright area is the grafted chitosan matrix. All the TEM micrographs of nanocomposite hydrogels revealed that the distance between the two adjacent dark lines, the spacing of the two silicate layers, results in an intercalated structure. Indeed, parts of the silicate layer can be seen in Figure 4(a-d). The results of the TEM analysis are consistent with the XRD data (Figure 3), and support that CS-*g*-poly(AA-*co*-HEMA)/mica nanocomposite hydrogels have an intercalated structure and no significant if any level of an exfoliated structure.

3.5 Equilibrium water absorbency

3.5.1 Effect of monomer type (AA or HEMA) on the properties of the grafted CS hydrogels

The equilibrium water absorbency of CS alone was rather low but was significantly affected by the copolymerization with AA, but not with HEMA (Table 1). CS-g-poly(AA) had ten-fold higher water absorbency, whereas the water absorbency of the CS-g-poly(HEMA) was not significantly different to that for CS alone (Table 1). The water absorbency of the CS-g-poly(AA-co-HEMA) decreased ~1.2- and 3.2-fold as the AA: HEMA ratios decreased from 3:1 to 1:1 and 1:3, respectively (Table 1). That the water absorbency of CS-g-poly(AA-co-HEMA) increased as the content of AA increased is due to the increase in the density of hydrophilic groups from the carboxylic acid contents, which then provides a greater repulsion of the anionic portion allowing for the expansion of the polymer chains. This also then explains the increased water absorbency of the CS-g-poly(AA)

hydrogels over that of the CS hydrogels. On the other hand, CS-g-poly(HEMA) had very low water absorbency because HEMA is not as polar as AA but rather has a rather rigid chain due to the methacrylate substituent group. The longer chain of the poly(HEMA) hydrogel thus is likely to have resulted in more molecular entanglements that limited the chain expansion³⁹ and caused the water absorbency of the CS-g-poly(HEMA) hydrogel to decrease. Thus, although CS-g-poly(HEMA) would be unlikely to be beneficial to intercalate with mica, the HEMA moiety is more compatible with human cells than the other types of monomer moieties.

3.5.2 Effect of mica loading

The equilibrium water absorbency of the CS-g-poly(AA-co-HEMA) hydrogel at a 1:1 AA: HEMA molar ratio was ~5.4- and 5-fold higher than that of CS or CS-g-poly(HEMA), respectively, but almost half that of the CS-g-poly(AA) hydrogel (Table 1). The addition of mica at 5, 7 or 10% (w w⁻¹ of monomer) caused a 1.2-fold drop in the equilibrium water absorbency from that seen with the mica-free CS-g-poly(AA-co-HEMA) hydrogel, but did not vary significantly between the three different mica loading levels (Table 1). In contrast, when the mica loading was increased to 15% w w⁻¹ of monomer, the water absorbency was significantly decreased a further 1.3-fold compared to that seen with the 5 – 10% w w⁻¹ mica loaded CS-g-poly(AA-co-HEMA), or 1.54-fold less than that for the mica-free CS-g-poly(AA-co-HEMA). This is because the polymer chains were inserted into the spacing between the silicate layers of mica and so the polymer chains were restricted in these limited spaces and so less able to expand. Another reason could be the degree of rigidity of the nanocomposite hydrogel that is induced by the mica. This also supports the notion that the structure of this nanocomposite hydrogel was intercalated.

3.6 Antibacterial activity

Particle sizes of the CS, CS-g-poly(AA-co-HEMA) hydrogels and CS-g-poly(AA-co-HEMA)/mica nanocomposite hydrogel were in the range of 200 - 400 µm by the sieve size 50-100 mesh which is anticipated to have an important effect on the bacterial growth inhibitio. This was therefore evaluated using a co-culture of *S. aureus* with each hydrogel type and evaluating the bacterial growth relative to the control culture by measuring the culture turbidity by absorbance (after removal of the hydrogel by filtration), and by total plate counts of replication competent ("viable") cells, over a 24 h time period.

3.6.1 Turbidity method

This well used method assumes that the turbidity of a medium solution increases solely due to the increase in the number of bacterial cells. Although this method is easy to perform the bacteria sample must be in a liquid suspension state, and typically it can only be used to detect bacteria in the range of 10⁶ to 10⁷ bacteria ml⁻¹. Moreover, the measurement of bacterial growth in the lag phase is less accurate and is an indirect measurement that needs a calibration curve, where a direct measurement of bacterial counts must be performed.

The preliminary results of the antibacterial activity testing of the CS-g-poly(AA-co-HEMA) hydrogel, evaluated by measuring the optical density at 610 nm every 2 h and compared with the negative control (containing only the medium and the gram-positive *S. aureus*), revealed three phases in the growth cycle (Figure 5). The lag phases of S. aureus growth in the negative control and in the presence of CS-g-poly(AA-co-HEMA) hydrogel were similar, lasting for 4 h. Then, during the exponential phase, the growth rate of *S. aureus* grown in MHB containing the CS-g-

poly(AA-*co*-HEMA) hydrogel was lower than that of the negative control during the first 2 h of growth (4 - 6 h of total culture time), but then this growth rate decreased in the control culture from after 6 h up to reaching the start of the stationary phase (12 h), whereas the growth rate did not slow down in the cultures with CS-*g*-poly(AA-*co*-HEMA) until 10 - 12 h of total culture time, by which time the total bacterial number (as culture optical density) was slightly higher (1.5-fold) than in the control culture. From 12 - 24 h of total culture time, *S. aureus* in both conditions remained in stationary phase. Thus, the presence of the CS-*g*-poly(AA-*co*-HEMA) hydrogel appeared to render a slower early exponential growth rate of *S. aureus* (or to delay it) but did not reduce the final bacterial density reached after 12 - 24 h in the stationary phase. Since we did not count the viable bacteria that are attached to the gel, or wash them out from the gel, then the CS-grafted hydrogels may not be inhibitory at all but rather the bacteria grow attached to the gel surface and so are not in suspension first and only in suspension subsequently after the gel surface is full swollen and thus has the apparent delayed kinetics appearance.

3.6.2 The total Plate count method

The antibacterial activities of sterile sodium ampicillin (positive control), CS and grafted CS hydrogels against *S. aureus* were determined by the total plate count method. The mean CFU ml⁻¹ and the relative inhibition of CS and grafted CS hydrogels are summarized in Table 2. The relative inhibition observed with the CS hydrogel was 2.9-fold greater at 6 h of culture time (early log phase) than that after 8 h of culture (the late log phase). When the CS was grafted with poly(AA), the antibacterial activity was significantly improved 1.53- and 4.23-fold after both 6 and 8 h of culture at 93 and 89% relative inhibition, respectively, because of the

hydrophilicity of poly(AA),⁴¹ and the biological activity of the free amino groups at the C-2 position of the native CS.⁴² The higher antibacterial activities of the CS-*g*-poly(AA) hydrogel can be caused by the interaction between the negative charges on the bacteria surface with the positive surface of the CS-*g*-poly(AA). The more positively charged hydrogels could promote bacterial adhesion onto the hydrogel surface and reduce the remaining amount in the free suspension, resulting in a decrease in the bacteria colonies in the liquid medium. It is relevant to note here that the amount (molar ratio) of the AA or HEMA monomers that were grafted onto the CS is almost the same for the three different grafted CS derivatives studied here.

It was anticipated that the pores on the CS-g-poly(AA) hydrogel surface would improve the ability to capture bacteria. Although, the relative inhibition of the CS-g-poly(AA-co-HEMA) hydrogel would be higher than that of CS, because of the hydrophilicity resulting from the carboxyl group of poly(AA), the surface of the CS-g-poly(AA-co-HEMA) hydrogel is much rougher than the ungrafted CS hydrogel surface, which may increase bacterial adhesion sites and result in a higher antibacterial activity in the CS-g-poly(AA-co-HEMA) hydrogel than that of the CS. However, the relative inhibition of the CS-g-poly(AA-co-HEMA) hydrogel was found to actually be 1.35- and 3.3-fold lower than that of the CH-g-poly(AA) hydrogel in the early (6 h) and late (8 h) log phases, respectively. This is likely to be due to the decreased hydrophilicity of the HEMA moiety. Thus, graft copolymerization of CS with a 1:1 molar ratio of AA: HEMA can delay (or inhibit) the growth of *S. aureus* in the early exponential phase.

The antibacterial activity of the CS-g-poly(AA-co-HEMA)/mica nanocomposite hydrogels are summarized in Table 2. The relative inhibition of CS-g-poly(AA-co-HEMA)/mica nanocomposite hydrogels having mica loadings at 7 and

10% w w⁻¹ of the monomer was slightly higher (1.3- and 1.11-fold) at a culture time of 6 h than that of the CS and CS-*g*-poly(AA-*co*-HEMA) hydrogel, respectively. This finding is in agreement with those reported by Wang et al..¹⁵ However, CS-*g*-poly(AA-*co*-HEMA) exhibited higher relative inhibition against *S. aureus* growth by 1.2- and 1.1-fold comparing with 10 and 7% w w⁻¹ mica loading, respectively, at 8 h of culture. Increasing the mica loading to 15% w w⁻¹ of the monomer significantly decreased the apparent antibacterial activity 2.03- and 2.13-fold of that seen with no mica addition, and 2.25- and 1.9-fold of that seen with a 7% w w⁻¹ mica loading after 6 and 8 h of culture, respectively. This result agreed quite well with Meng et al.,¹⁶ finding that CS intercalated mica hydrogels could kill more bacteria than the neat CS or the clay minerals.

Nanocomposite hydrogels can generate a larger surface area to absorb more bacterial colonies and so give a greater chance to increase the antibacterial activity through interactions between the positive charges of the CS hydrogel and the negative charges on the cytoplasmic cell membrane of the bacteria. In addition, S. aureus does not have an outer membrane to prevent the influx of foreign molecules and so it can be inhibited more easily. However, the higher mica loading at 15% w w of the monomer revealed a significantly decreased level of relative inhibition of S. aureus growth. This might be because the higher mica content screens and prevents the polymer chains from adhering with the bacteria to trigger the antibacterial activity.

3.6.3 Minimum inhibition concentration (MIC)

The MIC obtained for the CS-g-poly(AA) at 1.56 mg ml⁻¹ against the 0.01 A₆₁₀ Units of *S. aureus* cultured in MHB for 24 h (i.e. to the late stationary phase) at room temperature was 16- and >16-fold better than that of CS and CS-g-poly(HEMA),

respectively (Table 3). These MICs agree with that of viable counts and relative inhibition of *S. aureus* in the log phase of growth (Table 1). The extent of the water absorbency and acidity of the hydrogels plays influencing roles as described in the total plate count method for the MIC result. The more the hydrogel expanded, the higher the number of colonies of *S. aureus* that could be trapped and inhibited through the diffusion effect by water in the hydrogel. The higher acidic moiety of the CS-*g*-poly(AA) hydrogels, which carry a higher positive charge, may enhance the inhibitory effect with CS. It is worth noting that the presence of the COO group in the poly(AA) containing hydrogels (CS-*g*-poly(AA) and CS-*g*-poly(AA-*co*-HEMA)) becomes a major driving force for bacterial adhesion in the positively charged CS. AA in the feed is a key factor governing the antibacterial property in the resulting hydrogel and nanocomposites hydrogels. The high MIC value for the CS-*g*-poly(HEMA) was potentially caused by the proposed semi-IPN structure and the rigid conformation of poly(HEMA) chains grafted onto the CS backbones.

Surprisingly, the CS-*g*-poly(AA-*co*-HEMA)/mica nanocomposite hydrogels with mica loadings of 5, 7, 10 and 15% w w⁻¹ of the monomer had the same MIC values as each other and as that for the CS-*g*-poly(AA-*co*-HEMA) hydrogel (Table 3). This correlates with the almost constant water absorbency observed for the CS-*g*-poly(AA-*co*-HEMA) and the CS-*g*-poly(AA-*co*-HEMA)/mica nanocomposite hydrogels regardless of the mica loadings but relatively lower water absorbency at 15% w/w. Likewise, a much higher concentration of CS (25 mg ml⁻¹) or CS-*g*-poly(HEMA) (>25 mg ml⁻¹) or CS-*g*-poly(AA-*co*-HEMA)/mica nanocomposite hydrogels (12.5 mg ml⁻¹) is required for inhibiting *S. aureus* after 24 h of incubation.

Typical SEM micrographs of *S. aureus* cells cultured for 24 h in the MHB media alone (negative control), and in the various grafted CS copolymer and CS-g-

poly(AA-co-HEMA)/mica nanocomposite hydrogels are shown in Figure 6. Since the positive control in the total plate count did not produce any viable cells, then the positive control in MIC was not performed. The normal roundish-shapes of *S. aureus* cells were evident when cultured in the MHB media alone and also as adhered on the surface of mica (Figure 6(a,b), respectively). However, the cell walls of some of the *S. aureus* in or on the CS-g-poly(HEMA) and CS-g-poly(AA-co-HEMA) hydrogels after culture for 24 h were destroyed to give open cells (Figure 6(c) as shown in Figure 6(d)). Moreover, of the *S. aureus* cells that were adsorbed and immobilized on the surface and in the pores of the CS-g-poly(AA-co-HEMA)/mica nanocomposite hydrogels, some had distorted shapes and were destroyed to give fractured cell walls and these were randomly distributed in the hydrogel matrix (Figure 6(e-h)).

Although the water absorbency of the nanocomposite hydrogels was relatively lower than that of the grafted CS hydrogel, the hydrogels had larger surface area to absorb more bacterial colonies. With this compensation, the MIC values of nanocomposite hydrogels are not different from that of the grafted CS hydrogel. Thus, CS-g-poly(AA-co-HEMA) hydrogel or CS-g-poly(AA-co-HEMA)/mica nanocomposite hydrogels were at an equilibrium condition and gave similar MIC values.

The MIC values and SEM micrographs support that the mica content in the grafted CS hydrogel did not influence the antibacterial activity. On the other hand, the different results from the plate count method are caused by the absorbance assays undertaken in the mid- and late-log phases of growth at 6 and 8 h, respectively, whilst the MIC was evaluated at a late stationary phase (24 h). The different culture times could have resulted in different cell numbers due to different chances of cell adsorption by the nanocomposite hydrogels, as well as growth and death rates

4. Conclusion

CS was used to graft with AA and/or HEMA to give the grafted-CS hydrogels. CS-g-poly(AA-co-HEMA)/mica nanocomposite hydrogels were synthesized at different mica loadings and all hydrogels were characterized by FT-IR spectroscopy, SEM, XRD, TEM and equilibrium water absorbency. FT-IR spectroscopy indicated that the CS was grafted at the NH₂ and OH sites on the CS backbone. The water absorbency of the CS-g-poly(AA) hydrogel was the highest whilst those of CS and CS-g-poly(HEMA) were the lowest. The CS-g-poly(AA-co-HEMA)/mica nanocomposite hydrogels had an intercalated structure, as revealed by XRD and TEM analyses.

At the fixed 1:1 molar ratio of AA: HEMA, the extent of water absorbency of the nanocomposite hydrogels was constant at 5, 7 and 10% (w w⁻¹ of the monomer) mica loading but slightly decreased at 15% w w⁻¹ mica loading. The CS-g-poly(AA) hydrogel can inhibit the early-to-mid-log phase growth of *S. aureus* up to 93% with a MIC value as low as 1.56 mg ml⁻¹. For the CS-g-poly(AA-co-HEMA)/mica nanocomposite hydrogels, the relative inhibition was very similar (at ~81%) with mica loadings of 5, 7 and 10% w w⁻¹ of the monomer, but abruptly decreased at a 15% w w⁻¹ mica loading. Regardless of the mica loading levels in the CS-g-poly(AA-co-HEMA)/mica nanocomposite hydrogels, the MIC value at the late stationary phase was constant at 12.5 mg ml⁻¹. The CS-g-poly(HEMA) had a greater MIC (>25 mg ml⁻¹) than CS (25 mg ml⁻¹). Several possible explanations for the different inhibitory activities against *S. aureus* are discussed, but await further research for clarification.

Acknowledgements

The authors would like to acknowledge the financial support from the Thailand Research Fund under the Research Team Aided Program Contract no. RTA5080004. Partial financial support from the Graduate School, Chulalongkorn University is acknowledged. The provision of research facilities by the Imaging Polymer Laboratory of Chulalongkorn University's Department of Imaging and Printing Technology, Faculty of Science is highly appreciated. English edition by the Publication Counselor Unit of the Research Division, Faculty of Science, Chulalongkorn University, and fruitful suggestion provided by Dr. Robert Butcher are highly appreciated.

References

- 1. Devine, D. M.; Higginbotham, C. L. Eur Polym J 2005, 41, 1272.
- 2. Rinaudo, M. Prog Polym Sci 2006, 31, 603.
- 3. Dos Santos, K. S. C. R.; Coelho, J. F. J.; Ferreira, P.; Pinto, I.; Lorenzetti, S.G., Ferreira, E. I.; Higa, O. Z.; Gil, M. H. Int J Pharm 2006, 310, 37.
- 4. Mahdavinia, G. R.; Pourjavadi, A.; Hosseinzadeh, H.; Zohuriaan, M. J. Eur Polym J 2004, 40, 1399.
- 5. Jalal Zohuriaan-Mehr, M. Iran Polym J 2005, 14, 235.
- 6. Carenza, M. Int J Radiat Appl Instrum C Radiat Phys Chem 1992, 39, 485.
- 7. Schweikl, H.; Hartmann, A.; Hiller, K-A.; Spagnuolo, G.; Bolay, C.; Brockhoff, G.; Schmalz, G. Dent Mater 2007, 23, 688.
- 8. Pawlowska, E.; Poplawski, T.; Ksiazek, D.; Szczepanska, J., Blasiak, J. Mutation Res 2010, 696, 122.

- 9. Tanodekaew, S.; Prasitsilp, M.; Swasdison, S.; Thavornyutikarn, B.; Pothsree, T.; Pateepasen, R. Biomaterials 2004, 25, 1453.
- Sahu, K.; Verma, Y.; Sharma, M.; Rao, K. D.; Gupta, P. K. Skin Res Tech 2010, 16, 428.
- 11. Tang, C.; Chen, N.; Zhang, Q.; Wang, K.; Fu, Q.; Zhang, X. Polym Degrad Stabil 2009, 94, 124.
- 12. Wang, X.; Du, Y.; Luo, J.; Yang, J.; Wang, X.; Shi, X.; Hu, Y. Polymer 2006, 47, 6738.
- 13. Wang, X.; Du, Y.; Luo, J.; Yang, J.; Wang, W.; Kennedy, J. F. Carbohydr Polym 2009, 77, 449.
- 14. Xie, Y.; Wang, A.; Liu, G. Polym Compos 2010, 3, 89.
- 15. Wang, X.; Du, Y.; Luo, J.; Lin, B.; Kennedy, J. F. Carbohydr Polym 2007, 69, 41.
- 16. Meng, N.; Zhou, N.; Zhang, S.; Shen, J. Appl Clay Sci 2009, 42, 667.
- 17. Bozhilov, K. N.; Xu, Z.; Dobrzhinetskaya, L. F.; Jin, Z-M.; Green II, H. W. Lithos 2009, 109, 304.
- Tjong, S. C. Synthesis and structure-property characteristics of clay-polymer Nanocomposites, Nanocrystalline Materials; Oxford: Elsevier, 2006; Chapter 10; p. 311.
- 19. Hsu, S.; Tseng, H.; Hung, H.; Wang, M.; Hung, C.; Li, P.; Lin, J. Appl Mater Interfaces 2009, 1(11), 2556.
- 20. Li, P.; Wei, J.; Chiu, Y.; Su, H.; Peng, F.; Lin, J. Appl Mater Interfaces 2010, 2, 1608.
- 21. Patil, D. R., Fanta, G. F. J Appl Polym Sci 1993, 47, 1765.
- 22. Lanthong, P.; Nuisin, R.; Kiatkamjornwong, S. Carbohydr Polym 2006, 66, 229.

- 23. Mun, G. A.; Nurkeeva, Z. S.; Dergunov, S. A.; Nama, I. K.; Maimakov, T.P.; Shaikhutdinov, E. M.; Lee, S. C.; Park, K. React Funct Polym 2008, 68, 389.
- 24. Sun, T.; Zhou, D.; Xie, J.; Mao, F. Eur Food Res Technol 2007, 225, 451.
- 25. Zhang, J.; Wang, Q.; Wang, A. Carbohydr Polym 2007, 68, 367.
- 26. Singha, V.; Sharmaa, A. K.; Tripathi, D. N.; Sanghib, R. J Hazard Mater 2009, 161, 955.
- 27. Huacai, G.; Wan, P.; Dengke, L. Carbohydr Polym 2006, 66, 372.
- 28. Mishra, D. K.; Tripathy, J.; Srivastava, A.; Mishra, M. M.; Behari, K. Carbohydr Polym 2008, 74, 632.
- 29. Casimiroa, M. H.; Botelho, M. L.; Leal, J. P.; Gil, M. H. Radiat Phys Chem 2005, 72, 731.
- 30. Semenzato, S.; Lorenzetti, A.; Modesti, M.; Ugel, E.; Hrelja, D.; Besco, S.; Michelin, R. A.; Sassi, A.; Facchin, G.; Zorzi, F.; Bertani, R. Appl Clay Sci 2009, 44, 35.
- 31. Dai, H.; Li, H.; Wang, F. Surf Coat Technol 2006, 201, 2859.
- 32. Bayramoğlu, G.; Arica, M. Y. Colloids Surf A 2002, 202, 41.
- 33. Wang, J. P.; Chen, Y. Z.; Zhang, S. J.; Yu, H. Q. Bioresour Technol 2008, 99, 3397.
- 34. Luckachan, G. E.; Pillai, C. K. S. Carbohydr Polym 2006, 64, 254.
- 35. Kittur, F. S.; Kumar, A. B. V.; Tharanathan, R. N. Carbohydr Res 2003, 338, 1283.
- 36. Krishna Rao, K. S. V.; Chung, I.; Ha, C. S. React Funct Polym 2008, 68, 943.
- 37. Sivudu, K. S.; Thomas, S.; Shailaja, D. Appl Clay Sci 2007, 37, 185.
- 38. Sperling, L. H. Introduction to Physical Polymer Sciences. 4th ed.; New York: John Wiley & Sons, 2006; p. 477.

- 39. Zhou, Y.; Yang, D.; Gao, X.; Chen, X.; Xu, Q.; Lu, F.; Nie, J. Carbohydr Polym 2009, 75, 293.
- 40. Mohan, Y. M.; Lee, K.; Premkumar, T.; Geckeler, K. E. Polymer 2007, 48, 158.
- 41. Oh, S. T.; Han, S. H.; Ha, C. S.; Cho, W. J. J Appl Polym Sci 1996, 59, 1871.
- 42. Je, J.; Kim, S. J Agric Food Chem 2006, 54, 6629.



Table 1. The water absorbency of hydrogels derived from CS, AA and /or HEMA grafted-CS copolymers and CS-g-poly(AA-co-HEMA)/mica nanocomposites.

D.L	AA: HEMA	Mica	Water absorbency
Polymer	(mol ratio)	(w w ⁻¹ of monomer)	$(g g^{-1})^1$
CS			10 <u>+</u> 2
CS-g-poly(AA)			101 <u>+</u> 4
CS-g-poly(HEMA)			11 <u>+</u> 1
CS-g-poly(AA-co-HEMA)	3:1		64 <u>+</u> 2
	1:1		54 <u>+</u> 3
	1:3		20 <u>+</u> 2
	1:1	5	45 <u>+</u> 3
	1:1	7	44 <u>+</u> 1
	1:1	10	46 <u>+</u> 2
	1:1	15	35 <u>+</u> 5

¹Data are shown as the mean \pm 1 SD and are derived from 5 repeats. Means within the column are significantly different (p<0.05).

Table 2. Total plate counts (replication competent cells) and the relative inhibition of growth of *S. aureus* in the presence of sodium ampicillin and the hydrogels of CS, AA and/or HEMA grafted-CS copolymers and CS-g-poly(AA-co-HEMA)/mica nanocomposites with various mica loadings.

		6 h cu	lture time	8 h culture time		
Sample type	Mica (% w w ⁻¹)	CFU ml ⁻¹ (x 10 ⁹) ¹	Relative inhibition (%)	CFU ml ⁻¹ (x 10 ⁹) ¹	Relative inhibition (%)	
Negative control ²	Q,	6.95 <u>+</u> 1.51	-	8.15 <u>+</u> 1.25	-	
Positive control ³		0	100	0	100	
CS ⁴		2.7 <u>+</u> 0.25	61	6.4 <u>+</u> 1.68	21	
CS-g-poly(AA) ⁴		0.52 <u>+</u> 0.48	93	0.91 <u>+</u> 0.85	89	
CS-g-poly(HEMA) ⁴		2.18 <u>+</u> 0.28	69	5.95 <u>+</u> 1.25	27	
CS-g-poly(AA-co-HEMA) ⁴		1.90 <u>+</u> 0.19	73	2.92 <u>+</u> 0.07	64	
CS-g-poly(AA-co-HEMA) ⁴	7	1.4 <u>+</u> 0.37	81	3.6 ± 0.55	57	
CS-g-poly(AA-co-HEMA) ⁴	10	1.5 <u>+</u> 0.34	81	3.9 ± 0.31	54	
CS-g-poly(AA-co-HEMA) ⁴	15	5.0 <u>+</u> 1.68	36	5.9 <u>+</u> 2.4	30	

 $^{^{1}}$ CFU ml $^{-1}$ is shown as the mean \pm 1 SD and are derived from 6 repeats. Means within a column or across a row are significantly different (p<0.05).

²Negative control contains only the MHB medium and *S. aureus*.

³Positive control contains 250 mg of the sodium ampicillin, MHB medium and *S. aureus*.

⁴All hydrogel samples were co-cultured with S. aureus in MHB media at 250 mg ml⁻¹.

Table 3. Minimum inhibition concentration of hydrogels derived from CS, AA and/or HEMA grafted-CS copolymers and CS-g-poly(AA-co-HEMA)/mica nanocomposites with various mica loadings.

Sample test	Mica (% w w ⁻¹)	CFU ml ⁻¹ $(x \ 10^8)^1$	MIC (mg ml ⁻¹) ²
Negative control ³	-	18 <u>+</u> 1.0	-
CS ⁴		10 <u>+</u> 0.6	25
CS-g-poly(AA) ⁴		3.0 <u>+</u> 0.4	1.56
CS-g-poly(HEMA) ⁴		6.6 <u>+</u> 3.5	> 25
CS-g-poly(AA-co-HEMA) ⁴		1.2 <u>+</u> 0.5	12.5
CS-g-poly(AA-co-HEMA) ⁴	5	1.1 <u>+</u> 0.4	12.5
CS-g-poly(AA-co-HEMA) ⁴	7	5.1 ± 0.6	12.5
CS-g-poly(AA-co-HEMA) ⁴	10	4.6 <u>+</u> 0.4	12.5
CS-g-poly(AA-co-HEMA) ⁴	15	4.9 <u>+</u> 4.9	12.5

 $^{^{1}}$ CFU ml $^{-1}$ is shown as the mean \pm 1 SD and is derived from 3 repeats. Means within the column are significantly different (p<0.05).

²MIC are shown as mg ml⁻¹ for a 2% (v v⁻¹) seeding of a late log phase culture of *S. aureus* in MHB media and evaluated at late stationary phase (24 hr of culture).

³Negative control contains only the MHB medium and *S. aureus*.

⁴All hydrogel samples were co-cultured with S. aureus in MHB media at 250 mg ml⁻¹.

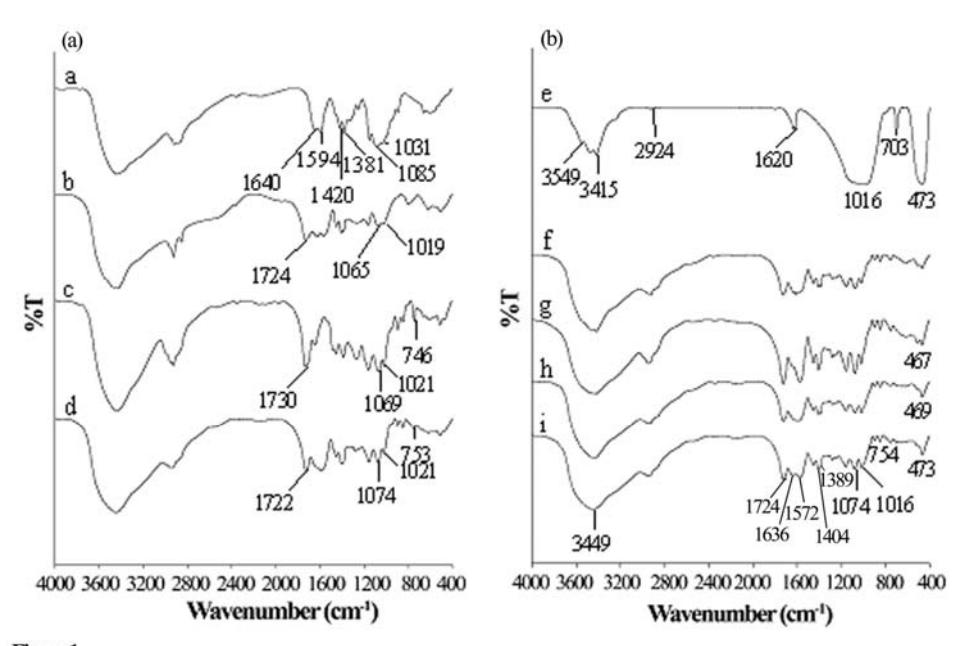


Figure 1

Representative FT-IR spectra of (A): (a) CS, and (b) CS-g-poly(AA), (c) CS-g-poly(HEMA) and (d) CS-g-poly(AA-co-HEMA) hydrogels, the last being synthesized with an AA: HEMA, N-MBA: CH, APS: CH and TEMED: CH molar ratios of 1, 0.11, 0.07 and 0.58, respectively; (B): (e) mica, and CS-g-poly(AA-co-HEMA)/mica nanocomposite hydrogels with mica loadings of: (f) 5%, (g) 7%, (h) 10% and (i) 15% w w-1 based on the monomer. 104x72mm (600 x 600 DPI)

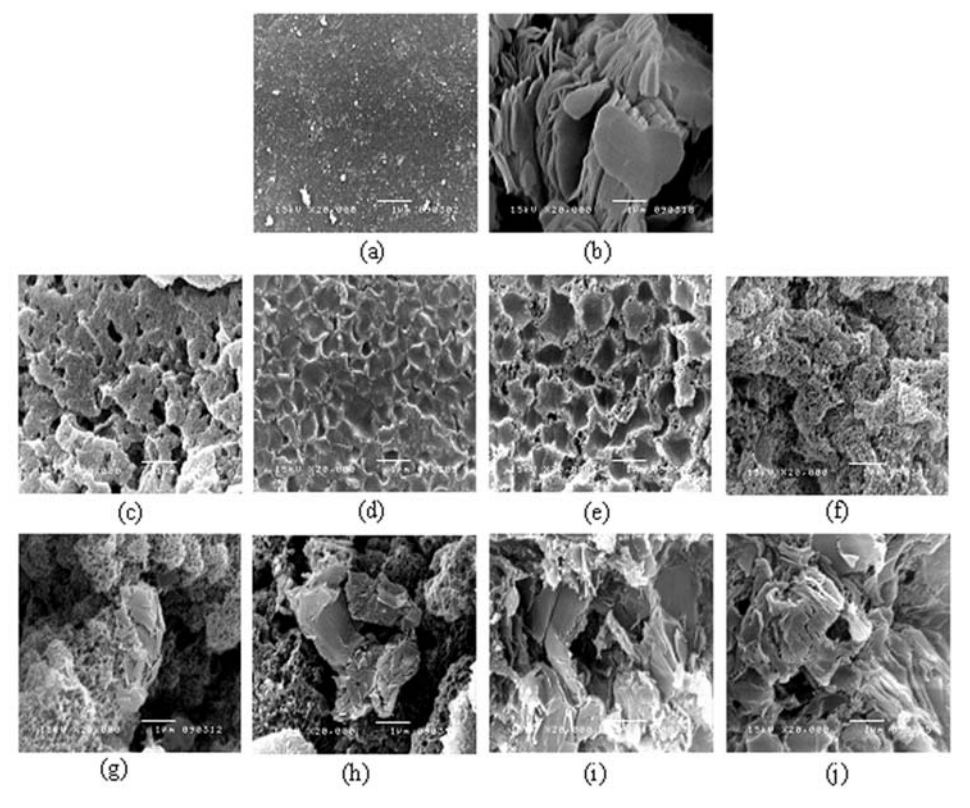
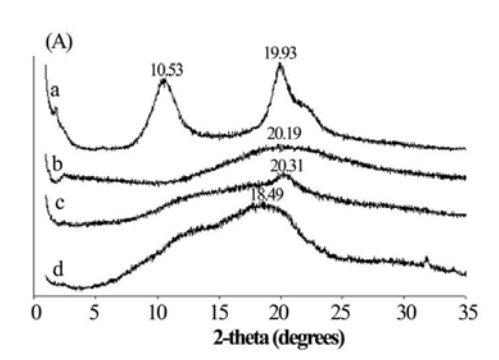


Figure 2

Representative SEM micrographs of (a) CS, (b) mica, (c) CS-g-poly(AA), (d) CS-g-poly(HEMA), (e, f) CS-g-poly(AA-co-HEMA), and CS-g-poly(AA-co-HEMA)/mica composite hydrogels synthesized with mica loading levels of (g) 5%, (h) 7%, (i) 10% and (j) 15% w w-1 of the monomer. 158x140mm (400 x 400 DPI)



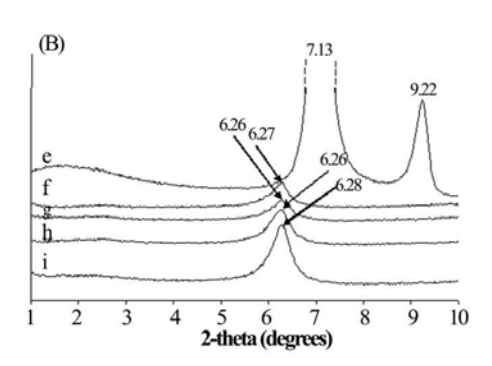


Figure 3

Representative XRD patterns of hydrogels synthesized from (A): (a) CS, (b) CS-g-poly(AA) synthesized with 1 g CS, 54 mmol AA, and N-MBA, APS and TEMED at 10%, 10% and 40% w w-1 of CS, respectively, (c) CS-g-poly(AA-co-HEMA) and (d) CS-g-poly(HEMA); (B): (e) mica, and CS-g-poly(AA-co-HEMA)/mica nanocomposite hydrogels synthesized with mica loadings of (f) 5%, (g) 7%, (h) 10% and (i) 15% w w-1 based on the monomer, 1 g CS, an AA: HEMA molar ratio of 1:1, and N-MBA, APS and TEMED at 10%, 10% and 40% w w-1 of CS, respectively.

60x24mm (600 x 600 DPI)

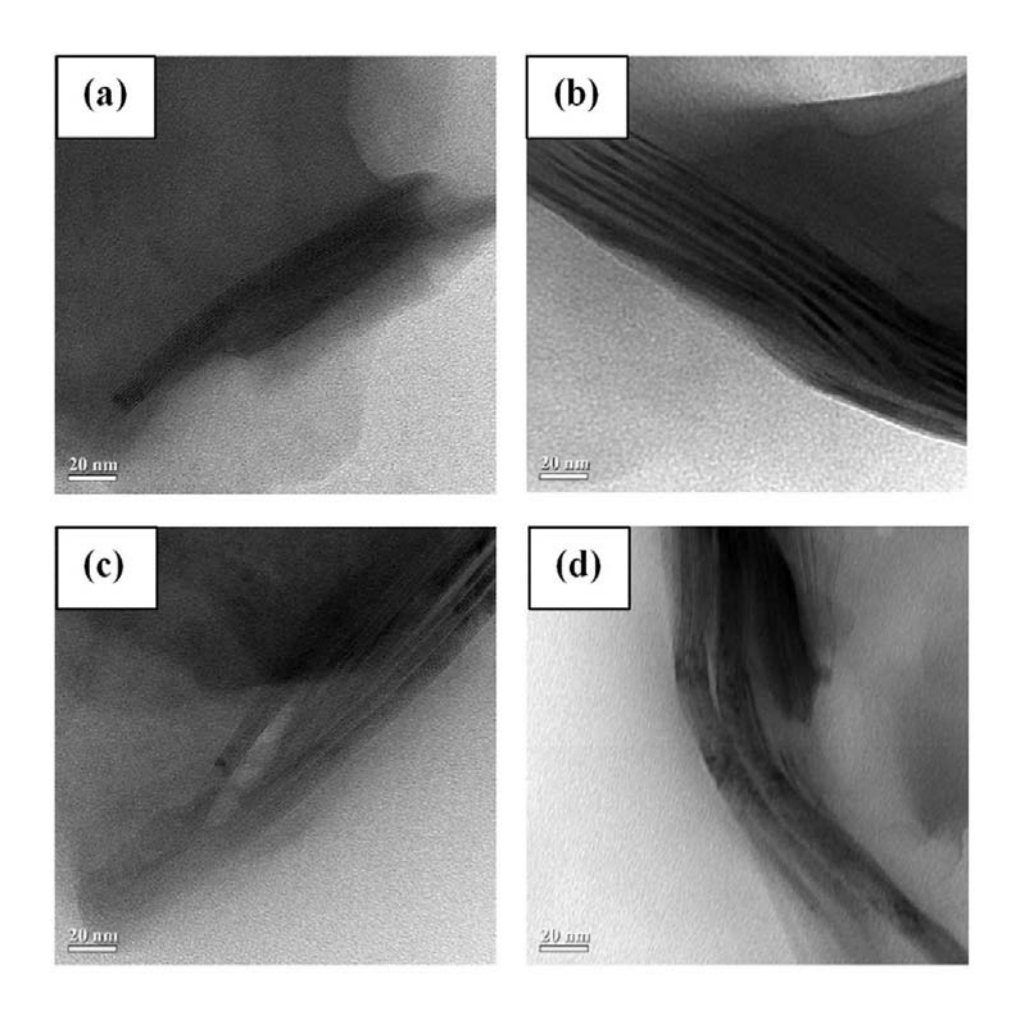


Figure 4

Representative TEM micrographs of CS-g-poly(AA-co-HEMA)/mica composite hydrogels synthesized with mica loadings of (a) 5%, (b) 7%, (c) 10% and (d) 15% w w-1 based on the monomer. $104x115\text{mm} \ (300 \ x \ 300 \ \text{DPI})$

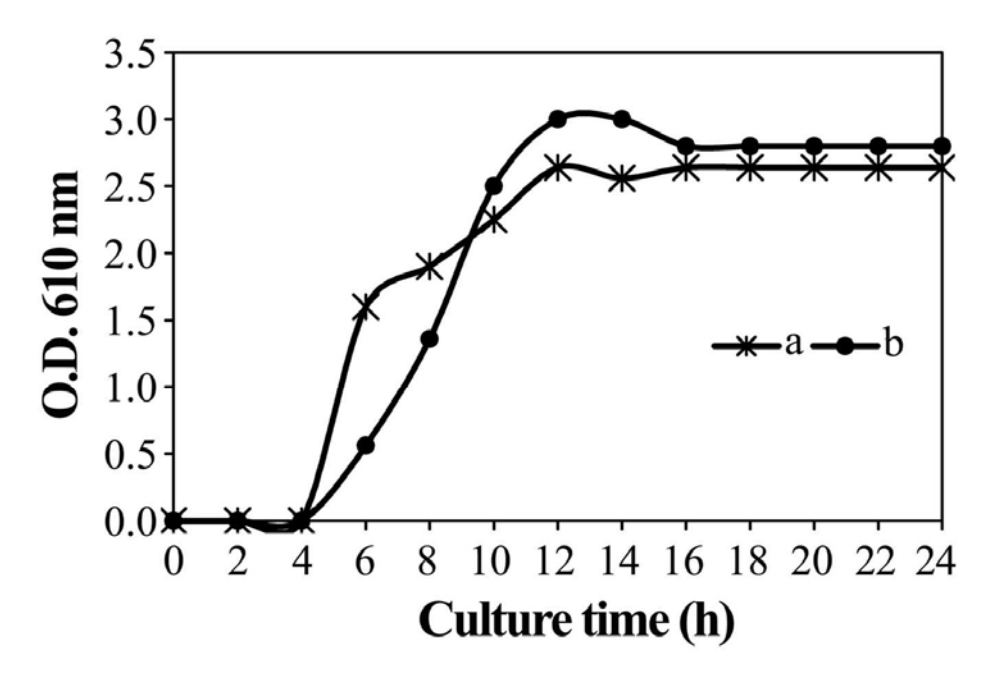


Figure 5

The optical density at 610 nm of S. aureus cultured in HMB media at various culture times with (a) the negative control, or 250 mg ml-1of (b) CS-g-poly(AA-co-HEMA) hydrogel prepared with 1 g CS, a AA: HEMA molar ratio of 1:1, and N-MBA, APS and TEMED at 10%, 10% and 40% w w-1 of CS, respectively, with polymerization performed at 250 pm and 60 °C for 60 min. 59x45mm (600 x 600 DPI)

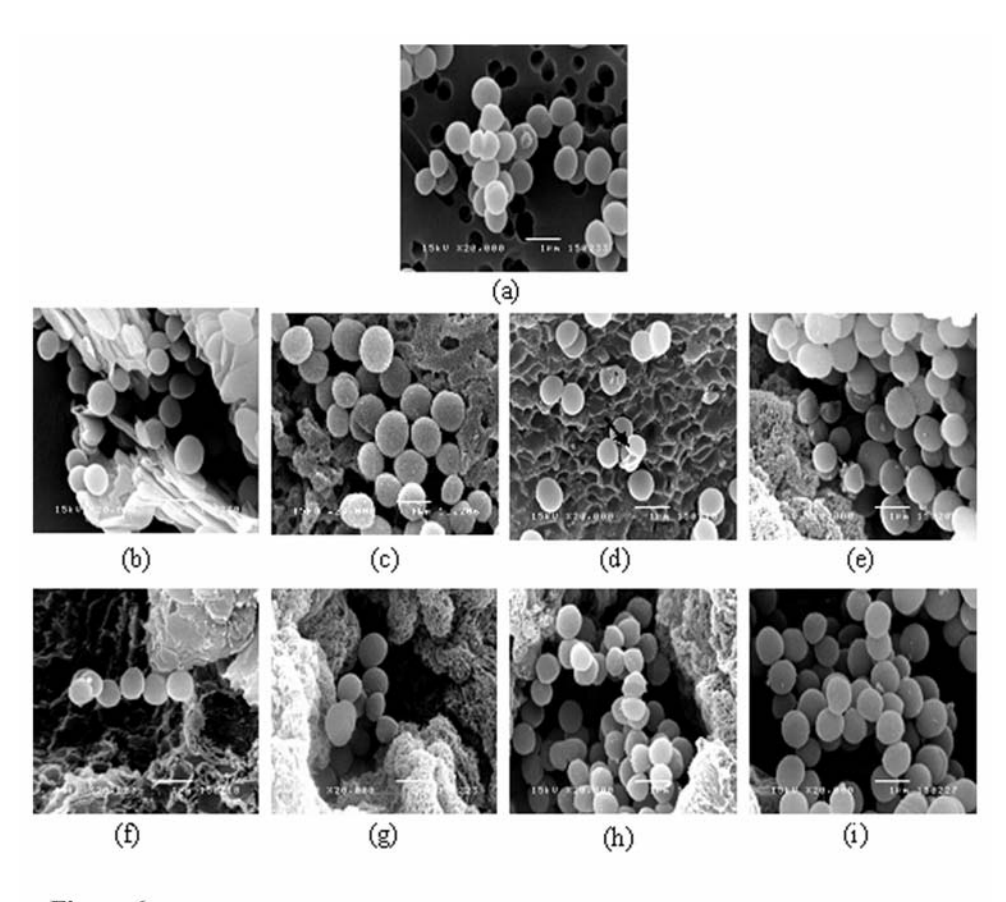


Figure 6

Representative SEM micrographs of S. aureus after co-culture for 24 h with (a) negative control, (b) mica, (c) CS-g-poly(AA), (d) CS-g-poly(HEMA), (e) CS-g-poly(AA-co-PHEMA) and CS-g-poly(AA-co-PHEMA)/mica nanocomposites with mica loadings of: (f) 5%, (g) 7%, (h) 10% and (i) 15% w w-1 based on the monomer. The arrow in (d) highlights a damaged cell. 152x142mm (600 x 600 DPI)

KAPOK I: CHARACTERISTCS OF KAPOK FIBER AS A POTENTIAL PULP SOURCE FOR PAPERMAKING

Somporn Chaiarrekij,* Apiporn Apirakchaiskul, Kuntinee Suvarnakich, and Suda Kiatkamjornwong

The potential use of kapok fiber for pulping and papermaking has been investigated. The kapok fibers were cooked using the optimal dosage of sodium hydroxide determined from the experiments. Then, the pulp was refined twice using a disc refiner with a disc gap of 1/100 inch and this kapok pulp was mixed with commercial hardwood pulp and/or softwood pulp at different blend ratios to make papers. Addition of the kapok pulp to the mixed pulps improved the tensile and burst strengths of the sheets but decreased the tear resistance and elongation. Brightness and opacity of the sheets were also dropped with the addition of kapok pulp to the mixed pulps. Water repellency of the sheets prepared from the kapok pulp mixed with the commercial pulps was also improved. These results indicate that kapok fiber can be a quality pulp source for papermaking, especially for packaging paper.

Keywords: Kapok fiber; Properties; Raw material; Papermaking

Contact information: Department of Imaging and Printing Technology, Faculty of Science, Chulalongkorn University, Phayathai Road, Bangkok, 10330 Thailand; *Corresponding author: Huaja@hotmail.com

INTRODUCTION

The kapok tree, Ceiba pentandra (L.) Gaertn. (Malvales: Malvaceae), formerly Bombacaceae family, is cultivated widely in Southeast Asia, as well as other parts of East Asia and Africa. The kapok fiber is an agricultural product obtained from the fruits of the kapok tree (Tang et al. 2008; Qiuling and Lin 2009). Kapok fibers have a hollow structure with a thin fiber wall and large lumen (Hong et al. 2005; Lim and Huang 2007). The diameter including the fiber wall is $16.5 \pm 2.4 \, \mu m$. The lumen diameter is $14.5 \pm 2.4 \, \mu m$ μ m and the fiber length is 25 \pm 5 μ m (Huang and Lim 2006). Kapok fibers are fluffy, light-weight and too inelastic to be spun, and so are good for stuffing beds, pillows and cushions. Chemical compositions of kapok fiber were differently reported by two groups of researchers. The first one mentioned that kapok fiber is chemically composed of 64% cellulose, 13% lignin and 23% pentosan on a weight basis (Kobayashi et al. 1977) while the other stated that it comprises of 35% cellulose, 21.5% lignin, 22% xylan and 13% of acetyl groups on a weight basis (Hori et al. 2000). Besides all those mentioned chemical compositions, they also contain a waxy cutin on the fiber surface which makes them water repellent and oil absorbent. Thus, they are also useful in oil removal applications (Hori et al. 2000; Khan et al. 2004; Huang and Lim 2006; Rengasamy et al. 2011).

There are few reports on utilizing blended kapok fibers for papermaking, such as, the blend of 75:25 (w/w) kapok fibers: bamboo pulp was treated with detergent and

sodium hydroxide before being used to produce paper (Malab et al. 2001). In this case, the combination of the two non-wood fibers significantly reduced the volume of the bamboo pulp, and the amounts of chemical reagents and energy consumption, without adversely affecting the paper strength properties. Another study has indicated that kapok fibers could potentially be pulped to produce paper (Chaiarrekij et al. 2008), but this claim has not been established and any products have not been further characterized. However, it has been observed that paper sheets made from kapok pulp seemed to demonstrate superior water resistant behavior even without any sizing agents being added.

Consequently, the optimum set of pulping conditions for the kapok fibers to give the best strength properties was investigated. This optimal set of pulping conditions was then employed to produce kapok pulp. The influence of kapok pulp on paper properties when the kapok pulp was mixed with commercial hardwood pulp and softwood pulp was also determined. The hypothesis being tested was that kapok pulp might increase the strength properties of the hybrid paper prepared from mixtures of kapok pulp with conventional commercial softwood pulp and/or hardwood pulp. It was thought that as well as providing better strength, paper made of kapok pulp might possess superior water resistance, which is generally required for a packaging paper.

EXPERIMENTAL

Materials

Before pulping, the kapok fibers (sourced from the north eastern part of Thailand) were washed, cleaned, and immersed in water for three weeks prior to manually squeezing out the excess water and cutting to 3-5 cm in length. The moisture content was determined using the moisture balance (FD-600, Kett Electric Laboratory, Japan). The commercial softwood (SW) pulp from Pine and hardwood (HW) pulp from Eucalyptus were obtained from the Crofton Pulp & Paper Mill, Canada and the Phoenix Pulp & Paper Public Co., Ltd, Thailand, respectively.

Methods

The experiment was divided into 2 parts. The first part was about determination of optimal pulping condition for kapok fiber, while the second part was about examining the effects of kapok pulp addition to commercial softwood and hardwood pulps on the properties of the resultant pulp and paper.

Determination of optimal pulping condition for kapok fiber

Kapok fibers were separately pulped using 10, 15, 20, and 25% (w/w) NaOH, based on the oven-dried pulp weight. The liquor-to-wood ratio was 17:1. The pulping was carried out in an autoclave digester, (UEC-2017A, Universal Engineering, India) with an initial digesting temperature at 40 °C. The pulp matrix was then gradually heated to 120 °C over 30 min. Pulping was proceeded at this temperature for another 120 min. The pulp was then extensively washed with tap water to remove the alkalinity from the pulp by controlling with a pH meter (Hanna HI 98128, Hanna Instrument, U.S.A.).

Kapok pulps were refined twice through a disc refiner, using a 1/100 inch disc gap (Andritz Sprout, U.S.A.). The degree of refining was determined following the Canadian Standard Freeness (CSF) standard, using a freeness tester (CF/A, Regmed, Brazil) according to TAPPI Standard Method T227 om-04. Kapok pulps were disintegrated in a standard disintegrator (Formax T-100, Adirondack, U.S.A.) for 100,000 revolutions in hot water (80 °C) to remove latency. The average length of 5,000 fibers per sample was automatically determined using a fiber quality analyzer (FQA, Optest, Canada) according to the TAPPI Standard Method T271 om-98 using the following equations.

The arithmetic average length of individual fibers (L) is calculated from equation (1):

$$L = \underbrace{\sum n_i l_i}_{\sum n_i} \tag{1}$$

The length-weighted average length of the fibers (L_1) is calculated from equation (2):

$$L_1 = \frac{\sum n_i l_i^2}{\sum n_i l_i} \tag{2}$$

The weight-weighted average length of the fibers $(L_{\rm w})$ is calculated from equation (3):

$$L_{\rm w} = \frac{\sum n_i l_i^3}{\sum n_i l_i^2} \tag{3}$$

where the number of fibers (n_i) is the number of fibers in each class of length (l_i) .

The chemical composition of each pulp was determined using TAPPI Standard Method T222 om-98 for lignin determination, TAPPI Standard Method T203 cm-99 for alpha cellulose (α -cellulose) determination, and Browning's method for holocellulose determination (Browning 1963). The amount of hemicellulose was calculated from the difference between the holocellulose content and the alpha cellulose content.

Kapok pulp was also made into 60 g/m² handsheets on a Rapid-Köthen sheet former (RK-2A KWT, PTI, Austria) according to the ISO Standard Method 5269-2. The brightness and opacity of the handsheets were measured using an optical tester (Color Touch PC, Technidyne, U.S.A.), based on ISO Standard Methods 2470 and 2471, respectively. The tensile, burst, tear, and zero-span tensile strengths were measured using a tensile strength tester (Strograph E-S, Toyo Seiki, Japan), a burst strength tester

(SE002P, Lorentzen & Wettre, Sweden), a tear strength tester (Protear, Thwing-Albert, U.S.A.), and a modified tensile strength tester (Pendulum Tensile Strength Tester with special clamps adjustable to zero, Toyo Seiki, Japan), according to TAPPI Standard Method T494 om-01, T403 om-02, T414 om-04 and T231 cm-96, respectively. The contact angle of water in contact with surface of handsheet was automatically measured using the Pocket Goniometer PG-3 (Fibro System, Sweden) by capturing and processing the water droplet images. The dynamic mode was used to measure the rate of change of the contact angle as a function of time. The test was done following TAPPI standard T558 om-06.

The effects of the addition of kapok pulp to commercial softwood pulp and hardwood pulps on the properties of the resultant paper samples

Kapok pulp produced by using the set of optimal conditions previously described was bleached using 3% (w/w) aqueous hydrogen peroxide at a 1.5% consistency and 80 °C for 120 min. The product was disintegrated using a disintegrator (Formax T-100, Adirondack Machine, U.S.A.) for 100,000 revolutions in hot water (80 °C) to remove latency. Each commercial pulp was beaten in a valley beater (UEC-2018A, Universal Engineering, India) in which 360 g of the oven-dried pulp in 23 L of water was accommodated, according to TAPPI Standard method T200 sp-01. The softwood pulp and hardwood pulp were separately beaten to meet the Canadian Standard Freeness of 350 mL and 300 mL, respectively. Then, the bleached kapok pulp was mixed with the commercial beaten hardwood pulp, softwood pulp and mixed pulp (25:75 (w/w) softwood: hardwood) to make handsheets. These procedures of papermaking and paper characterization were repeated in the manner as described.

Statistical analysis

Parametric data were analyzed using the analysis of variance (ANOVA). In all cases, a p-value smaller than or equal to 0.05 was accepted as being a statistically significant difference. For all of the experiments, three replicates were performed.

RESULTS AND DISCUSSION

Determination of Optimal Pulping Condition

Chemical composition of kapok pulp

The effects of the sodium hydroxide solution on the chemical composition of the kapok pulp are summarized in Table 1. Analysis of the chemical composition of the pulps showed that an increased amount of sodium hydroxide in cooking liquor resulted in lower percentages of lignin, higher percentages of holocellulose and alpha cellulose, with lower percentages of hemicellulose. It should be noted that holocellulose is composed of alpha cellulose and hemicellulose. This finding was to be expected, since sodium hydroxide solution dissolves lignin. Carbohydrates, especially hemicellulose, can also be easily destroyed by sodium hydroxide, leaving a higher ratio of alpha cellulose behind. Since all of the P-values of the chemical compositions were lower than 0.05, the effects of sodium

hydroxide solution on kapok pulp chemical compositions were thus statistically significant.

 Table 1. Effects of Sodium Hydroxide Concentration on the Chemical

Composition of the Kapok Pulp

Pulp Chemical Composition	NaOH Dosage (% w/w)				
	10	15	20	25	P-value
Lignin (%)	19.20	18.27	17.57	17.53	0.0109*
Holocellulose (%)	76.12	76.53	78.49	78.50	0.0005*
Alpha cellulose (%)	65.63	69.87	69.65	69.96	0.0002*
Hemicellulose (%)	10.49	6.66	8.84	8.54	0.0007*
* Statistically significant since P-value is lower than 0.05					

Kapok pulp and fiber characteristics

The effects of sodium hydroxide treatment level on pulp yield, freeness and the average fiber length, characterized in terms of arithmetic, length-weighted, and weight-weighted criteria are summarized in Table 2, along with the percentage of fines.

Table 2. Pulp and Fiber Characteristics of the Kapok Pulp after Soda Pulping

Pulp and Fiber Properties		NaOH Dosage (% w/w)		
	10	15	20	25
Pulp yield (%)	62.40	51.25	44.69	40.46
Freeness (CSF, mL)	401	362	296	277
Average fiber length-Arithmetic (mm)	0.91	0.91	0.83	0.81
Average fiber length-Length weighted (mm)	1.51	1.49	1.32	1.28
Average fiber length-Weight weighted (mm)	2.26	2.17	1.93	1.83
Fines (%)	21.5	21.6	22.7	23.7

The results in Table 2 indicate that high sodium hydroxide concentration could also result in a lower pulp yield because of the removal of lignin and extractives. Also, high sodium hydroxide dosage could lead to carbohydrate degradation, especially with the hemicellulose, due to a peeling reaction. This might also contribute to the lower pulp yield.

Table 2 shows that increasing the concentration of sodium hydroxide significantly decreased the degree of the pulp freeness. Thus, there was a decrease in the pulp's drainage capacity. This was probably due to an increasing amount of fines which would have a significantly greater surface area than fibers for water absorption. Also relevant are the removal of hydrophobic lignin, the dissolution of hemicellulose and possibly the saponification of the cutin wax by the alkali with "solvation" of the cellulose. The latter two possibilities were supported by the results from contact angle studies in which the contact angle with water decreased when the amount of alkali was increased (Fig. 1).

Figure 1 also shows that the handsheets in the dry state (at a zero contact time) had the greater water contact angles. However, after contact with the water, the contact angles decreased due to wetting, absorption, penetration, and spreading of the water under the influence of the cellulosic hydrophilic interactions.

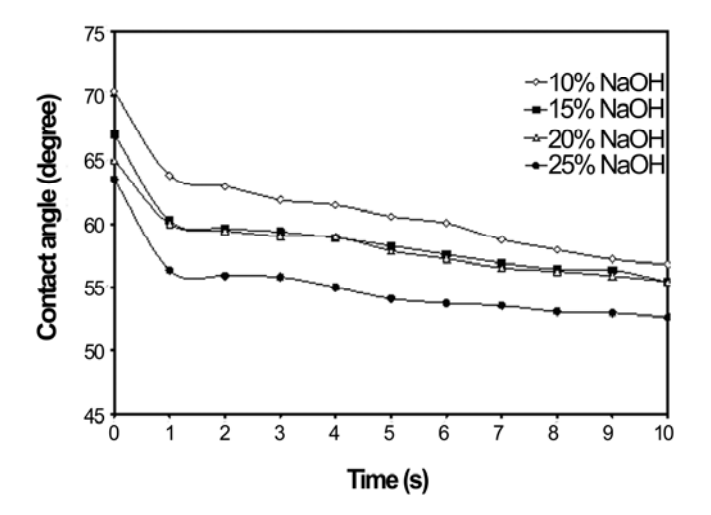


Fig. 1. The effects of different sodium hydroxide concentrations on water contact angles of the kapok fiber sheets.

It should be noted that weight weighted average fiber length is one of the average fiber length values, but it emphasizes more on the content of long fibers as compared to the length weighted fiber length and the arithmetic average fiber length, respectively. When the amount of sodium hydroxide increased, the average fiber length significantly decreased, whilst the fines content was increased (Table 2). This was likely to have occurred because the fibers were damaged by a peeling reaction under the strong alkali conditions leading to carbohydrate degradation (Sjöström 1993). Thus, the greater the amount of carbohydrate that was degraded by the alkali, the lower would be the mean fiber length and the greater would be the amount of fiber fines.

Kapok handsheet properties

The effects of the sodium hydroxide solution on the kapok handsheet properties are summarized in Table 3.

Table 3. Effects of Sodium Hydroxide Concentration on the Kapok Handsheet Properties

Pulp and Paper Properties	NaOH Dosage (% w/w)				
	10	15	20	25	P-value
Apparent density (g/cm ³)	0.68	0.80	0.82	0.88	0.1264
ISO opacity (%)	97.9	97.5	97.4	97.0	0.0235*
ISO brightness (%)	21.3	19.1	18.6	18.1	0.1917
Tensile index (N m/g)	80.3	100.4	111.5	101.3	0.0002*
Elongation (%)	1.75	2.01	2.10	2.05	0.0335*
Burst index (kPa m ² /g)	4.44	5.73	5.96	5.98	0.0348*
Tear index (mN m ² /g)	1.78	1.68	1.60	1.59	0.4005
Zero span tensile index (N m/g)	59.5	58.2	56.7	55.9	0.9801
* Statistically significant since P-value is lower than 0.05					

Increasing the amount of sodium hydroxide solution led to an increase in the apparent density of the sheets which was defined as handsheet grammage divided by

handsheet thickness, but a lower opacity (Table 3). Such effects are likely to be due to the role of sodium hydroxide solution in breaking up lignin molecules within the fiber cell wall. As the hydrophobic lignin was removed, the fiber surface became more hydrophilic, encouraging fiber swelling and conformability. This would result in a more compacted sheet that in turn, which could lead to fewer air-to-fiber interfaces and a lower opacity. In addition, the increasing content of fines and the greater amount of fiber contact areas would help to improve fiber bonding, leading to denser sheets, as indicated by the higher apparent density. Shorter fibers and a greater amount of fines also provided a basis for more effective filling of existing voids, which might also have contributed to lower opacity of the sheet. However, the effect of sodium hydroxide solutions on the apparent density appeared in this case to be statistically insignificant while its effect on opacity was statistically significant.

Pulp brightness would be expected to increase when greater amounts of sodium hydroxide solution were used, since more lignin would be removed. However, the observed trend was the opposite of this expectation, as indicated by the statistical evaluation (Table 3). However, greater concentrations of sodium hydroxide solution might reduce pulp brightness through an alkali darkening reaction, resulting in structural changes of the chromophoric groups in the residual lignin. These groups could also absorb light and thus cause the brightness of the pulp to decrease. An additional plausible explanation might be that the sodium hydroxide solution mediated the removal of lignin and caused greater sheet compactness with a resultant reduced level of light scattering of the sheet, whilst the greater amount of fines might also lead to sheet compactness.

The tensile index defines the tensile strength of paper. It is the tensile strength divided by the grammage. The burst index defines the burst strength of the paper and is equal to the burst strength divided by the grammage. Fiber bonding is highly likely to affect the tensile strength and burst strength. Increasing sodium hydroxide dosage provided higher tensile and burst strengths due to increasing fiber bonding, since lignin was removed and fibers became more conformable (Table 3). Increased fiber bonding caused by the greater sodium hydroxide dosage also led to the higher elongation. However, it should be noticed that using too high dosage of sodium hydroxide was detrimental to tensile and burst strengths as a result of carbohydrate degradation by peeling reaction at a strong alkali condition. The effects of the sodium hydroxide concentration in cooking liquor on the tensile index, the elongation and the burst index were statistically significant.

The tear index, the tear resistance value divided by the grammage, defines the tear resistance of the paper. Tear resistance is affected by many factors, such as the intrinsic fiber strength, the fiber length, and fiber bonding. The most important factor for well-bonded sheets is the fiber strength. The zero span tensile index is defined by the zero-span tensile strength divided by the grammage. Generally, zero span tensile index is a function of both the intrinsic fiber strength and the fiber bonding; however, the intrinsic fiber strength is a major contributing factor. The tear index decreased when the sodium hydroxide concentration increased (Table 3). The same observation was found for the zero span tensile index. This effect could be caused by the peeling reaction that destroys endwise, the chains of cellulose and hemicellulose and by the alkaline hydrolysis that leads to a drop in the degree of polymerization of the fibers (Shatalov and Pereira 2005).

The decrease in tear resistance might also be caused by the shorter fiber length and the greater amount of fines that are created. However, the effects of sodium hydroxide dosage on the tear and zero span tensile index values were so small that they were statistically insignificant.

Overall, the optimum condition for kapok fiber pulping was that of the cooking liquor containing 20% (w/w) of sodium hydroxide, which gave the maximum tensile properties as discussed. Thus, kapok pulp that was prepared using a 20% (w/w) sodium hydroxide dosage was used in subsequent experiments. However, the pulp was bleached before being mixed with commercial pulps.

Effects of Kapok Pulp Addition to Commercial Softwood and Hardwood Pulps on the Properties of the Resultant Pulp and Paper

Fiber length distributions of kapok, softwood and hardwood pulps

The fiber length distributions of the kapok pulp that was produced using the cooking liquor of 20% (w/w) sodium hydroxide and the commercial softwood pulp and hardwood pulp are shown in Fig. 2.

The kapok pulp had an intermediate amount of short fibers that was less than that of the hardwood pulps. The softwood pulp gave the lowest short fiber content. The kapok pulp was also intermediate in the amount of both medium and long fibers. These were lower than that from the hardwood pulp. The softwood pulp contained the greater amount of long fibers.

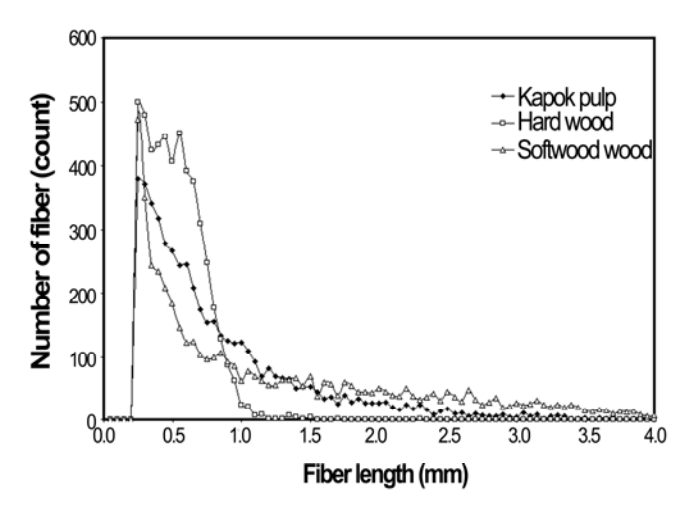


Fig. 2. Fiber length distributions of the kapok, hardwood and softwood pulps.

Fiber length, fines content and zero span tensile index of kapok, softwood and hardwood pulps

Fiber length, fines content and zero span tensile index of kapok, softwood and hardwood pulps are compared and illustrated in Table 4.

Table 4. Fiber Length, Fines Content and Zero Span Tensile Index of Kapok and the Commercial Pulps

Pulp Properties	Pulp Types					
	Kapok Softwood (SW) Hardwood (HW)					
Average fiber length-Arithmetic (mm)	0.83	1.25	0.50			
Fines (%)	22.7	43.2	34.0			
Zero span tensile index (N m/g)	56.7	82.6	44.2			

After being refined to the freeness of 300 mL as shown in Table 4, the average fiber length of the kapok pulp (0.834 mm) was between those of the softwood pulp (1.253 mm) and hardwood pulp (0.496 mm). The kapok pulp also had the lowest level of fines, followed by the hardwood pulp and softwood pulp, respectively.

As shown in Table 4, the sheets made from the softwood and hardwood pulps had the greatest and least zero-span tensile index at 82.6 and 44.2 N m/g, respectively. That made from kapok pulp was 56.7 N m/g. Since kapok fiber was brittle, this led to the lower zero span tensile index of kapok pulp.

Apparent density

The apparent densities of the sheets that were prepared from different ratios of the kapok pulp to the commercial softwood (SW), hardwood (HW) and softwood-hardwood mixed pulps, are shown in Fig. 3.

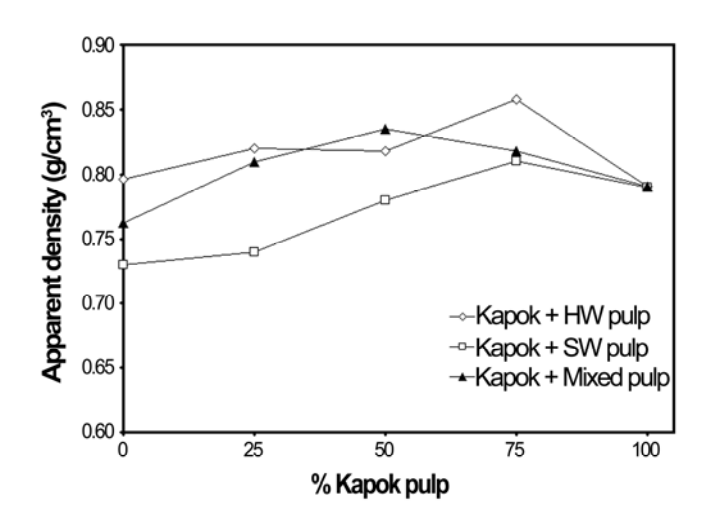


Fig. 3. Apparent density of the sheets made from kapok pulp mixed with the commercial hardwood (HW) pulp and softwood (SW) pulp at the indicated percentages.

The sheets made from the hardwood pulp had a greater apparent density than those containing either the softwood pulp or the kapok pulp. That is because the shorter fibers of the hardwood pulp fill the voids and pores in the sheet structure, making the sheets more compact. The inclusion of kapok pulp increased the apparent density of the sheets in all of the pulp mixtures. This could be because the kapok fibers have very thin cell wall, being easily collapsed, making more compact sheets. However, sheets derived

from the pure kapok pulp were not greater in apparent density, as seen by the fact that the kapok fibers become easily entangled. Thus, pure kapok sheets gave poor sheet formation and an irregular sheet surface.

Tensile index and burst index

The sheets made from kapok pulp gave the highest tensile index (Fig. 4). This could be because the kapok fibers were long and the lumens were easily collapsed when forming paper, producing highly bonded regions and denser sheets with a resulting superior sheet tensile index.

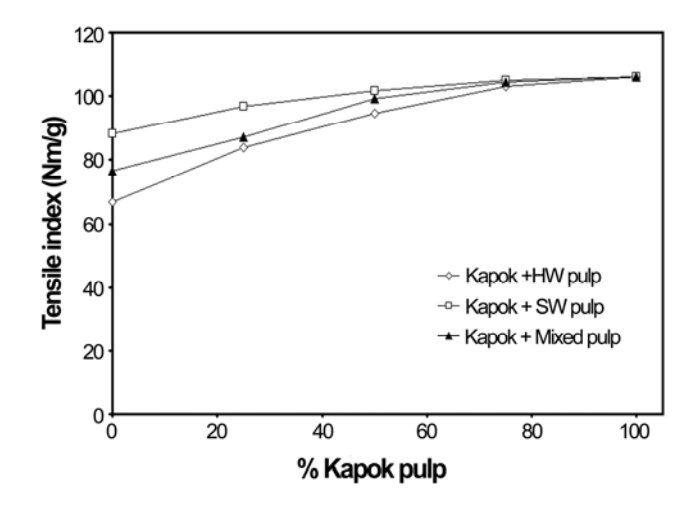


Fig. 4. Tensile index of the sheets made from kapok pulp mixed with the commercial hardwood (HW) pulp and softwood (SW) pulp at the indicated percentages.

The sheets made from the hardwood pulp produced the lowest tensile index. Those made from a 75:25 (w/w) blend of the hardwood: softwood pulps had a medium tensile index. Those made from the pure softwood pulp gave the greatest tensile index. With respect to kapok-commercial pulp mixtures, as the ratio of kapok pulp increased, the tensile index also increased (Fig. 4). However, the results were more prominent when the kapok pulp was mixed with the hardwood pulp than with the softwood pulp.

The sheets derived from the pure kapok pulp gave the highest burst index, the values being somewhat similar to those of the sheets made from the softwood pulp (Fig. 5). This is because both kapok fiber and the softwood fiber are long and have extensive contact areas that are available for fiber bonding. The sheets made from the hardwood pulp had the lowest burst index. This is because the hardwood pulp contained a greater amount of short fibers, resulting in poor bonding. As the ratio of the kapok pulp in mixtures with the hardwood pulp or the 75:25 ratios (w/w) of hardwood pulp: softwood pulp increased, the burst indexes of the resultant paper significantly increased, because fiber bonding was greatly improved.

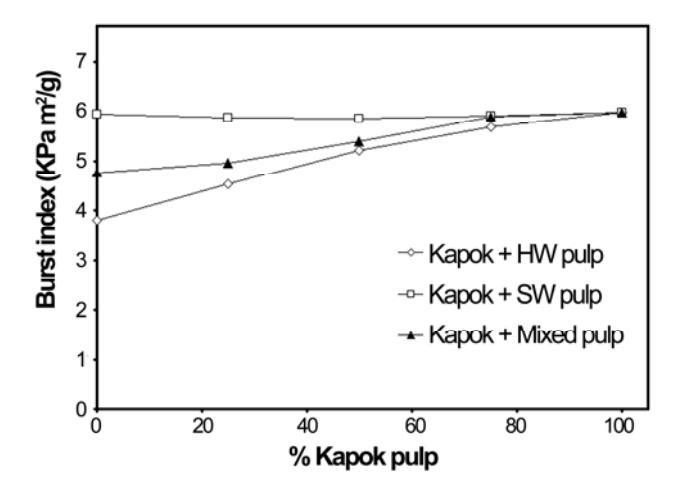


Fig. 5. Burst index of the sheets made from kapok pulp mixed with the commercial hardwood (HW) pulp and softwood (SW) pulp at the indicated percentages.

Tear index and elongation

One of the key characteristics of kapok fibers is their brittleness. Thus, the sheets made from the kapok pulp had the lowest tear index relative to those made from the commercial softwood pulp, the hardwood pulp, and the softwood-hardwood mixed pulp. For kapok-commercial pulp mixtures at different ratios, it was clearly observed that as the ratio of kapok pulp increased, the tear index significantly decreased (Fig. 6).

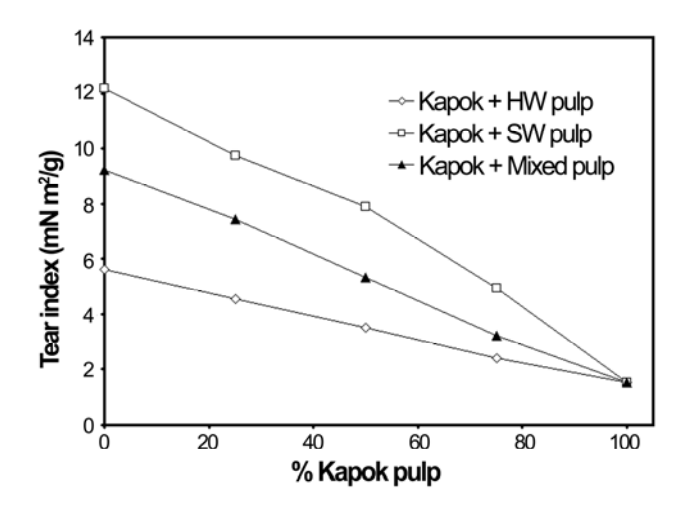


Fig. 6. Tear index of the sheets made from kapok pulp mixed with the commercial hardwood (HW) pulp and softwood (SW) pulp at the indicated percentages.

The elongation of the sheets that were prepared from different ratios of the kapok pulp is compared in Fig. 7. Sheets made from kapok pulp had the lowest elongation. This is because the key characteristics of kapok fibers are their brittleness and inelasticity, which might reduce the elongation of the sheets when a load was applied. Thus, as the

ratio of the kapok pulp was increased, the elongation significantly decreased in all pulp mixtures.

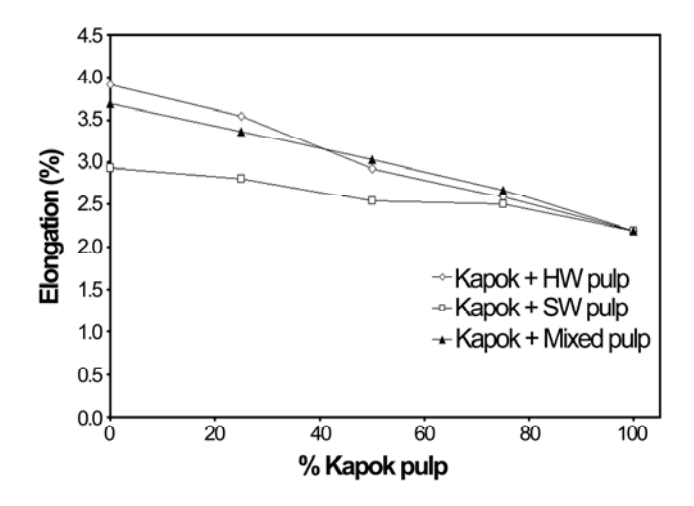


Fig. 7. Elongation of the sheets made from kapok pulp mixed with the commercial hardwood (HW) pulp and softwood (SW) pulp at the indicated percentages.

Water contact angle

The water contact angles of the sheets made from kapok pulp mixed with the commercial softwood pulp and hardwood pulp are shown in Fig. 8. As seen in Fig. 8, K 100 represented handsheets made from 100% kapok pulp. HW100 indicated handsheets made from 100% hardwood pulp while SW100 illustrated handsheets made from 100% softwood pulp. M100 designated handsheets made from mixed pulp (25:75 (w/w) softwood pulp: hardwood pulp). Handsheets prepared from kapok pulp mixed with hardwood, softwood and mixed pulps with different percentages characterized by K: HW, K: SW and K: M with the percentage indicated in parenthesis.

The results indicated that as the time of contact increased, the water contact angles decreased because of absorption and penetration of the water droplets into the sheet. Those made from 100% kapok pulp gave the greatest values for the water contact angle. This effect was due to the unique characteristics of the kapok fibers having a wax coating on the surface. Although the kapok fibers were pulped, some of the wax was still present. When mixed with the commercial pulps (softwood, hardwood and mixed pulps), as the ratio (w/w) of the kapok pulps increased, the water contact angle values increased.

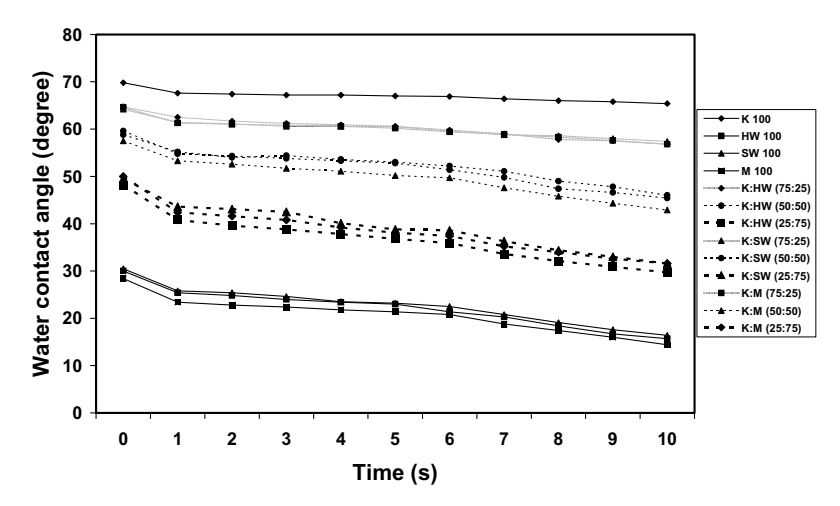


Fig. 8. Water contact angles of the sheets from the kapok (K) pulp mixed with the commercial hardwood (HW) pulp, softwood (SW) pulp and mixed (M) pulp at the indicated percentages.

CONCLUSIONS

- 1. When kapok pulp was mixed with the commercial softwood pulp and/or hardwood pulp, the tensile and burst strengths of the blended sheets increased but with the lower tear resistance and elongation due to the excellent tensile strength and brittleness of kapok pulp.
- 2. Brightness and opacity of the blended sheets decreased when higher amounts of kapok pulp were added in the pulp mixture due to the yellowness of the kapok pulp.
- 3. Handsheets containing kapok pulp gave greater water contact angles due to the hydrophobic nature of kapok fibers.
- 4. Thus, kapok pulp can potentially be mixed with the commercial softwood pulp and/or hardwood pulp to produce commercial packaging paper when the strength and light weight characteristics are required.

ACKNOWLEDGMENTS

This research was financially supported by a Research Team Aid Grant from the Thailand Research Fund and Commission of Higher Education under the contract number RTA5080004. The authors would like to thank the Department of Imaging and Printing Technology of Chulalongkorn University, and the Product and Technology Development Center of Siam Cement Group Paper Company Limited for providing relevant research facilities.

REFERENCES CITED

Browning, B. L. (1963). *Methods in Wood Chemistry*, Interscience Publishers, New York.

- Chaiarrekij, S., Wongsaisuwan, U., and Watchanakit, S. (2008). "Papermaking from Kapok fiber," *Thai Petty Patent*, 4279, June 13, 2008.
- Hong, X., Wei-dong, Y., and Mei-wu, S. (2005). "Structure and Performances of the Kapok Fiber," *Journal of Textile Research* 26(4), 4-6.
- Hori, K., Flavier, M. E., Kuga, S., Lam, T. B. T., and Liyama, K. (2000). "Excellent oil absorbent kapok [*Ceiba pentandra (L.) Gaertn.*] fiber: Fiber structure, chemical characteristics, and application," *J. Wood Sci.* 46(5), 401-404.
- Huang, X. F., and Lim, T. T. (2006). "The performance and mechanism of hydrophobic—oleophilic kapok filter for oil/water separation," *Desalination* 190(1-3), 295-307.
- Khan, E., Virojnagud, W., and Ratpukdi, T. (2004). "Use of biomass sorbents for oil removal from gas station runoff," *Chemosphere* 57, 681-689.
- Kobayashi, Y., Matsuo, R., and Nishiyama, M. (1977). "Method for adsorption of oils," *Japanese Patent*, 52,138,081, November, 17, 1977.
- Lim, T.-T., and Huang, X. (2007). "Evaluation of Kapok (*Ceiba pentandra* (L.) Gaertn.) as a Natural Hollow Hydrophobic-Oleophilic Fibrous Sorbent for Oil Spill Cleanup," *Chemosphere* 66, 955-963.
- Malab, S. C., Agrupis, S., Cabalar, L., and Ballesteros, R. (2001). "Paper sheets from bamboo and kapok," *PCARRD Press Release* No.153, December, 14, 2001.
- Qiuling, C., and Lin, W. (2009). "Structure and Property Contrast of Kapok Fibre and Cotton Fibre," *Contton Textile Technology* 37(11), 668-670.
- Rengasamy, R.S., Dipayan, D., and Karan, P.C. (2011). "Study of Oil Sorption Behavior of Filled and Structured Fiber Assemblies Made from Polypropylene, Kapok and Milkweed Fibers," *Journal of Hazardous Materials* 186(1), 526-532.
- Shatalov, A. A., and Pereira, H. (2005). "Kinetics of polysaccharide degradation during ethanol-alkali delignification of giant reed-Part 1. cellulose and xylan," *Carbohydr. Polym.* 59(4), 435-442.
- Sjöström, E. (1993). *Wood Chemistry-Fundamentals and Applications*, 2nd ed., Academic Press, San Diego.
- Tang, A.-m., Sun, Z.-h., Fu, X., Zi, M., Zhang, H.-w., Chen, G., and Lin, Y. (2008). "Chemical and Structural Characteristics of Kapok Fibers," *Zhongguo Zaozhi Xuebao/Translations of China Pulp and Paper* 23(3), 1-5.

Article resubmitted: July 31, 2011;

Elsevier Editorial System(tm) for Journal of Chromatography A Manuscript Draft

Manuscript Number:

Title: Comparative study of the mesostructure of natural and synthetic polyisoprene by SEC-MALS and AF4-MALS

Article Type: Full Length Article

Keywords: Field flow fractionation; size exclusion chromatography; polyisoprene; multi angle light

scattering; rubber

Corresponding Author: Mr. Stéphane Dubascoux,

Corresponding Author's Institution: Montpellier SupAgro

First Author: Stéphane Dubascoux

Order of Authors: Stéphane Dubascoux; Chalao Thepchalerm; Eric Dubreucq; Suwaluk Wisunthorn;

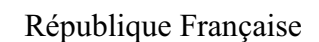
Laurent Vaysse; Suda Kiatkamjornwong; Charoen Nakason; Frédéric Bonfils

Suggested Reviewers: Stepan Podzimek stepan.podzimek@synpo.cz expert in AF4 and polymer science

Bruno Grassl bruno.grassl@univ-pau.fr expert in polymer science

Yacine Hemar y.hemar@auckland.ac.nz expert in physico-chemistry of colloidal system

Opposed Reviewers:





CENTRE INTERNATIONAL D'ETUDES SUPERIEURES EN SCIENCES AGRONOMIQUES

DEPARTEMENT DES SCIENCES POUR LES AGRO-BIOPROCEDES

UMR INGENIERIE DES AGROPOLYMERES ET TECHNOLOGIES EMERGENTES (UMR 1208 IATE, CIRAD-INRA-MONTPELLIER SUPAGRO-UM2)

Dr. Stéphane Dubascoux Tel: +33 (0) 499613016

Email: stephane.dubascoux@supagro.inra.fr

Montpellier, 05th July 2011

Cover letter

Dear Managing Editor,

Please find enclosed the submission of our regular research paper entitled: "Comparative study of the mesostructure of natural and synthetic polyisoprene by SEC-MALS and AF4-MALS". In this article, we present the first original results about natural and synthetic rubber characterization by asymmetrical flow field flow fractionation (AF4). Mesostructure evaluation by AF4 is compared with that obtained with size exclusion chromatography.

Up to now, there is a real lack of information concerning natural rubber mesosctructure and more precisely about the presence and the nature of microaggregates (gel content) among the linear polyisoprene chains. AF4 allows assessing simultaneously both the distribution of polyisoprene chains and gel content. Results obtained allow to validate the AF4 fractionation (compared to SEC results) and to consider the gel part of polyisoprene samples.

For these reasons, we think that our article matches with the topic of your journal and is appropriate for publication in journal of chromatography A.

Sincerely yours,

The authors: Stephane Dubascoux, Chalao Thepchalerm, Eric Dubreucq, Suwaluk Wisunthorn, Laurent Vaysse, Suda Kiatkamjornwong, Charoen Nakason, Frederic Bonfils

1 Comparative study of the mesostructure of natural and synthetic

- 2 polyisoprene by SEC-MALS and AF4-MALS.
- 3 Stephane Dubascoux*¹, Chalao Thepchalerm^{1,2,6}, Eric Dubreucq¹, Suwaluk Wisunthorn³,
- 4 Laurent Vaysse⁴, Suda Kiatkamjornwong⁵, Charoen Nakason², Frederic Bonfils*⁶
- 6 ¹ Montpellier SupAgro, UMR IATE 1208, 2 Place Viala, 34060 Montpellier, France
- ² Center of Excellence in Natural Rubber Technology, Faculty of Science & Technology,
- 8 Prince of Songkla University, Pattani campus, Thailand
- 9 ³ Faculty of Science and Industrial Chemistry, Prince of Songkla University, Surat Thani
- 10 campus, Thailand

5

15

- 11 ⁴ CIRAD, UMR IATE 1208, KU-CIRAD laboratory, Agroindustry building 3, 7th Floor,
- 12 Kasetsart University, Bangkok 10900, Thailand
- 13 ⁵ Faculty of Science, Chulalongkorn University, Bangkok, Thailand
- 14 ⁶ CIRAD, UMR IATE 1208, 2 Place Viala, 34060 Montpellier, France

Abstract

This paper presents results from the first analyses of the mesostructure of natural rubber (NR) by asymmetrical flow field flow fractionation (AF4). The results are compared with those obtained by size exclusion chromatography (SEC) in terms of average molar masses, radius of gyration and insoluble part (or gel quantity). Comparable results were obtained for the sample not containing gel. Conversely, for samples with gel, significant differences were found due to the presence of microaggregates. In fact, contrary to SEC, AF4 fractionation enables partial fractionation of polyisoprene chains and microaggregates in a single run without preliminary treatment. The results presented here also highlight the special structure (very compact spheres) of microaggregates in NR compared to chemical crosslinked microaggregates in synthetic polyisoprene. The advantages and drawbacks of both techniques for analysing NR samples are also discussed.

Introduction

30

31 For natural rubber (NR), as for numerous biopolymers, it is rather simplistic to speak about 32 macromolecular structure. Indeed, biopolymers often exhibit a complex associative structure, 33 a mixture of macromolecular chains, microaggregates and macroaggregates [1,2]. Because of 34 that, the term mesoscopic structure or mesostructure, which includes both macromolecular 35 structure and aggregate characterization, is increasingly being used. Although NR 36 mesostructure has been studied for many years, the origins of its unique properties are not yet 37 fully clear. Recently, Kim et al. [3,4] revisited the mesostructure of NR. Kim et al. [3,4] analysed NR samples with SEC-MALS and showed that the soluble part injected into a SEC 38 39 system contained very few branched macromolecules, contrary to earlier published studies [5-40 7]. Kim et al. [3,4] showed that the soluble part of NR in solution in tetrahydrofuran (THF) was composed of a mixture of linear chains and assumed compact microaggregates ($R_g \approx 110$ -41 42 130 nm). They showed that to more effectively ascertain the mesostructure of NR, as is the 43 case with most polymers, a MALS detector coupled with SEC is required to avoid a 44 misunderstanding of the structure. From a mechanistic point of view, many mechanisms have 45 been proposed to explain the associative structure of NR [8-11]. The most recent proposal is Tanaka's group scheme involving a protein and a phospholipid at each end of the poly(cis-46 47 1,4-isoprene) chain. These two reactive end chains would appear to be involved in what they 48 called the "naturally occurring network" of NR [12,13]. 49 Today, many tools are available for macromolecule analysis. Of these techniques, size 50 exclusion chromatography (SEC) and field flow fractionation (FFF) are tools of choice to 51 fractionate macromolecules according to their sizes. SEC is beyond doubt the most popular 52 and developed technique for polymer separation. However, a recent study has also highlighted 53 some difficulties for NR separation with SEC coupled with a multi-angle light scattering 54 (MALS) detector because of an abnormal elution phenomenon [3]. This abnormal elution is

due to co-elution of microaggregates with short chains. Kim et al. [3] showed that the abnormal elution occurring with NR could be overcome by treating the SEC columns with an ionic surfactant. After treatment, it was possible to separate these compact microaggregates from linear random coil polyisoprene chains [3]. However, it is difficult to be sure whether or not all microaggregates elute and the procedure is rather cumbersome. The solution to this SEC limitation for NR sample analysis might be the use of techniques based on field flow fractionation. Recent reviews have demonstrated the potentiality of FFF in various fields, such as polymer science [14], biomolecule characterization [15], nanoparticles [16] or the environment [17]. Moreover, FFF could easily be coupled on-line with different detectors, such as a refractive index detector, an ultra-violet detector, a light scattering or inductively coupled plasma mass spectrometer [18]. Recently, Messaud et al. [14] emphasized the fact that field flow fractionation techniques can provide effective simultaneous separation of polymer and microgel. The most popular FFF techniques used for polymer fractionation are thermal flow field flow fractionation (Th-FFF) and Flow Field Flow Fractionation (Fl-FFF or F4) [14]. The main difference between these two sub-techniques is the field used for the fractionation. Fractionation takes place in a channel and the field is a thermal gradient for Th-FFF, while it is a crossflow stream carried through an ultrafiltration membrane in the case of Fl-FFF [19]. Up to now, only Th-FFF has been used for NR characterization [20-23]. However, during Th-FFF, macromolecules are separated according to their size and their chemical composition. Thus, heterogeneity in the chemical composition of a given polymer can complicate the determination of macromolecular structure. Asymmetrical Fl-FFF (AsFl-FFF or AF4) is Fl-FFF where the channel is semi-permeable and asymmetric, involving less sample dilution [19]). Natural rubber has been analysed by Th-FFF using either the polyisoprene calibration curve [20,22,23] or a multi-angular light scattering detector (MALS) [21]. Lee and Molnar [23] compared the analysis of natural rubber by Th-FFF and SEC. They

55

56

57

58

59

60

61

62

63

64

65

66

67

68

69

70

71

72

73

74

75

76

77

78

used a calibration curve made with linear standards poly(cis-1,4-isoprene). The analysed NR samples (RSS1 type) had a number-average molar mass (M_n) of about 0.8 million g.mol⁻¹ and a weight-average molar mass (M_w) of about 29 million g.mol⁻¹, M_w being three times higher than that given by SEC. Lee and Molnar [23] showed that the high molar masses and microgels disappeared after mastication of a NR sample in an extruder. The range of molar masses found was between 10,000 and 10 million g.mol⁻¹ (non-masticated RSS). Filtration of the solution through filters with 5 µm pores led to a shift in the fractogram towards lower retention times. This phenomenon was observed for non-masticated rubber but not for masticated rubber. This shift to lower molar masses was attributed to the removal and/or degradation of microgels (or ultra-high molar mass species). They quantified the gel rate (as a % of total rubber, w/w) in the NR samples by Th-FFF and found slightly lower values (RSS 13%, masticated RSS 0%) than with their conventional method – i.e. filtration through a 125 μm wire mesh after 24 h in toluene (RSS 15%, masticated RSS 0%). Fulton and Groves [21] analysed two synthetic polyisoprenes (IR305, Natsyn2200), a polybutadiene (Europrene BR40) and a natural rubber (SMR5L) in cyclohexane by Th-FFF-MALS without any filtration. They showed that the IR305 sample was essentially linear with no gel, as confirmed later by Kim et al. [3] by SEC-MALS, contrary to the Natsyn2200 sample, which had a 25% gel rate and was branched for molar masses above 5.10⁵ g.mol⁻¹. While there was no steric effect in the separation process for the two synthetic polyisoprenes, they observed such an effect for the polybutadiene and the NR samples. As a consequence of this phenomenon, very large entities eluted together with the smaller molecules. Bang et al. [24] used AF4 to characterize and determine the molar mass distribution of styrene-butadiene rubber. This paper presents the first study of synthetic and natural polyisoprene fractionation by AF4 coupled with MALS in an organic solvent (tetrahydrofuran). The peak shape is discussed and the results in terms of average molar masses, radius of gyration and gel content are compared

80

81

82

83

84

85

86

87

88

89

90

91

92

93

94

95

96

97

98

99

100

101

102

103

with those obtained by SEC-MALS. The comparison of AF4-MALS with SEC-MALS also made it possible to evaluate the discrepancies between the two techniques for analysing NR samples.

Material & methods

Samples

111	In order to compare SEC and AF4 results on synthetic polyisoprene and natural rubber (NR),
112	four samples were chosen for their differences in mesostructure. The two synthetic poly(cis-
113	1,4-isoprenes) were Kraton IR 307 (Kraton polymer, Houston, USA) and Nippol 2200 (Zeon
114	Corporation, Louisville, USA). The main difference between these two synthetic
115	polyisoprenes is the gel rate: no gel in the IR307 sample and presence of microgel in Nippol
116	2200. The two natural rubbers, M160 and M121, were TSR5CV (Technically Specified
117	Rubber with a Constant Viscosity) made from monoclonal Hevea brasiliensis latex. The
118	preparation of the samples was described previously [25].
119	In order to reach a sample concentration of 1 mg.mL ⁻¹ , 30 ± 5 mg of the samples was
120	dissolved in about 30 mL of HPLC grade tetrahydrofuran (THF, VWR, West Chester, USA)
121	stabilized with 2,6-di-tert-butyl-4-methylphenol – BHT – (Sigma Aldrich, Saint Louis, USA)
122	at 250 mg.L ⁻¹ . The flasks were precisely weighed (± 0.01 mg) before and after filling with
123	THF to determine the exact concentration of the solutions. The solvent (THF + BHT) was
124	filtered at 0.1 µm before use. Each sample was analysed in triplicate to evaluate measurement
125	repeatability. All solutions were stored in the dark in a water bath at 30°C for 7 days and
126	gently shaken at 30 rpm (rotational agitator REAX 2, Heidolph, Schwabach, Germany) for 1
127	hour each day for optimum dissolution. Before injection, the macrogel and part of the
128	microgels were removed from all the solutions by filtration at a 1 μm cutoff with Acrodisc
129	glass filters (Pall, Port Washington, USA) to avoid both clogging of the column during SEC
130	analysis and a steric effect (resulting in inverse elution) on AF4 fractionation [21].
131	Two monodisperse polystyrene standards at 200 and 1460 kDa from Polymer Standard
132	Service (PSS, Mainz, Germany) were used to assess the quality of the separation/fractionation
133	and detector response for each SEC/AF4 injection series.

AF4 experiments

The AF4 system was a Postnova AF2000 MT series (Postnova Analytics GmbH, Landsberg, Germany) equipped with a channel adapted for organic solvents and a 350 µm spacer. The membrane was made of cellulose material treated for compatibility with organic solvents with a cut-off of 5 kDa (Postnova Analytics GmbH, Landsberg, Germany). The temperature setpoint of the AF4 oven containing the channel was 45°C. The detector flow was kept constant at 0.65 mL.min⁻¹. The focusing step consisted of a flow delivered by the injection port of about 0.2 mL.min⁻¹ with a crossflow of 1 mL.min⁻¹ for 6 minutes. Then, a 1 min transition time was applied to avoid a major pressure drop during the switch from the focus step to the elution step. The programme to decrease the linear crossflow during the elution step was as follows:

Table 1

An autosampler (PN 5300 model, Postnova Analytics GmbH) was used to carry out the 100 µL sample injections.

Detection was carried out with a 7-angle multi-angle light scattering detector (PN 3070 model, Postnova Analytics GmbH) in line with a refractive index detector (2414 model, Waters Corporation, Milford, USA). The data gathered were processed with AF2000 software (Postnova Analytics GmbH) after blank subtraction for the DRI signal (used as a concentration detector) and according to the Berry model with 2nd order polynomial formalism. In fact, it has been shown that this formalism is well adapted for entities with a radius up to 50 nm [26]. As the refractive index detector signal changes during transition steps due to the AF4 functioning principle, five blank (mobile phase) injections were carried out in

each injection series. The refractive index detector signal from the blank injections was subtracted for each sample injected.

For one series, each sample triplicate was injected once. Two series were carried out (i.e. a total of 6 injections was carried out for each sample) with different operators in order to evaluate the reproducibility of the analysis. Prior to each series of injections, the membrane was replaced and the detector was recalibrated.

SEC experiments

The SEC system was based on an on-line ERC 3112 degaser (ERC, Saitama, Japan), a Waters 515 pump (Waters Corporation, Milford, USA) and 3 MIXED-A columns in series: 2 styragel columns (porosity 20 μ m, 300 mm \times 7.5 mm I.D.) from Waters and 1 PLgel column (porosity 20 μ m, 300 mm \times 7.5 mm I.D.) from Varian (Varian, Walnut Creek, USA). All the columns were kept in an oven at 45°C. The detectors were an 18-angle multi-angle light scattering detector (Dawn DSP model, Wyatt Technology, Santa Barbara, USA) and a refractive index detector (Optilab rEX model, Wyatt Technology). Data from angles 5 to 16 were collected and processed with Astra software version 5.3.1 (Wyatt Technology) according to the Berry method with a 2nd order polynomial model. Similarly to the AF4 injection series, each sample triplicate was injected once. Two series were carried out (i.e. a total of 6 injections carried out for each sample).

Theory/calculation

180 Light scattering theory

- 181 For the Berry method with a 2nd order polynomial fit, $[Kc/\Delta R(\theta)]^{1/2}$ is plotted against
- $\sin^2(\theta/2)$. According to the light scattering theory, this plot makes it possible to determine M_{wi}
- and Rgi for each slice of the fractogram from AF4 or the chromatogram from SEC,
- respectively, according to equation 1.

$$\left[\frac{\kappa c}{\Delta R(\theta)}\right]_{i}^{1/2} = \left[\frac{1}{M_{wi}} + \frac{16\pi^2}{3_0^2} \frac{\langle R_g^2 \rangle_i}{M_{wi}} \sin^2\left(\frac{\theta}{2}\right)\right]^{1/2} \quad Equation \ 1$$

- where K is an optical constant
- c is the solute concentration (in g.mL⁻¹)
- 188 θ is the scattering angle
- $\Delta R(\theta)$ is the excess Rayleigh ratio, the ratio of scattered and incident light
- intensity
- M_{wi} is the weight-average molar mass of the solute
- λ_0 is the wavelength of the laser beam in a vacuum (in nm)
- R_g is the gyration radius of the solute (nm)
- 194

179

The optical constant K is given by equation 2.

$$K = \frac{4\pi^2 n_0^2}{N_A^2} \left(\frac{dn}{dc}\right)^2 \quad Equation \ 2$$

- where n_0 is the refractive index of the solvent
- 198 N_A is Avogadro's number
- 199 $\left(\frac{dn}{dc}\right)$ is the differential refractive index increment of the polymer in the solvent
- 200 used

201

For detailed information about the light scattering theory, refer to [27,28].

203

204

Molar mass and radius definitions

The different molar masses calculated and presented are defined as:

206
$$M_n = \frac{\sum_i N_i M_i}{\sum_i N_i}$$
 $M_w = \frac{\sum_i N_i M_i^2}{\sum_i N_i M_i}$ $M_z = \frac{\sum_i N_i M_i^3}{\sum_i N_i M_i^2}$ Equation 3, 4 & 5

207 Where N_i is the number of polymers with molecular weight M_i 209 The radius of gyration (<R_g> or R_z) or root mean square radius (r.m.s) is defined for a non-210 rigid particle as:

$$< R_g > = \frac{\sum_i c_i M_i \langle R_g^2 \rangle_i}{\sum_i c_i M_i} \quad Equation \ 6$$

Gel content calculation

In order to evaluate the amount of gel retained by the 1 μ m filter, the whole peak from the concentration detector (refractive index detector) observed in SEC or AF4 separation was integrated using 0.13 as the value of dn/dc [29]. This gel content was called the "filtrate gel on 1 μ m" or Gel_{>1 μ}. In previous papers this quantity of aggregates (macro and micro) was called "total gel". However, as shown by Kim *et al.* [3] and as we will see later in this paper, a not insubstantial quantity of microaggregates passes through the 1 μ m filter. As a consequence, the real total gel (G_T) is:

$$G_T = Gel_{>111} + Gel_{<111} \quad Equation 7$$

Gel $_{1\mu}$ is the quantity of microaggregates with a size smaller than 1 μ m. Gel $_{1\mu}$ cannot be determined by SEC-MALS, except by treating the columns with tetrabutylammonium bromide (TBABr) as shown previously [3]. This procedure is rather cumbersome, whereas it will be shown that Gel $_{1\mu}$ can easily be estimated using AF4 analysis of NR samples. Indeed, by knowing the initial concentration of the sample before filtration, it is possible to determine from the fractogram (DRI signal) the concentration of the two populations in solution after filtration: polyisoprene chains and microaggregates smaller than 1 μ m.

230 Thus:

$$Gel_{>1\mu m} = \frac{c_1 \times 100}{c_0} \quad Equation \ 8$$

 $Gel_{<1\mu m} = \frac{c_2 \times 100}{c_0} \quad Equation 9$

Where C_0 is the initial concentration of the analysed sample, C_1 the concentration of the analysed sample passing through the 1 μ m filter (polyisoprene chains + microaggregates) and C_2 the concentration of only the microaggregates passing through the 1 μ m filter. C_1 can be determined either by SEC or AF4 by integrating the whole peak of the concentration detector (DRI). C_2 can be calculated only by AF4 integrating the part of the DRI peak containing microaggregates.

Results & Discussion

Qualitative description of fractograms

SEC-MALS profiles for the different samples are presented in Figure 1. M_w variations started with a linear decrease corresponding to a normal elution from large chains to small chains but displayed a deviation of the slope of this curve for samples containing gel (i.e. Nippol, M121 and M160, figure 1B, C & D). As described in the introduction and as previously detailed [3], SEC separation of rubber generally presents this abnormal elution due to co-elution of delayed large macromolecules, assumed to be microaggregates ($GEL_{<1\mu}$), with the small chains of poly(cis-1,4-isoprene). This particular elution was highlighted when either a change or an inversion of the slope presenting the variation in weight-average molar mass versus elution volume occurred. Regarding the detectors, the differential refractive index (DRI) signal during the SEC elution profile corresponded to a main Gaussian peak (with slight backtailing) for Nippol and M121, and to a bimodal molar mass distribution for the IR307 and M160 samples. The LS signal was more unimodal with back-tailing varying depending on the sample.

Figure 1

Unlike SEC, AF4 fractionated the macromolecules from small to large ones and the peak shapes appeared quite different. For poly(*cis*-1,4-isoprene) with gel (i.e. Nippol 2200, M160 and M121), the shape of the LS fractograms did not correspond to a Gaussian peak. The fractograms displayed a long front tailing, (i.e. a long and low signal increase) and an abrupt increase in the LS signal from 25 to 30 min (corresponding to a crossflow ranging from 0.5 to

0.3 mL.min⁻¹) (Figure 2). For the IR307 sample, the fractogram exhibited a clearly less pronounced increase in the LS signal (Figure 2A). As the IR307 sample did not contain gel, unlike the Nippol 2200 sample, this abrupt increase in the signal was due to microaggregates, as observed by Andersson et al. [30] for AF4 analysis of ethylhydroxyethyl cellulose. For the refractive index detector signal, the behaviour was unfamiliar, with a first peak close to void volume (elution starting at 7 min), corresponding to small chains, followed by either a slight increase in the concentration signal (for IR 307), or a decrease (for Nippol 2200), or quite a constant signal up to the end of the peak (for the two natural samples) (Figure 2). With both the DRI and LS detectors, the fractograms gave a continuous elution whatever the entities eluting, be they random coil or compact microaggregates (sphere-like). However, the evolution of the molar masses (M_{wi}) in line with the elution time was not linear from a qualitative viewpoint (Figure 2). For the IR307 sample, Figure 2A shows a change in slope for an elution time of 17-18 min ($M_{wi} \approx 600 \text{ kg mol}^{-1}$). A clear decrease in the variability of the measured R_{gi} was observed from this elution time ($t_e = 17-18$ min) (Figure 2). Indeed, for the first 18 minutes of the fractogram, Rgi values were very dispersed whatever the samples analysed using Berry 2 formalism (Figure 2), compared to SEC-MALS. This high dispersion of R_{gi} may have occurred because the concentrations of the injected solutions were too low (≈ 1 mg.mL⁻¹) for LS detection or because there was a lack of resolution for small molecule fractionation under our AF4 conditions. This initial slope change in M_{wi} was observed for other samples at times that varied depending on the sample (from 13 up to 17 min). With the Nippol sample, a second marked change appeared in the Mwi slope at an elution time of about 31 min (Figure 2B). This abrupt slope change was accompanied by a dramatic increase in the LS signal due to huge entities eluting ($250 < R_{gi} < 1000$ nm). This second change in the M_{wi} slope in line with the elution time was not visible for the other synthetic polyisoprene

267

268

269

270

271

272

273

274

275

276

277

278

279

280

281

282

283

284

285

286

287

288

289

(IR307), but was visible to a lesser extent for the two NR samples (M121 and M160) at an elution time of about 26-27 min (Figure 2C & D).

293

291

292

294 *Figure 2*

295

296

297

298

299

300

301

302

303

304

305

306

307

308

309

310

311

312

313

314

315

The M_{wi} AF4 profile for IR 307 confirmed the presence of only one population of chains with a M_{wi} ranging from 60,000 g.mol⁻¹ to 5 million g.mol⁻¹ (Figure 2A). Conversely, the Nippol AF4 profile clearly showed the presence of 2 distinct populations (Figure 2B). The first population was composed of isolated polyisoprene chains and the second one (starting at 32 min) was composed of microaggregates with sizes under 1 µm (Gel<14) with a drastic increase in the M_{wi} slope. For the two NR samples (M121 and M160) (Figure 2C and 2D), the M_{wi} profiles were quite different from that for Nippol. Isolated polyisoprene chains seemed to elute first up to about 27 min. After this elution time, the M_{wi} profile exhibited an increase in slope (from 27 to about 35 min), reaching a quasi-plateau (from 35 min). This behaviour suggests that this population was quite monodisperse. These two parts could be attributed to co-elution of isolated polyisoprene chains and $Gel<_{1\mu}$ in the first case and $Gel<_{1\mu}$ only for the plateau. Large differences were observed for the Mwi=f(Ve) and Rgi=f(Ve) slopes, the sizes (Rgi) and the molar masses (M_{wi}) of the second populations for Nippol compared to the two natural polyisoprene samples (Figure 2). These results tend to confirm that the gel was not intrinsically the same for natural and synthetic polyisoprene. Indeed for NR, the radius for the $Gel \le_{1\mu}$ was about 150 nm for a molar mass close to 15 million g.mol⁻¹ whereas for Nippol for the same molar mass the radius was about 240 nm (i.e. 60% higher), as illustrated in Figure 3. Moreover, there was no "plateau effect" for Nippol compared to the NR samples. Thus, with a lower Rgi for the same Mwi, the microaggregates in the NR samples seemed more compact than in the Nippol synthetic polyisoprene. However, some of the difference observed in the slopes may have been due to an underestimation of $M_{\rm wi}$ for the microaggregates of the NR samples. Indeed, it cannot be ruled out that the dn/dc of NR microaggregates is not constant. Changes in the non-isoprene composition (lipids and/or proteins) of microaggregates cannot be excluded. A change in the proportion of non-isoprene compounds versus polyisoprene in the microaggregates could lead to a change in the dn/dc and so in the $M_{\rm wi}$ determined.

Figure 3

One of the main difficulties encountered with AF4 fractionation is to define a correct and unbiased integration range. For our data, the integration range for average molar mass and radius of gyration assessment was started when the Mwi and Rgi signals were stabilized (out of void peak influence) and stopped just before the end of the peak (shown as the red box in figure 4 for M160, for example). This choice of integration area was made in order to have results including almost all the peak surface and to avoid a decrease in repeatability for the AF4 results due to pre- and post-peak radius and mass dispersion and heterogeneity because of a low LS signal. This method was applied for the AF4 signals from IR307, M160 and M121. On the other hand, the treatment for Nippol 2200 was different. Indeed, the variation in M_{wi} in the second part of Nippol 2200 fractionation was quite high due to the presence of microaggregates with ultra high molar masses (over 10¹⁰ g mol⁻¹). Moreover, this final M_w increase was quite noisy and unrepeatable, probably due to the low associated RID signal. In fact, as presented in table 2 for example, increasing the Nippol 2200 integration range (from 9.5 - 35 min to 9.5 - 40 min), drastically increased the average molar masses, but also the standard deviation. Lastly, a 7% increase in RID integration area (hence in quantity) led to an increase of 4 orders of magnitude for the Mw and resulted in an increase in the standard

deviation from 25% to 71%. Consequently, for Nippol, the integration range was shortened, compared to the other samples, to avoid excessive variability in the results.

Table 2

In order to quantify aggregates exceeding 1 μ m (Gel $_{^{-1}\mu}$) (estimation of C_1 in eq. 9), the whole peak was integrated (green box in figure 4). The quantity of microaggregates smaller than 1 μ m (Gel $_{^{<1}\mu}$) (estimation of C_2 in eq. 10) was calculated according to a third integration range (the blue box in figure 4) starting from the middle of the zone we considered as a mixture of polyisoprene chains and microaggregates (data R_g =f(V_e)) up to the end of the peak.

Figure 4

Comparison of data between SEC-MALS and AF4-MALS

Average molar masses

 M_n , M_w and M_z were calculated from the SEC and AF4 results for each sample. The results are presented in Figure 5.

Figure 5

The number average molar mass M_n did not present significant differences whether determined by SEC or AF4 (Figure 5). The ratio of M_n obtained by AF4 to that obtained by SEC was ranged between 0.85 and 1.0. Unlike M_n , M_w and M_z were different, with a higher M_w and M_z obtained for AF4. As described previously, these larger M_w and M_z can be

explained by the presence of large microaggregates not observed with SEC. This observation is confirmed by the fact that for IR 307 (poly(*cis*-1,4-isoprene) without gel), M_w and M_z exhibited no significant difference between SEC and AF4 results. The difference between AF4 and SEC in terms of average molar masses was, as expected, higher for M_z than for M_w. The M_w ratios (M_{w-AF4}:M_{w-SEC}) ranged from 1.0 to 4.3 (for IR 307 and M121 respectively) whereas the M_z ratios (M_{z-AF4}:M_{z-SEC}) ranged from 1.0 to 18.6 (for IR 307 and Nippol respectively). For the three average molar masses considered (i.e. M_n, M_w or M_z), the AF4 results showed greater heterogeneity than for the SEC results, with high standard deviations. This lower reproducibility and repeatability was mainly due to the difficulty in defining the integration range, as previously explained, but also to the substantial variability generated by the refractive index detector baseline position. Indeed, the AF4 principle resulted in some noise, deviations and jumps in the DRI baseline and thus to some doubts / uncertainties on the baseline position, despite the blank subtraction. The large M_z difference (from AF4 to SEC) and RSD for Nippol was due to the large amount of microaggregates with ultra high molar masses and to the poor repeatability in the high mass range, as explained later on.

Determination of gel rates

The gel rates in the samples were calculated after SEC and AF4 analysis. $Gel_{>1\mu}$ was calculated for both the SEC and AF4 analyses whereas $Gel_{<1\mu}$ was only calculated after AF4 analysis. Figure 6 presents the $Gel_{>1\mu}$ rate after SEC and AF4 analyses. For the IR 307 and Nippol samples, the $Gel_{>1\mu}$ rate did not display any significant difference (no gel for IR307 and average $Gel_{>1\mu}$ slightly higher for Nippol with AF4). For the two NR samples, only M160 exhibited a significant difference in the $Gel_{>1\mu}$ rate between SEC and AF4 determination (23.8% for SEC and 17.2% for AF4). For M121, the lack of significant difference was due to the high variance of the AF4 result. The $Gel_{<1\mu}$ calculation was estimated at 9.5% for Nippol,

27% for M160 and 29% for M121 (no Gel $_{<1\mu}$ for IR 307). These large quantities of Gel $_{<1\mu}$ explained the large differences observed for M_w and M_z in the NR samples and the Nippol sample (higher M_w and M_z for AF4 analyses compared to SEC). However, as a result of such a large quantity of Gel $_{<1\mu}$ for the NR samples, assumed to be "lost" in not insubstantial proportions in SEC, the Gel $_{>1\mu}$ rate should have been much lower with AF4 compared to SEC for Nippol, M160 and M121. The slight difference observed between AF4 and SEC for the Gel $_{>1\mu}$ rate could be explained either by the large measurement variability for AF4, or by an overestimated Gel $_{>1\mu}$ calculation in AF4 analysis (potentially due to concentration peak area determination and therefore to blank subtractions). For the Gel $_{<1\mu}$ calculation, Kim *et al.* [3] obtained Gel $_{<1\mu}$ values close to 10% (calculated by SEC after ionic surfactant treatment of the columns) for NR samples similar to M160 and M121, meaning a difference with our Gel $_{<1\mu}$ values of about 15%.

Figure 6

Comparison of radii of gyration

As for the average molar masses, the R_g values obtained with AF4 were higher than those obtained with SEC, except for the IR307 sample, whose R_g was the same for both separation techniques (see table 3). Nevertheless, the differences in R_g obtained with the two techniques were less pronounced than for M_z . This was due to the narrower radius of gyration size range observed (typically varying from 20 to 200 nm) compared to the 10^2 - 10^3 order of magnitudes for the masses over the whole fractionation (up to 10^5 for Nippol). The variation in R_{gi} depending on the elution time with AF4 displayed a similar behaviour to that for M_{wi} (Figure 2). As the variation in R_{gi} was less significant than for M_{wi} , it implies that the material was becoming increasingly compact (greater increase for masses than for radii) towards the

end of the elution, especially for the second population, as previously illustrated in figure 3.
This observation confirms the presence of compact microaggregates highlighted by Kim *et al*.
[3].
Table 3

Conclusions

This work demonstrates the ability of AF4 to fractionate natural and synthetic poly(cis-1,4-isoprene). Distinct populations (characterized by a clear slope change in M_{wi} variation) corresponding to isolated polyisoprene chains and microaggregates smaller than 1 μ m (Gel $_{<1}\mu$) were detected. Average molar masses were determined and compared with those obtained by SEC. Similar M_n values were obtained but large differences were observed for M_w and M_z . These differences could be explained by a microgel population observed in AF4 but not during SEC separation. Moreover, microaggregates in the NR samples exhibited quite a different structure, appearing more compact than the microaggregates in the Nippol synthetic polyisoprene. Some problems (difficulties in defining the baseline, DRI signal jumps, etc.) due to the use of DRI with AF4 were encountered, in particular for gel rate determination. It seems obvious that some analytical developments are needed to optimize fractionation, increase the resolution for small polyisoprene chains and enable better reproducibility. However, these results are promising and microgel (Gel $_{<1}\mu$) can be considered for further individual studies and physico-chemical characterization.

Acknowledgements

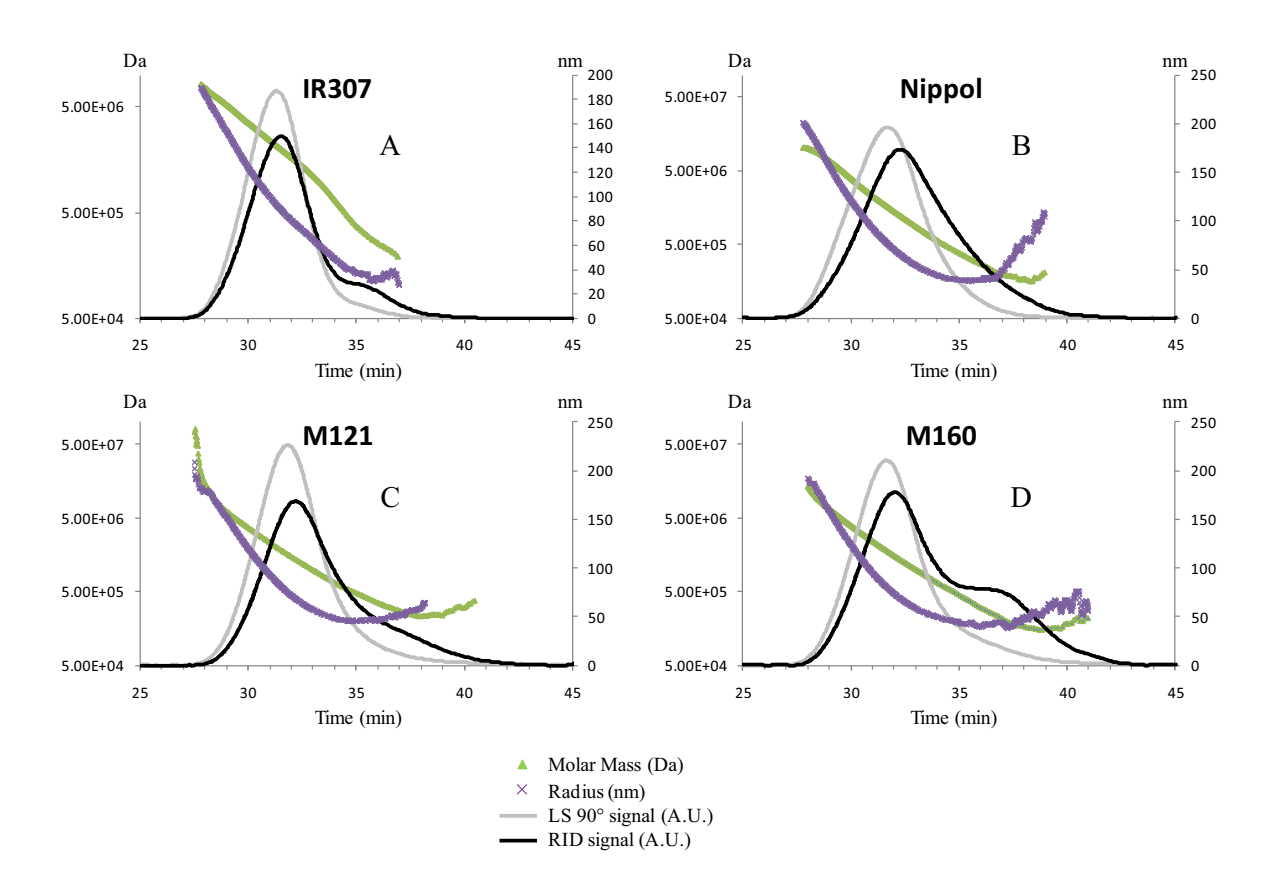
The authors gratefully thank Emilie Croizat and Christine Char for their valuable contribution to this project. A4F-MALS and SEC-MALS analyses were carried out on the LipPol-Green platform (http://www.supagro.fr/plantlippol-green/). We kindly thank CIRAD DRS and Agropolis fondation (http:// http://www.agropolis-fondation.fr) for financial support, and the Hubert Curien Programme for funding Miss Chalao Thepchalerm's scholarship.

445 **References**

- 446
- 447 [1] Hongsheng Liua, Fengwei Xiea, Long Yua, Ling Chena, L. Li, Prog. Polym. Sci. 34
- 448 (2009) 1348.
- 449 [2] L. Vaysse, F. Bonfils, P. Thaler, J. Sainte Beuve, in D.R. Höfer (Editor), Sustainable
- Solutions for Energy Generation, Royal Society of Chemistry, Cambridge, 2009, p.
- 451 335.
- 452 [3] C. Kim, M. Morel, J. Sainte Beuve, A. Collet, S. Guilbert, F. Bonfils, J. Chromatogr.
- 453 A 1213 (2008) 181.
- 454 [4] C. Kim, J. Sainte Beuve, S. Guilbert, F. Bonfils, Eur. Polym. J. 45 (2009) 2249.
- 455 [5] Angulo-Sanchez JL, Caballero-Mata P, Rubber Chem. Technol. 54 (1981) 34.
- 456 [6] K.N.G. Fuller, W.S. Fulton, Polymer 31 (1990) 609.
- 457 [7] J. Tangpakdee, Y. Tanaka, J. Rubber Res. 1 (1998) 14.
- 458 [8] S.N. Gan, J. Membrane Sci., Pure Applied Chemistry A33 (1996) 1939.
- 459 [9] J. Tangpakdee Sakdapipanich, T. Kowitteerawut, K. Suchiva, Y. Tanaka, Rubber
- 460 Chem. Technol. 72 (1999) 712.
- 461 [10] F. Ngolemasango, E. Ehabe, C. Aymard, J. Sainte-Beuve, B. Nkouonkam, F. Bonfils,
- 462 Polym. Int. 52 (2003) 1365.
- 463 [11] Y. Tanaka, L. Tarachiwin, Rubber Chem. Technol. 82 (2009) 283.
- 464 [12] S. Amnuaypornsri, J. Sakdapipanich, S. Toki, B.S. Hsiao, N. Ichikawa, Y. Tanaka,
- 465 Rubber Chem. Technol. 81 (2008) 753.
- 466 [13] J. Carretero-Gonzalez, T. A. Ezquerra, S. Amnuaypornsri, S. Toki, R. Verdejo, A.
- Sanz, J. Sakdapipanich, B.S. Hsiaod, M.A. Lopez–Manchadoa, Soft Matter 6 (2010)
- 468 3636.

- 469 [14] F.A. Messaud, R.D. Sanderson, J.R. Runyon, T. Otte, H. Pasch, S.K.R. Williams,
- 470 Prog. Polym. Sci. 34 (2009) 351.
- 471 [15] R. Qureshi, W. Kok, Anal. Bioanal. Chem. 399 (2011) 1401.
- 472 [16] G. Lespes, J. Gigault, Anal. Chim. Acta 692 (2011) 26.
- 473 [17] L.J. Gimbert, K.N. Andrew, P.M. Haygarth, P.J. Worsflod, Trends Anal. Chem. 22
- 474 (2003) 615.
- 475 [18] S. Dubascoux, I. Le Hecho, M. Hassellov, F. Von der Kammer, M.P. Gautier, G.
- 476 Lespes, J. Anal. At. Spectrom. 25 (2010) 613.
- 477 [19] M.E. Schimpf, K.D. Caldwell, G.J. C., Field Flow Fractionation Handbook, Wiley
- 478 Interscience, 2000.
- 479 [20] W.-S. Kim, C.H. Eum, A. Molnar, J.-S. Yu, S. Lee, Analyst 131 (2006) 429.
- 480 [21] W.G. Fulton, SA, J. Nat. Rubber Res. 12 (1997) 154.
- 481 [22] S. Lee, C. Eum, A. Plepys, B. Korean Chem. Soc. 21 (2000) 69.
- 482 [23] S. Lee, A. Molnar, Macromolecules 28 (1995) 6354.
- 483 [24] D.Y. Bang, D.Y. Shin, S. Lee, M.H. Moon, J Chromatogr. A 1147 (2007) 200.
- 484 [25] C. Kim, M. Morel, J. Sainte Beuve, S. Guilbert, F. Bonfils, Polym. Eng. Sci. 50 (2010)
- 485 240.
- 486 [26] M. Andersson, B. Wittgren, K.-G. Wahlund, Polymer 46 (2003) 4279.
- 487 [27] I. Teraoka, Polymer Solutions: An Introduction to Physical Properties, New York,
- 488 2002.

- 489 [28] P.J. Wyatt, Anal. Chim. Acta 272 (1993) 1.
- 490 [29] C. Kim, A. Deratani, F. Bonfils, J. Liq. Chromatogr. Relat. Technol. 33 (2010) 37.
- 491 [30] M. Andersson, B. Wittgren, K.G. Wahlund, Anal. Chem. 73 (2001) 4852.



 $\label{eq:Figure 1: Chromatograms (from the RID and LS detector at 90°) and variation in R_g and M_i \\ depending on the elution time during SEC analysis$

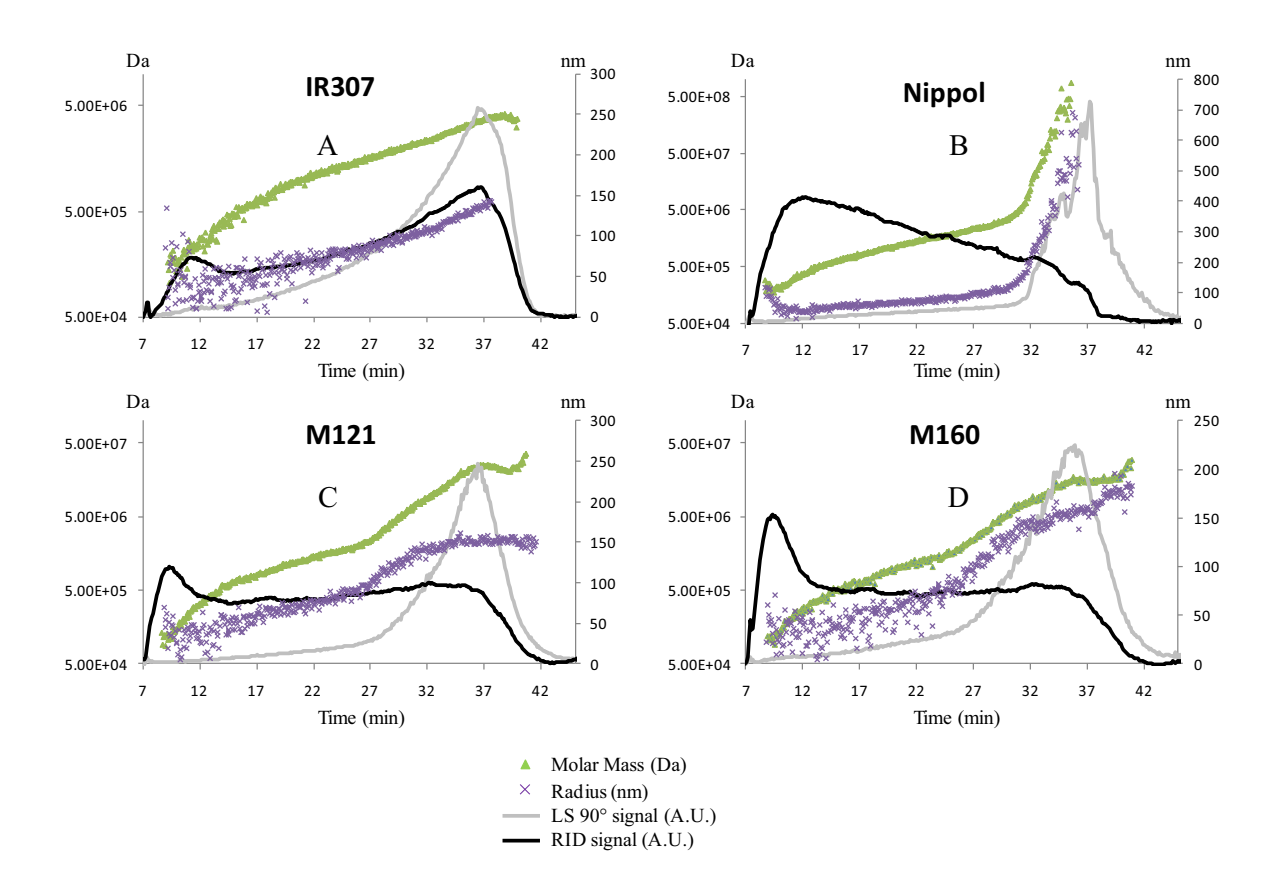


Figure 2: Fractograms (from the RID and LS detector at 90°) and variation in R_g and M_i depending on the elution time during AF4 analysis

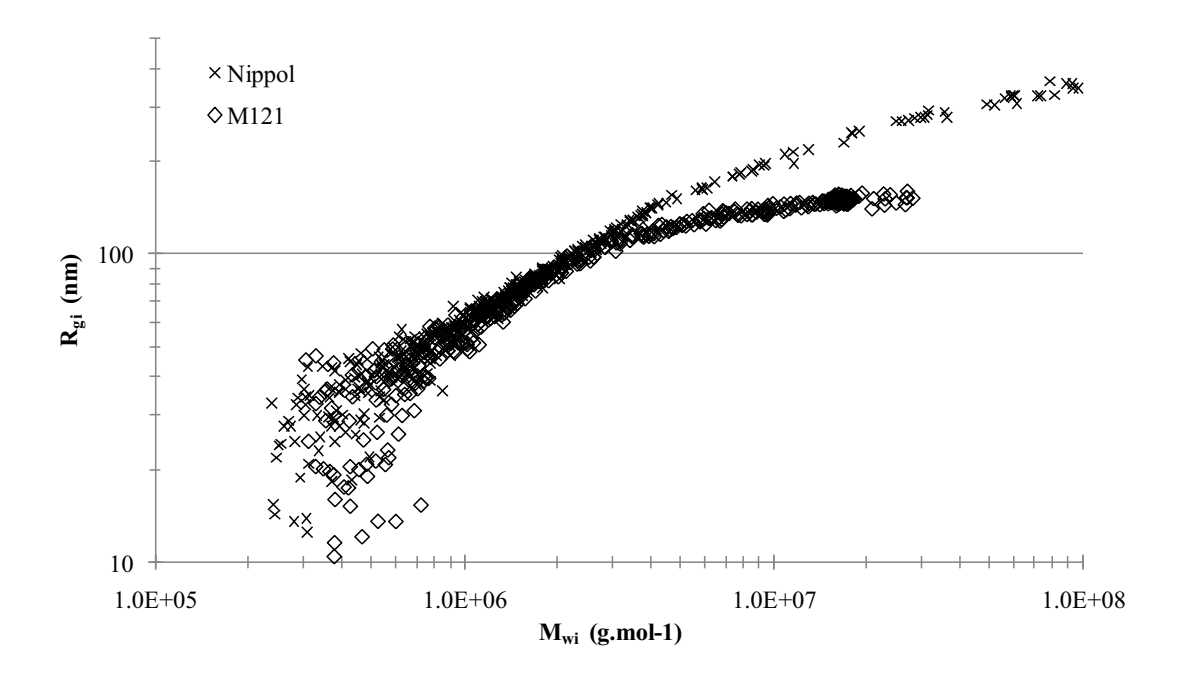


Figure 3: Variation of the radius of gyration (R_{gi}) depending on molar masses (M_{wi}) for the Nippol 2200 and M121 samples.

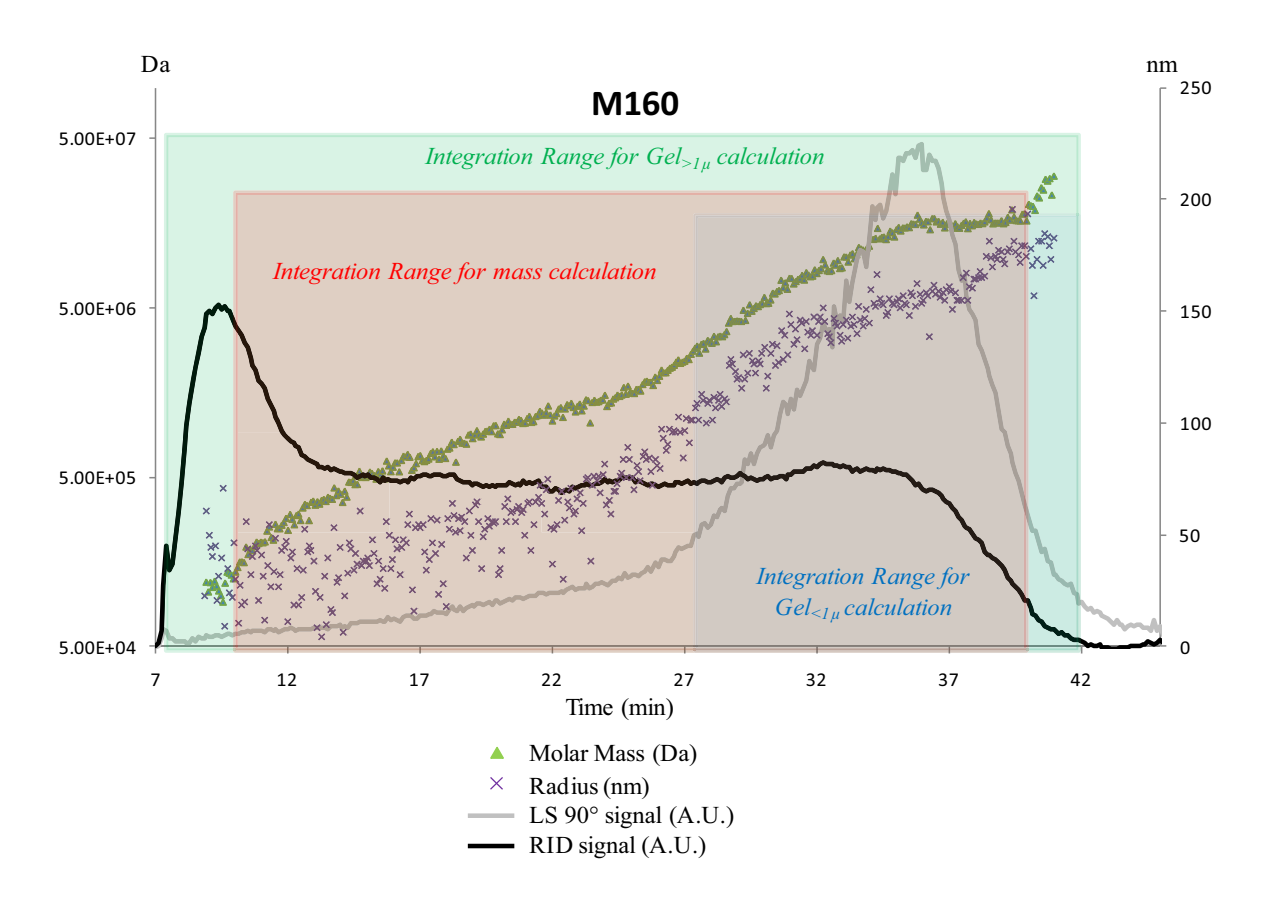


Figure 4: Determination of the AF4 integration range for the M160 sample

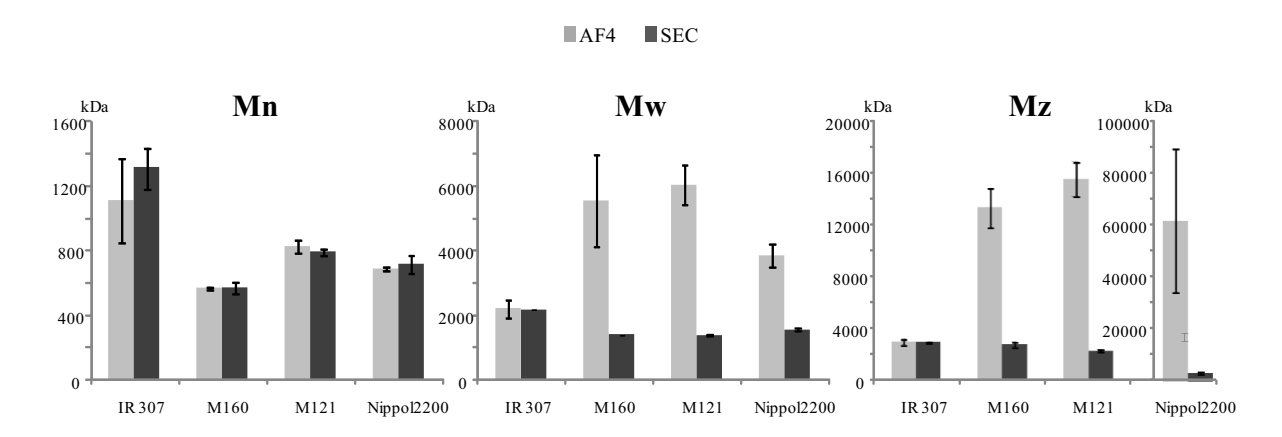


Figure 5: Comparison of masses obtained by SEC and AF4

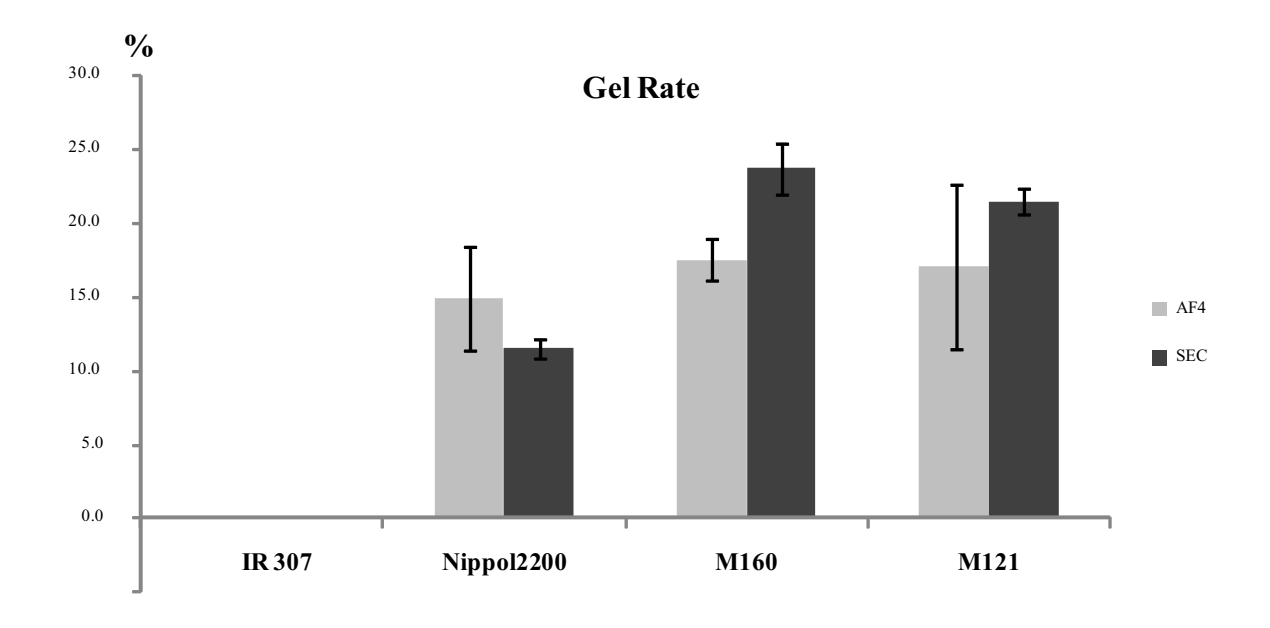


Figure 6: Comparison of filtrate gel on 1 μm (Gel $_{^{>1}\mu}$) rate calculated by AF4 and SEC

Step	Duration (min)	Crossflow (mL.min ⁻¹)	Type of rate		
1	1.5	1	Constant		
2	30	From 1 to 0.08	Linear		
3	9	0.08	Constant		
4	7	0	Constant		

 Table 1: AF4 crossflow programme during elution

Tables 2

	integration start	integration end	M _n (Da)	RSD	M _w (Da)	RSD	Mz (Da)	RSD	
Nippol	9.5 min	35 min	6.95E+05	4%	3.61E+06	25%	4.24E+07	62%	Integration :+7%
2200	9.5 min	40 min	7.48E+05	4%	9.36E+10	71%	1.40E+14	81%	of surface area

Table 2: Nippol 2200 mass calculation (M_n , M_w and M_z with respective RSD from one AF4 series) with different integration ranges

		R _g (nm)	SD (nm)	CV
ID207	AF4	115.8	3.8	4.0%
IR307	SEC	112.1	1.4	1.3%
Nippol	AF4	249.9	28.8	28.8%
	SEC	108.5	4.2	3.9%
M160	AF4	136.5	7.0	4.3%
	SEC	102.8	2.3	2.2%
M121	AF4	133.5	7.8	3.4%
	SEC	92.5	2.4	2.6%

⁽¹⁾ SD: standard deviation, CV: coefficient of variation ((SD/mean) x 100)

Table 3: $R_{\rm g}$ determined by AF4 and SEC

Elsevier Editorial System(tm) for Colloids and Surfaces B: Biointerfaces Manuscript Draft

Manuscript Number:

Title: Surface-quaternized chitosan particles as an alternative and effective organic antibacterial filler

Article Type: Full Length Article

Keywords: chitosan; particle; heterogeneous quaternization; minimum inhibitory concentration.

Corresponding Author: Dr. Voravee Hoven, Ph.D.

Corresponding Author's Institution: Chulalongkorn University

First Author: Oraphan Wiarachai, MS

Order of Authors: Oraphan Wiarachai, MS; Nuttha Thongchul, PhD; Suda Kiatkamjornwong, PhD; Voravee Hoven, Ph.D.

Abstract: Taking advantage of the large surface area that is covered with permanent positive charges of quaternary ammonium entities, this research aimed to develop environmentally friendly, organic antibacterial fillers from quaternized chitosan particles that may be applicable for biomedical devices, health and textile industries. The particles were formulated by ionic crosslinking of chitosan with tripolyphosphate followed by quaternization that was conducted under heterogeneous condition via either direct methylation or reductive N-alkylation with a selected aldehyde followed by methylation. Sub-micron, spherical, and positively charged quaternized chitosan particles were formed, as determined by 1H-NMR, FT-IR, PCS, and TEM analysis. Antibacterial activity tests performed by viable cell counts suggested that all quaternized chitosan particles exhibited superior antibacterial activity against the model Gram-positive bacteria, S.aureus, as compared to the native chitosan particles at neutral pH. Only some quaternized chitosan particles, especially those having a high charge density and bearing large alkyl substituent groups, were capable of suppressing the growth of the model Gramnegative bacteria, E. coli. The inhibitory efficiency of the quaternized chitosan particles was quantified in terms of the minimum inhibitory concentration (MIC).



June 12, 2011

Dear Sir/Madam:

I would like to send a manuscript, entitled "Surface-quaternized chitosan particles as an alternative and effective organic antibacterial filler" to be considered for publication as a full paper in Colloids and Surfaces B: Biointerfaces. On behalf of all authors, namely, Oraphan Wiarachai, Nuttha Thongchul, Suda Kiatkamjornwong, Voravee P. Hoven, I hereby confirm that this manuscript or its contents in some other form has not been published previously by any of the authors and/or is not under consideration for publication in another journal at the time of the submission.

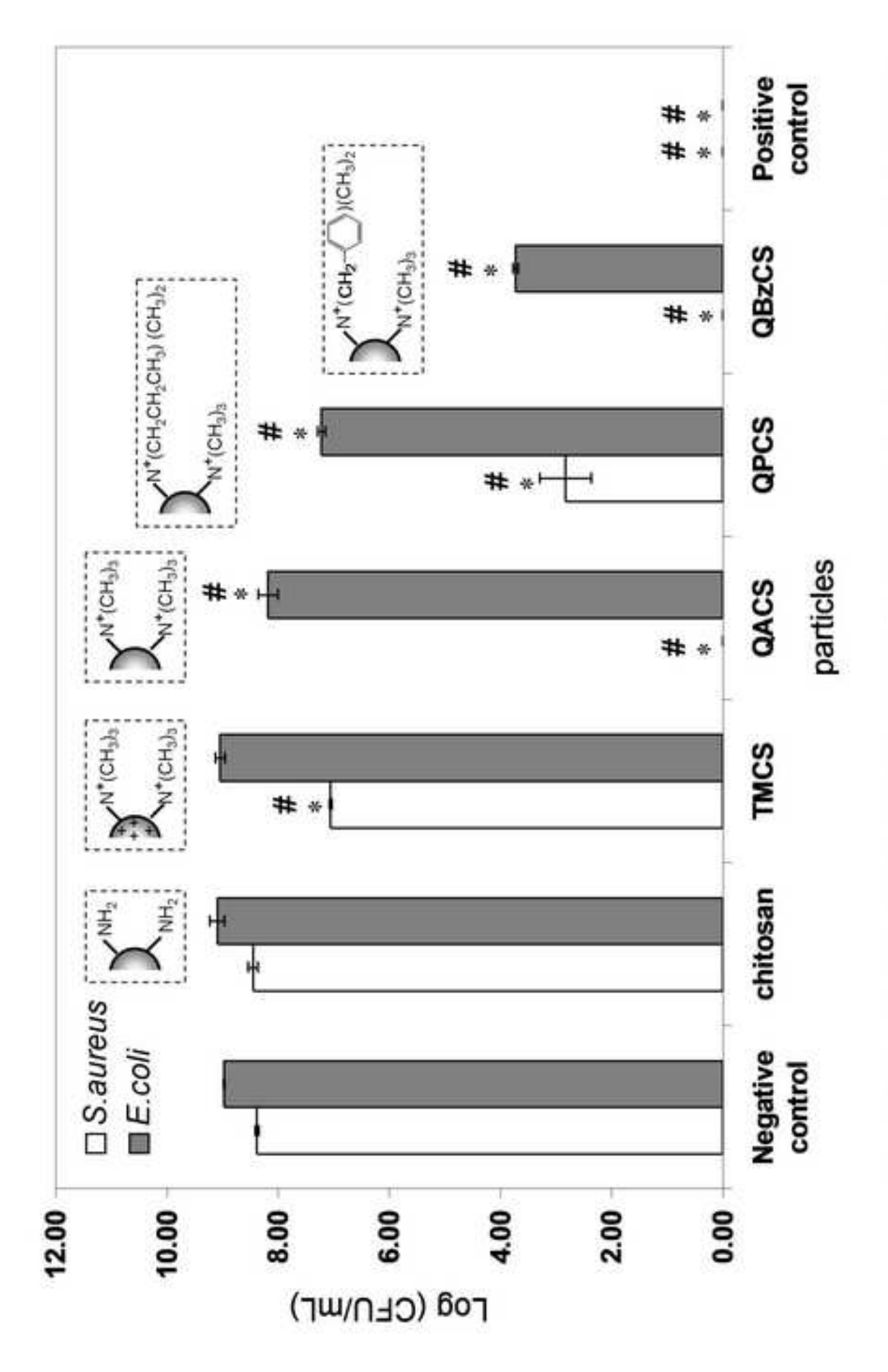
This work introduces surface-quaternized chitosan particles as an effective, environmentally friendly, organic antibacterial filler that may be incorporated into materials that require antibacterial activity. Based on the minimum inhibitory concentration, it was found that some surface-quaternized chitosan particles are more effective in inhibiting the bacterial growth than the quaternized chitosan solution. The fact that the heterogeneous quaternization used for the preparation of surface-quaternized chitosan particles can simply be done without the requirement for tedious purification process opens up an opportunity to produce such effective antibacterial filler at a large scale and that is very beneficial from industrial perspective.

The authors believe that the content of this contribution would be of interest to **Colloids and Surfaces B: Biointerfaces** audiences. Should there be any further information which may be required or if any problems arise, please contact me at the address shown below.

Sincerely yours,

Vp. Horeen

Voravee P. Hoven, Ph.D. Corresponding Author



[*p < 0.01 (compared with the negative control), "p < 0.01 (compared with the chitosan particles)]

Research highlights

- Quaternized chitosan particles prepared by heterogeneous quaternization exhibited significantly higher antibacterial activity against *S. aureus* (Gram positive bacteria) and *E. coli* (Gram negative bacteria) than the particles prepared by homogeneous quaternization.
- Only some quaternized chitosan particles, especially those having a high charge density and bearing a large alkyl substituent, were capable of suppressing the growth of *E. coli*, the Gram-negative bacteria.

Surface-quaternized chitosan particles as an alternative and effective organic antibacterial filler

Oraphan Wiarachai^{a,b}, Nuttha Thongchul^c, Suda Kiatkamjornwong^d, Voravee P. Hoven^{e*}

^a Program in Petrochemistry and Polymer Science, Faculty of Science, Chulalongkorn University, Phayathai Road, Pathumwan, Bangkok 10330, Thailand

^b Center for Petroleum, Petrochemicals, and Advanced Materials, Chulalongkorn University, Phayathai Road, Pathumwan, Bangkok 10330, Thailand

^c Institute of Biotechnology and Genetic Engineering, Chulalongkorn University, Phayathai Road, Pathumwan, Bangkok 10330, Thailand

^d Department of Imaging and Printing Technology, Faculty of Science, Chulalongkorn University, Phayathai Road, Pathumwan, Bangkok 10330, Thailand

^e Organic Synthesis Research Unit, Department of Chemistry, Faculty of Science, Chulalongkorn University, Phayathai Road, Pathumwan, Bangkok 10330, Thailand

* Corresponding author. Tel: +66-2218-7626-7 ext 102; fax: +66-2218-7598 E-mail address: vipavee.p@chula.ac.th.

ABSTRACT

Taking advantage of the large surface area that is covered with permanent positive charges of quaternary ammonium entities, this research aimed to develop environmentally friendly, organic antibacterial fillers from quaternized chitosan particles that may be applicable for biomedical devices, health and textile industries. The particles were formulated by ionic crosslinking of chitosan with tripolyphosphate followed by quaternization that was conducted under heterogeneous condition via either direct methylation or reductive Nalkylation with a selected aldehyde followed by methylation. Sub-micron, spherical, and positively charged quaternized chitosan particles were formed, as determined by ¹H-NMR. FT-IR, PCS, and TEM analysis. Antibacterial activity tests performed by viable cell counts suggested that all quaternized chitosan particles exhibited superior antibacterial activity against the model Gram-positive bacteria, S.aureus, as compared to the native chitosan particles at neutral pH. Only some quaternized chitosan particles, especially those having a high charge density and bearing large alkyl substituent groups, were capable of suppressing the growth of the model Gram-negative bacteria, E. coli. The inhibitory efficiency of the quaternized chitosan particles was quantified in terms of the minimum inhibitory concentration (MIC).

Keywords: chitosan; particle; heterogeneous quaternization; minimum inhibitory concentration

1. Introduction

Incorporation of antibacterial fillers is an efficient approach to introduce antibacterial activity to materials. There are many types of filler that can be incorporated into the materials to induce their antibacterial activity such as antibiotic [1], nitric oxide [2], halogen species [3, 4], biocide [5] and heavy metal [6-8]. From several types of antibacterial fillers, heavy metal in the form of silver nanoparticles (AgNPs), are well recognized to exhibit an effective antibacterial activity and are widely used in many applications such as medical devices [9], paint [10], coating [11] and textiles [12]. Recently, it has been reported that the AgNPs could affect human tissues from diverse routes of exposure including the respiratory system, skin, and gastrointestinal tract [13]. It has been proposed that AgNPs may interact with thiol groups of proteins and enzymes within mammalian cells, some of which are key components in the antioxidant defense mechanism of the cell. Inhibition of this mechanism would then result in an increase in the concentration of reactive oxygen species that can alter or damage the function of the cells. Also, it has been found that the AgNPs can be released from commercial clothing (socks) into the wash water [14], and so could increase the risk of environmental contamination. Therefore, it is highly desirable if the antibacterial fillers can be developed from natural, nontoxic and environmentally friendly material.

Chitosan is a natural biopolymer derived from the deacetylation of chitin, an abundantly available biopolymer found in the exoskeletons of insects, the shell of crustaceans, and fungal cell walls. It is nontoxic, biodegradable, biocompatible and possesses antibacterial properties [15]. In fact, the potential of chitosan particles as an effective antibacterial agent/filler has been realized and continuously reported. Early work by Qi and co-workers demonstrated that chitosan in the form of nanoparticles exerted a higher antibacterial activity against *E. coli, S. choleraesis, S. typhimurium, and S. aureus* than chitosan solution, and it was proposed that the greater surface area of the particles provided a

more intimate contact with the surface of bacterial cells [16]. Ye and co-workers, on the other hand, have shown that cotton fabrics coated with core-shell particles, having poly(*n*-butyl acrylate) as the core and chitosan as the shell, exhibited an excellent antibacterial activity against *S. aureus* with a reduction in viable bacteria numbers of more than 99% [17].

In general, chitosan would exhibit its antibacterial activity only in acidic medium, due to the poor solubility of chitosan above its pKa (pH 6.5). Quaternization of the amino groups to introduce permanent positively charged quaternary ammonium groups has been recognized as a potential way to enhance the antibacterial activity of chitosan over a broader pH range. The reaction can simultaneously introduce the permanent positive charge and hydrophobicity, the two parameters that are believed to affect the antibacterial activity [18-20]. Synthetic routes and applications of quaternized derivatives of chitosan have been recently reviewed and published [21, 22], whilst the application of quaternized chitosan particles has been reported. For example, particles fabricated from chitosan that was formerly quaternized by hexyl bromide were incorporated as bactericidal fillers in poly(methyl methacrylate) bone cement and tested against *S. aureus* and *S. epidermidis* under a neutral pH environment [23].

In order to promote ionic interactions with the negatively charged components of the bacterial cell membrane, the incorporation of metal ions [24-26] or cationic polymer [27] into chitosan particles has also been recently reported as an alternative approach. Qi and coworkers have suggested that the antibacterial activity can be enhanced by incorporating Cu²⁺ into chitosan particles [25]. Later, Du and co-workers have shown that chitosan particles loaded with various metal ion such as Ag⁺, Cu²⁺, Zn²⁺, Mn²⁺, Fe²⁺, exhibited higher antibacterial effect against *E. coli*, *S. choleraesuis*, and *S. aureus* than chitosan particles [24, 26]. In addition, Inphonlek and coworkers have found that core-shell nanoparticles having poly(methyl methacrylate) core coated with polyethyleneimine, and chitosan-mixed-

polyethyleneimine shells exhibited higher antibacterial activity against *S. aureus* and *E. coli* than chitosan nanoparticles [27].

Here in this research, we attempt to develop an environmentally friendly, organic antibacterial filler from chitosan particles. The permanent positive charges in the form of quaternary ammonium groups were introduced to the surface of pre-fabricated chitosan particles under heterogeneous condition via direct methylation or reductive *N*-alkylation using two different aldehydes, propionaldehyde and benzaldehyde, followed by methylation with methyl iodide. This method has the advantage that it can be performed conveniently in the absence of tedious purification process that is generally required for homogeneous quaternization. The success of this type of method for enhancing antibacterial activity especially in a neutral pH environment has been previously reported for the chitosan films [28]. And the fact that the addition of cationic metal species or polymers is no longer necessary truly simplifies the fabrication method.

2. Materials and methods

2.1. Materials

Chitosan flake (DAC 85%, $M_V = 45,000$ Da) was purchased from Seafresh Chitosan (Lab) Co., Ltd (Thailand). Propionaldehyde, methyl iodide (CH₃I), sodium borohydride (NaBH₄), sodium chloride (NaCl), sodium hydroxide (NaOH), sodium iodide (NaI) and tripolyphosphate (TPP) were purchased from Fluka (Switzerland). Acetic acid, benzaldehyde, ethanol (EtOH), and methanol (MeOH) were purchased from Merck (Germany). Dialysis membrane (cut-off molecular weight of 12,400 g/mol) was purchased from Sigma (USA). All reagents and materials were of analytical grade and used without further purification. *E. coli* and *S. aureus* were provided by National Center for Genetic Engineering and Biotechnology (BIOTEC), Thailand. Mueller-Hinton agar (MHA) and Mueller-Hinton broth (MHB) were

purchased from Difco (USA). Mueller Hinton agar plates were supplied by Department of Medical Science, Ministry of Public Health, Thailand. Ultrapure distilled water was obtained after purification using a Millipore Milli-Q system (USA) that involves reverse osmosis, ion exchange, and a filtration step.

2.1. Preparation of surface-quaternized chitosan particles

Chitosan particles were prepared using TPP as a crosslinking agent according to the published procedure by Qi *et al.* [16] Preparation of quaternized *N*-alkyl chitosan particles were done following the method of Vallapa *et al.* [28]. In brief, an anhydrous methanol solution of a selected aldehyde (10 mL) having a desired concentration was added into a flask containing chitosan particles (0.03 g). After stirring for a given time at ambient temperature (~28-30°C), NaBH₄ (0.3 g, 0.8 mol) was added into the reaction mixture and the solution was stirred for 24 h. The resulting *N*-alkyl chitosan particles were then isolated by centrifugation at 12,000 rpm for 30 min. The supernatant was discarded and the particles were centrifugally washed as above with methanol three times and then dried *in vacuo*. An anhydrous methanol solution (10 mL) containing NaI (0.30 g, 2 mmol) and NaOH (0.13 g, 3 mmol) was then added into a flask containing chitosan or *N*-alkyl chitosan particles (0.03 g) and CH₃I was then added via syringe. The reaction mixture was stirred at 50°C for a given time. The particles were isolated and purified as above mentioned.

2.2. Characterization of surface-quaternized chitosan particles

Fourier Transform-Infrared (FT-IR) spectra were collected using a Nicolet Impact 410 FT-IR spectrometer. All samples were prepared as KBr pellets. All ¹H NMR spectra were recorded in a 1% (v/v) solution of CF₃COOH/D₂O or D₂O using a Varian model Mercury-400 nuclear magnetic resonance spectrometer (USA) operating at 400 MHz. Chemical shifts

(δ) are reported in parts per million (ppm) relative to tetramethylsilane (TMS) or using the residual protonated solvent signal as a reference. The size and the morphology of all particles were examined by transmission electron microscope (TEM, Model JEM-2100, Japan) with the average diameter calculated using Semafore software and reported from the measurement of 100 randomly selected particles. The ζ -potential values of the particles were determined using a Nanosizer Nano-ZS (Malvern Instruments, UK) at 25°C with a scattering angle of 173°. All data are displayed as the mean \pm one standard deviation and are derived from at least three independent experiments. The data were calculated using the Helmholtz-Smoluchowski equation.

2.8. Evaluation of antibacterial activity

All glasswares used for the tests were sterilized in an autoclave at 121 °C for 15 min prior to use. All particles were sterilized by exposing to UV radiation for 60 min prior to the tests. The antibacterial test was performed according to a modified method of Qi *et al.* [16]. Chitosan and quaternized chitosan particles (2.5 mg) were added to 5 mL of MHB in test tubes and aseptically inoculated with 50 μ L of the freshly prepared bacterial suspension in distilled water (OD₆₀₀ = 0.5). The pH of the broth was about 7.4. The negative and positive controls were a broth solution alone and a broth solution with ampicillin (50 mg/mL), respectively. After mixing, broth cultures were incubated at 37 °C in a shaking incubator (Model G-25, New Brunswick Scientific Co., Inc., USA), at 110 rpm for 24 h. Then, 100 μ L of the bacterial solution was removed and 10-fold serially diluted down to 10⁶-fold the original level. A 100 μ L aliquots of each diluted bacterial suspension was then spreaded onto the MHA plates for total plate counting. After incubating at 37 °C for 18 h, the number of colonies, and thus replication competent bacteria, were then counted as a measure of the

assumed viable number of bacteria. The results after correction for the dilution factor were expressed as mean colony forming units per volume (CFU/mL).

To determine the minimum inhibitory concentration (MIC) of all particles, the particles were first suspended in 5 mL of MHB and two-fold serial dilutions prepared. Each set of serial dilutions was then inoculated under aseptic conditions with 50 μ L of the freshly prepared bacterial suspension in distilled water (OD₆₀₀ = 0.5). After incubating at 37 °C for 24 h, the total plate count enumeration of the CFU/mL was evaluated as described above. The lowest concentration of the particles that inhibited the growth of bacteria was considered as the minimum inhibitory concentration (MIC).

All tests of antibacterial activity were performed in triplicate per sample, upon at least three independent samples and expressed as mean \pm standard deviation (SD). Statistical analysis was performed using the Statistical Package for the Social Science (SPSS) version 17.0 software. Statistical comparisons made by One-Way Analysis of Variance (ANOVA) with the Least Square Difference (LSD) tests were used for post hoc evaluations of differences between groups. The threshold level for accepting statistical significance was set at p < 0.01.

3. Results and Discussion

3.1. Preparation and characterization of surface-quaternized chitosan particles

Chitosan particles were first fabricated by ionic crosslinking between positively charged chitosan and negatively charged TPP. The process was conducted at ambient temperature in the absence of any surfactant or oil phase. The resulting chitosan particles appeared as fine white powder after drying and were insoluble in water, dilute acidic and alkali solutions. As outlined in Scheme 1, chitosan particles were then surface-modified by heterogeneous reductive *N*-alkylation with selected aldehyde, namely propionaldehyde and

benzaldehyde which yielded N-propyl chitosan particles and N-benzyl chitosan particles, respectively. Subsequent methylation with CH₃I thus formed quaternized N-propyl chitosan (QPCS) particles and quaternized N-benzyl chitosan (QBzCS) particles, respectively. Furthermore, the quaternization (Scheme 1) was also conducted directly on chitosan particles by methylation with CH₃I and gave quaternary ammonium-containing chitosan (QACS) particles as products. The optimized conditions for the preparation of each surfacequaternized chitosan particles via heterogeneous quaternization, so as to yield the highest degree of quaternization in terms of reaction time and reagent concentration were empirically identified (Table S1, Supplementary Material) based on the results from water contact angle and ζ-potential measurements following the criteria as previously described [28]. Another type of quaternized particles designated as N,N,N-trimethylchitosan (TMCS) particles were prepared for comparison. Although the quaternary ammonium entity (trimethyl, -N(CH₃)₃) of the TMCS particles is similar to that of the QACS particles, the TMCS particles were prepared differently by ionic gelation of N,N,N-trimethylchitosan synthesized homogeneously from chitosan according to the method reported by Sieval et al. [29]. In other words, TMCS particles should not only bear positive quaternary ammonium groups at the particles' surface which is the case for the QACS particles, but also inside the particles.

Chemical functionalities of all quaternized chitosan particles were first identified by FT-IR analysis. As shown in Fig. 1, absorption peaks at 1650 and 1544 cm⁻¹ can be assigned to the C=O stretching (Amide I) and N-H bending (Amide II) of the glucosamine unit of chitosan, respectively. The decrement of the N-H bending signal at 1544 cm⁻¹ and the appearance of the C-H deformation signal in a range of 1470-1460 cm⁻¹ in the spectra of all quaternized chitosan particles implied that the amino groups were functionalized by alkyl substituents introduced by either reductive *N*-alkylation/methylation or direct methylation. Nonetheless, the C-H deformation peak belonging to the TMCS particles was obviously weak

as opposed to those observed for other particles implying that there was smaller content of quaternary ammonium groups in the TMCS particles.

The degree of success in the quaternization of chitosan particles was also confirmed by ^{1}H NMR analysis. As illustrated in Fig.2, the multiplet in the range of $\delta 3.3$ - 4.4 ppm comes from the six carbon atoms at the 2', 3, 4, 5, 6, and 6' positions, while the two singlets at $\delta 1.9$ and $\delta 2.9$ ppm are due to the methyl protons from the acetyl groups (position A) and at the 2 position of N-acetyl glucosamine unit, respectively. For the QPCS and QBzCS particles, it should be emphasized that not all of the amino groups of chitosan were alkylated in the first step of reductive N-alkylation. As a consequence, the signals of the methyl protons appearing in Fig.2(d-e) would come from methyl groups attached to both alkylated and nonalkylated amino functionalities. The signal at $\delta 3.1$ -3.3, $\delta 3.0$, and $\delta 2.7$ ppm can be assigned to the methyl protons of the trisubstituted $(-N^+(C\underline{H}_3)_3)$ or $NR^+(C\underline{H}_3)_2$, position B), disubstituted (- $N(C\underline{H}_3)_2$ or $-NR(C\underline{H}_3)$, position C) and monosubstituted (-NH(C \underline{H}_3), position D) amino groups, respectively. The trace signals of methylene protons ($\delta 1.0$ ppm) and methyl protons $(\delta 0.85 \text{ ppm})$ observed on the spectrum of QPCS particles (Fig.2(e)) can be used as additional evidences confirming the attachment of propyl groups at the amino moieties of chitosan in the step of reductive N-alkylation. For the QBzCS particles (Fig.2(f)), the signals of aromatic protons at δ 7.4 ppm together with the benzylic protons at 1.0 ppm could be used to verify the attachment of benzyl groups at the amino positions of chitosan.

Based on the ^{1}H NMR analysis, the degree of quaternization (%DQ) can also be estimated. To simplify the calculation, it was assumed that the majority of quaternary ammonium groups existed in the form of $^{-}N^{+}(C\underline{H}_{3})_{3}$ and only a few were present in the form of $NR^{+}(C\underline{H}_{3})_{2}$. This assumption is based on the fact that the non-alkylated or free amino groups (-NH₂) left after the *N*-reductive alkylation step are less bulkier than the alkylated amino group (-NHR) and should thus be more accessible for nucleophilic substitution of CH₃I. Such

characteristics should favor the formation of $-N^+(C\underline{H}_3)_3$ as opposed to that of the $NR^+(C\underline{H}_3)_2$. The %DQ can thus be calculated from the relative ratio between the integration of the nine protons from the three methyl groups of the quaternized *N*-alkyl chitosan at the position $\delta 3.1$ -3.3 ppm and the peak integration of the six protons of chitosan ($\delta 3.3$ -4.4 ppm). Accordingly, the calculated %DQ value based on the content of $N^+(C\underline{H}_3)_3$ was 2.1, 7.1, 4.2, and 5.7 % for TMCS, QACS, QPCS, and QBzCS particles, respectively. It should be taken into account that the quaternized chitosan particles were not completely soluble in the CF₃COOH/D₂O, the solvent used for NMR analysis. As a result, the %DQ values obtained from 1H NMR analysis are not capable of reflecting the actual degree of surface quaternization, they can only be used as a qualitative measure of the extent of surface substitution. The fact that %DQ of TMCS particles was the lowest agrees quite well with the data formerly described based on FT-IR analysis (Fig.1).

TEM analysis revealed that all particles were quite spherical in shape and had average diameters in a sub-micron range of 260 -490 nm (Fig. 3). The dimension of QACS particles was quite comparable to that of the TMCS particles implying that the preparation method did not have significant impact on the particle size and morphology. On the other hand, the size of chitosan particles seemed to be greater when being modified by a larger alkyl substituent (propyl, benzyl) which came from the aldehyde used in the reductive *N*-alkylation step. The charge characteristic of the quaternized chitosan particles was determined by photon correlation spectroscopy (PCS). As shown in Fig. 3, all particles prepared by heterogeneous quaternization via reductive *N*-alkylation followed by methylation (QPCS and QBzCS particles) or direct methylation (QACS particles) exhibited greater zeta potential values than those of chitosan and TMC particles. Indeed, comparing TMCS and QACS particles, it seems that the heterogeneous quaternization approach was more efficient in enhancing positive charges of the chitosan particles than the homogeneous one. This may stem from the fact that some positive charges of

TMC were neutralized following ionic crosslinking with the negatively charged TPP upon the particle formation. In accord with this notion is that the TMCS particles formed by the crosslinking of TMC and TPP were not completely soluble in CF₃COOH/D₂O. As a result, the %DQ of TMC particles (2.1%) was much lower than that of the originally synthesized TMC (%DQ = 11.8%) indicating the consumption of the positive charges during crosslinking. Unlike the TMCS particles, the introduction of trimethyl groups to chitosan particles via direct methylation to yield the QACS particles was performed after the particle formation. Thus, the positive charge density generated thereafter was not depleted by the crosslinking. A similar explanation can be applied for the QPCS and QBzCS particles, where again the quaternization was applied after the particle formation. Interestingly, the presence of the larger alkyl substituents (propyl and benzyl) somewhat promoted the subsequent methylation accounting for why the ζ -potential was raised above +35 eV for both the QPCS and QBzCS particles. It is postulated that the more hydrophobic environment created by the propyl and benzyl substituents may increase a chance of CH₃I, a small organic molecule of low polarity, to reach the amino active sites of chitosan chain during methylation. Previous work has also demonstrated that the degree of surface quaternization can be tailored by adjusting the CH₃I concentration used in the methylation step [28].

3.2 Antibacterial efficacy of surface-quaternized chitosan particles

The antibacterial activity of surface-quaternized chitosan particles were tested against the representative Gram-positive and Gram-negative bacteria, *S. aureus* and *E. coli*, respectively, and reported as the total number of replication competent (viable) cells as mean colony forming units per volume (CFU/mL). In the case of *S. aureus*, all quaternized chitosan particles, TMCS, QACS, QPCS and QBzCS particles, exhibited significantly higher antibacterial ratio (> 95%) than the chitosan particles at pH 7.4 (Fig. 4), supporting that the

introduction of the positive charges via quaternization can effectively improve the antibacterial activity of chitosan particles especially in neutral media. In contrast, the antibacterial action of chitosan particles cannot be detected given that their viable counts closely resembled those of the negative control. This outcome is in line with our previous observation on chitosan film implying that chitosan particles would exhibit its potential in suppressing the bacterial growth only when they are in acidic media in which they are positively charged [28]. This also further suggested that the chelation of the amino groups of chitosan as proposed by others [30, 31] is definitely not the major mechanism that controls the antibacterial activity at this particular condition. These evidences support that the superior antibacterial activities of some quaternized chitosan particles, especially QPCS and QBzCS particles, to the chitosan particles are mainly due to their higher charge density in near neutral pH condition than the latter (See Fig. 3 for ζ -potential data). Overall, this trend is in accordance with previously observed data reported by Qi and coworkers [16], who proposed that the positively charged chitosan particles should interact favorably with negatively charged cell membranes, causing an increase in membrane permeability and eventually rupture and leakage of intracellular components. This proposed mechanism is particularly reasonable in the case of the Gram-positive bacteria, such as S. aureus since their outer membrane consists of negatively charged teichoic acid, that is believed to be responsible for the electrostatic binding with the positively charged particles.

Although the TMCS particles exhibited a slightly lower ζ -potential than the chitosan particles, they still inhibited the growth of *S. aureus*, potentially suggesting that the inhibition did not solely rely on the contact-inhibitory mechanism which should be charge density-dependent, but may also be influenced by the charge inside the particles or the ability to dissolve in the media considering that TMC is water soluble and not all of the TMC molecules were crosslinked by TPP during the particle formation. In fact, this release-inhibitory

mechanism involving surface leaching of soluble chitosan and/or its quaternized derivatives has been recently proposed by Fernandez-Saiz and co-workers [32] and also in our earlier work on the surface-quaternized chitosan films [28]. Similar explanations may also be applied in the case of QACS particles whose charge density (ζ -potential = +29.3 mV) was slightly higher than those of both chitosan particles (ζ -potential = +27.1 mV) and TMCS particles (ζ -potential = +23.2 mV). Having the same type of quaternary ammonium groups (-N(CH₃)₃), the QACS particles exhibited better antibacterial action against *S. aureus* than the TMCS particles indicating that the heterogeneous quaternization was potentially a more effective route to promote the antibacterial activity of chitosan particles than the homogeneous one. This is extremely important considering that the higher charge density can be achieved via heterogeneous route without sacrificing the positive charges to the crosslinking process. The lowering of the ζ -potential upon ionotropic crosslinking of TMC by TPP has also been reported by Sadeghi and co-workers [33]. It is also conceivable that the uncrosslinked surface-modified quaternized layer on the surface of QACS particles may leach out easier than the quaternary entities trapped or crosslinked by TPP inside and/or on the surface of TMCS particles.

The trend observed for the representative Gram-negative bacteria, $E.\ coli$ is quite different from that seen with the Gram-positive $S.\ aureus$ described above. In comparison with the negative control and chitosan particles, the quaternized chitosan particles with only slightly higher charge density, namely TMCS, and QACS particles, did not possess significant antibacterial activity against $E.\ coli$ (Fig. 4). QACS particles exhibited % antibacterial activity of 82.9% whereas the detrimental action of TMCS cannot be detected. On the other hand, the quaternized chitosan particles with larger alkyl groups having higher charge density, namely QPCS and QBzCS particles, exerted much higher antibacterial action against the $E.\ coli$. With a similar ζ -potential, the QBzCS particles displays a greater inhibitory action than the QPCS particles which is reasonable considering that the uppermost

layer of the outer membrane of *E. coli* contains lipopolysaccharide that should interact favorably with hydrophobic entities of the particles. In addition, the fact that QACS film was reported to exhibit much lower % antibacterial activity against *S. aureus* (26%antibacterial ratio) and *E.coli* (29% antibacterial ratio) [28], in comparison with the QACS particles apparently suggests that the antibacterial efficacy can be magnified by the enhanced surface area of the particles.

Comparatively, as outlined in Fig. 4, it was found that $E.\ coli$ had a greater resistance to quaternized chitosan particles than the $S.\ aureus$. This can be explained by three reasons. Firstly, the absence of an outer membrane and the presence of negatively charged teichoic acid within a thick peptidoglycan layer (20-80 nm) on the surface of $S.\ aureus$ should make them more attractive to the positively charged, quaternized chitosan particles and more specific to be damaged by positively charged molecules than $E.\ coli$. Secondly, the presence of a number of small channels of porins within the outer membrane of $E.\ coli$ may help block the entrance of the particles into the bacterial cell, making them more difficult to inhibit than $S.\ aureus$. Finally, the smaller dimension of $S.\ aureus$ (sphere, i.d. ~ 0.5 -1 μ m) may partly account for more intimate contact with the quaternized chitosan particles, making the antibacterial activity more effective than the $E.\ coli$ (rod, 0.3-1.0 \times 1.0-6.0 μ m).

Minimum inhibitory concentration (MIC) is the lowest concentration of an antimicrobial agent that can inhibit the growth of the target microorganism. From a practical perspective, this value is a key indication of the inhibitory efficiency of the substance against the microorganism. In this study, the MIC values of chitosan, TMCS, QACS, and QBzCS particles were evaluated by viable cell counting methods. The MIC values for each type of particle were identified by comparing the viable cell counts (log (CFU/mL)) between the suspension having the designated particles and the negative control). Results for all quaternized chitosan particles are displayed in Table 1. The fact that the concentration of as

high as 1000 mg/mL was neccessary for chitosan particles to express their inhibitory power explained why no inhibitory action was detected when previously tested with 0.5 mg/mL or 500 μg/mL chitosan particles (Fig.4). To start suppressing the growth of *E. coli* by chitosan particles demanded a concentration as high as 2000 μg/mL. These results support the previous assumption that *E. coli* is more tolerant than *S. aureus*. However, using the same growth media for bacteria, MHB, much lower MIC values of 234 and 117 μg/mL against *S. aureus* and *E. coli*, respectively have been reported for the chitosan particles also prepared by ionotropic crosslinking by TPP [24]. It is suspected that this difference may be a result of their particles having a much smaller size (~54 nm) and so possess a greater available surface area than ours (~320 nm). Therefore, a significantly lower quantity of chitosan particles was required in their case. In contrast, Sadeghi and co-workers [33] reported a two-fold higher MIC value for the TPP-crosslinked chitosan particles against *S. aureus*. This is reasonable given that their particles had a comparable size (~250 nm) to ours but with less ζ- potential (+15.9 eV).

As anticipated, the QACS particles with lower MIC were more potent in prohibiting bacterial growth than the TMCS particles. This MIC value (62.5 µg/mL) was apparently lower than those reported for TMC solutions with various degree of quaternization (%DQ) [33, 34] indicating their superior antibacterial efficacy. This outcome truly indicated the potential of heterogeneous route for the preparation of quaternized chitosan particles as opposed to the conventional homogeneous one which is obviously suffered from the drawback of a deteriorated antibacterial activity because the particles have to be formed after quaternization. The data demonstrated by Sadeghi and co-workers (also shown in Table 1) can be used as a good example [33]. The variation in experimental parameters such as molecular weight and degree of deacetylation of chitosan, %DQ, growth media, pH, initial bacteria concentration, bacterial source, method used for determination of the antibacterial

activity (i.e. optical density (OD), total plate counts for viable cells) should be taken into account when comparing the results. Eventhough a greater quantity of QPCS and QBzCS particles was required to start their detrimental effect on both bacterial strains as compared with the QACS particles, their antibacterial action was more effective when the quantity of all particles were as equal to or above the MIC values of the QPCS and QBzCS particles. This can be evidenced from the data shown in Fig.4 (tested with 500 μ g/mL particles). Interestingly, the MIC values of both QACS and QBzCS particles were independent on the bacterial strain.

4. Conclusions

Quaternized chitosan particles having different alkyl substitutents can be successfully prepared by heterogeneous direct methylation or reductive N-alkylation/methylation as verified by 1 H NMR and FT-IR analyses. The particles were spherical in shape, having an average diameter in a range of 230-490 nm and carried positive charges with ζ -potential ranging from +23.2 to +46.8 mV. As determined by viable count method, it was found that all quaternized chitosan particles exhibited higher antibacterial activity against S. aureus (Gram positive bacteria) than the chitosan particles in neutral media. It is believed that the electrostatic binding between the positive charges on the particles and the negatively charged teichoic acid on the outer membrane of S. aureus was responsible for their superior antibacterial activity. In contrast, only the QPCS and QBzCS particles, which have a high charge density and relatively large alkyl groups, were capable of suppressing the growth of E. coli (Gram-negative bacteria). The fact that E. coli had greater resistance to all quaternized chitosan particles than the S. aureus may be explained as a result of their difference in shape and outer membrane properties. The minimum inhibitory concentration (MIC) data led to two important conclusive remarks: (1) the antibacterial efficiency of each particle was dose-

dependent and (2) having the same alkyl substituent as TMCS particles, QACS particles were a more potent antibacterial material indicating that the heterogeneous quaternization was a more effective method than the homogeneous one. The results obtained from this research suggested that the surface-quaternized chitosan particles may potentially be used as effective antibacterial fillers for biomedical applications.

Acknowledgments

This research was financially supported by Research Team Promotion Grant from the Thailand Research Fund (RTA50800004). The authors appreciated a language editing service provided by Dr. Robert Butcher, the Publication Counselling Unit (PCU), Faculty of Science, Chulalongkorn University.

References

- [1] M. Changez, V. Koul, A. K. Dinda, Efficacy of antibiotics-loaded interpenetrating network (IPNs) hydrogel based on poly(acrylic acid) and gelatin for treatment of experimental osteomyelitis: in vivo study, Biomaterials 26 (2005) 2095-2104.
- [2] B. J. Nablo, A. R. Rothrock, M. H. Schoenfisch, Nitric oxide-releasing sol-gels as antibacterial coatings for orthopedic implants, Biomaterials 26 (2005) 917-924.
- [3] Y. Y. Sun, G. Sun, Novel refreshable *N*-halamine polymeric biocides: *N*-chlorination of aromatic polyamides, Ind. Eng. Chem. Res. 43 (2004) 5015-5020.
- [4] Y. Sun, G. Sun, Synthesis, characterization, and antibacterial activities of novel *N*-halamine polymer beads prepared by suspension copolymerization, Macromolecules 35 (2002) 8909-8912.

- [5] S. M. Iconomopoulou, G. A. Voyiatzis, The effect of the molecular orientation on the release of antimicrobial substances from uniaxially drawn polymer matrixes, J. Control. Release 103 (2005) 451-464.
- [6] N. Cioffi, L. Torsi, N. Ditaranto, G. Tantillo, L. Ghibelli, L. Sabbatini, T. Bleve-Zacheo, M. D'Alessio, P. G. Zambonin, E. Traversa, Copper nanoparticle/polymer composites with antifungal and bacteriostatic properties, Chem. Mater. 17 (2005) 5255-5262.
- [7] M. Rai, A. Yadav, A. Gade, Silver nanoparticles as a new generation of antimicrobials, Biotechnol. Adv. 27 (2009) 76-83.
- [8] V. K. Sharma, R. A. Yngard, Y. Lin, Silver nanoparticles: Green synthesis and their antimicrobial activities, Adv. Colloid Interf. 145 (2009) 83-96.
- [9] F. Furno, K. S. Morley, B. Wong, B. L. Sharp, P. L. Arnold, S. M. Howdle, R. Bayston, P. D. Brown, P. D. Winship, H. J. Reid, Silver nanoparticles and polymeric medical devices: A new approach to prevention of infection, J. Antimicrob. Chemoth. 54 (2004) 1019-1024.
- [10] A. Kumar, P. K. Vemula, P. M. Ajayan, G. John, Silver-nanoparticle-embedded antimicrobial paints based on vegetable oil, Nat. Mate. 7 (2008) 236-241.
- [11] M. Wagener, Antimicrobial coatings, Polym. Paint Colour J. 196 (2006) 34-37.
- [12] N. Duran, P. D. Marcato, G. I. H. De Souza, O. L. Alves, E. Esposito, Antibacterial effect of silver nanoparticles produced by fungal process on textile fabrics and their effluent treatment, J. Biomed. Nanotechnol. 3 (2007) 203-208.
- [13] X. Chen, H. J. Schluesener, Nanosilver: A nanoproduct in medical application, Toxicol. Lett. 176 (2008) 1-12.
- [14] T. M. Benn, P. Westerhoff, Nanoparticle silver released into water from commercially available sock fabrics, Environ. Sci. Technol. 42 (2008) 4133-4139.

- [15] M. N. V. R. Kumar, R. A. A. Muzzarelli, C. Muzzarelli, H. Sashiwa, A. J. Domb, Chitosan chemistry and pharmaceutical perspectives, Chem. Rev. 104 (2004) 6017-6084.
- [16] L. F. Qi, Z. R. Xu, X. Jiang, C. H. Hu, X. F. Zou, Preparation and antibacterial activity of chitosan nanoparticles, Carbohyd. Res. 339 (2004) 2693-2700.
- [17] W. J. Ye, M. F. Leung, J. Xin, T. L. Kwong, D. K. L. Lee, P. Li, Novel core-shell particles with poly(*n*-butyl acrylate) cores and chitosan shells as an antibacterial coating for textiles, Polymer 46 (2005) 10538-10543.
- [18] X. L. Ye, X. G. Li, L. J. Yuan, L. H. Ge, B. S. Zhang, S. B. Zhou, Interaction of houttuyfonate homologues with the cell membrane of gram-positive and gramnegative bacteria, Colloid Surf. A-Physicochem. Eng. Asp. 301 (2007) 412-418.
- [19] M. E. I. Badawy, Structure and antimicrobial activity relationship of quaternary *N*-alkyl chitosan derivatives against some plant pathogens, J. Appl. Polym. Sci. 117 (2010) 960-969.
- [20] C. H. Kim, K. S. Choi, Synthesis and antibacterial activity of quaternized chitosan derivatives having different methylene spacers, J. Ind. Eng. Chem. 8 (2002) 71-76.
- [21] W. Sajomsang, Synthetic methods and applications of chitosan containing pyridylmethyl moiety and its quaternized derivatives: A review, Carbohyd. Polym. 80 (2010) 631-647.
- [22] V. K. Mourya, N. N. Inamdar, Trimethyl chitosan and its applications in drug delivery, J. Mater. Sci.-Mater. Med. 20 (2009) 1057-1079.
- [23] Z. L. Shi, K. G. Neoh, E. T. Kang, W. Wang, Antibacterial and mechanical properties of bone cement impregnated with chitosan nanoparticles, Biomaterials 27 (2006) 2440-2449.

- [24] W. L. Du, S. S. Niu, Y. L. Xu, Z. R. Xu, C. L. Fan, Antibacterial activity of chitosan tripolyphosphate nanoparticles loaded with various metal ions, Carbohyd. Polym. 75 (2009) 385-389.
- [25] L. F. Qi, Z. R. Xu, X. Jiang, Y. Li, M. Q. Wang, Cytotoxic activities of chitosan nanoparticles and copper-loaded nanoparticles, Bioorg. Med. Chem. Lett. 15 (2005) 1397-1399.
- [26] W. L. Du, Y. L. Xu, Z. R. Xu, C. L. Fan, Preparation, characterization and antibacterial properties against *E. coli* K88 of chitosan nanoparticle loaded copper ions, Nanotechnology 19 (2008) 085707.
- [27] S. Inphonlek, N. Pimpha, P. Sunintaboon, Synthesis of poly(methyl methacrylate) core/chitosan-mixed-polyethyleneimine shell nanoparticles and their antibacterial property, Colloid Surf. B-Biointerfaces 77 (2010) 219-226.
- [28] N. Vallapa, O. Wiarachai, N. Thongchul, J. S. Pan, V. Tangpasuthadol, S. Kiatkamjornwong, V. P. Hoven, Enhancing antibacterial activity of chitosan surface by heterogeneous quaternization, Carbohyd. Polym. 83 (2011) 868-875.
- [29] A. B. Sieval, M. Thanou, A. F. Kotze, J. C. Verhoef, J. Brussee, H. E. Junginger, Preparation and NMR characterization of highly substituted *N*-trimethyl chitosan chloride, Carbohyd. Polym. 36 (1998) 157-165.
- [30] M. Kong, X. G. Chen, C. S. Liu, C. G. Liu, X. H. Meng, L. J. Yu, Antibacterial mechanism of chitosan microspheres in a solid dispersing system against *E. coli*, Colloid Surf. B-Biointerfaces 65 (2008) 197-202.
- [31] R. G. Cuero, G. Osuji, A. Washington, *N*-Carboxymethylchitosan inhibition of aflatoxin production: Role of zinc, Biotechnol. Lett. 13 (1991) 441-444.

- [32] P. Fernandez-Saiz, J. M. Lagaron, M. J. Ocio, Optimization of the biocide properties of chitosan for its application in the design of active films of interest in the food area, Food Hydrocolloids 23 (2009) 913-921.
- [33] A. M. M. Sadeghi, F. A. Dorkoosh, M. R. Avadi, P. Saadat, M. Rafiee-Tehrani, H. E. Junginger, Preparation, characterization and antibacterial activities of chitosan, *N*-trimethyl chitosan (TMC) and *N*-diethylmethyl chitosan (DEMC) nanoparticles loaded with insulin using both the ionotropic gelation and polyelectrolyte complexation methods, Int. J. Pharm. 355 (2008) 299-306.
- [34] W. Sajomsang, P. Gonil, S. Saesoo, Synthesis and antibacterial activity of methylated *N*-(4-*N*,*N*-dimethylaminocinnamyl) chitosan chloride, Eur. Polym. J. 45 (2009) 2319-2328.

List of Figure and Scheme Captions

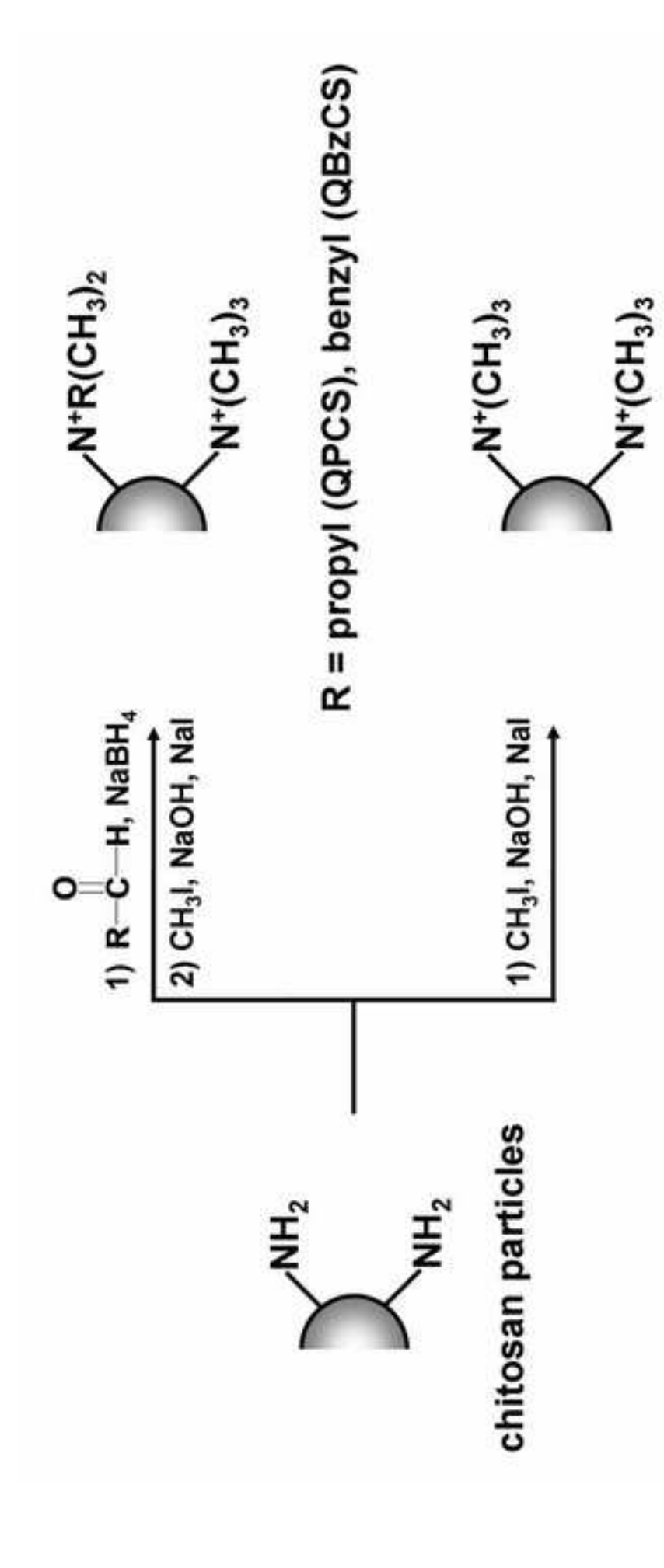
Scheme 1 Preparation of surface-quaternized chitosan particles by reductive *N*-alkylation/methylation (top row) and direct methylation (bottom row).

Fig. 1. FT-IR spectra of (a) chitosan particles, (b) TMCS particles, (c) QACS particles, (d) QPCS particles, and (e) QBzCS particles.

Fig. 2. ¹H-NMR spectra of (a) chitosan particles, (b) TMCS particles, (c) QACS particles, (d) QPCS particles, and (f) QBzCS particles.

Fig. 3. Representative TEM micrographs (x 12,000), average particles sizes and ζ - potentials of chitosan and quaternized chitosan particles. Micrographs shown are representative of at least 10 such fields of view per sample and 3 independent samples.

Fig. 4. Total replication competent (viable) cell counts of *S. aureus* and *E. coli* in suspension after incubation with different chitosan particles (0.5 mg/mL) for 24 h. Statistical significance with p < 0.01 of the viable count is compared with the negative control (*) and the chitosan particles (#). Below in the table is the corresponding antibacterial ratio.



QACS